Ferdowsi University of Mashhad

Journal of Agricultural Machinery

Iranian Society of Mechanical Engineers (ISME)

Vol. 10 No. 1

2020

ISSN: 2228-6829

Contents

Journal of Agricultural Machinery

Vol. 10 **No. 1** **2020**

Published by: Ferdowsi University of Mashhad, (College of Agriculture), Iran

Publisher: Ferdowsi University of Mashhad Press

Printed by: Printing office of Ferdowsi University of Mashhad

Address: College of agriculture, Ferdowsi University of Mashhad, Iran

P.O. BOX: 91775-1163

Fax: +98-05138787430

E-Mail: Jame@um.ac.ir

Web Site: http://jame.um.ac.ir

Contents

Journal of Agricultural Machinery
Vol. 10, No. 1, Spring- Summer 2020, p. 1-10

نشریه ماشین‌های کشاورزی
جلد ۱۰، شماره ۱، نیمسال اول ۱۳۹۹، ص ۱۰-۱

Design, Fabrication and Evaluation of a Novel System for Magnetic Field Application to the Seeds- Case study of Onion Seed

S. Rezaei[1], M. Dowlati[2*], R. Abbaszadeh[3]

Received: 02-11-2018
Accepted: 27-08-2019

Abstract

Non-chemical treatments are an approach for improving seed germination. In order to evaluate the effects of the magnetic field application on onion seed germination and seedling growth indices, a quadrupole magnetic field system was designed and fabricated. It was also compared with a dipole magnetic field system. In the quadrupole system, each coil consisted of three layers and the cores were moved inside the coils. These arrangements make it possible to change the magnetic field intensity in addition to input current setting. The experiments were conducted based on factors including the type of system (bipolar and quadrupole), magnetic flux density (75, 150, 300 and 600 μT) and duration of the field application (15, 30, 60 and 120 min). Germination percentage, germination rate, mean germination time, seedling vigor index, shoot length, root length, fresh weight of shoot and root, fresh weight of seedling, dry weight of shoot and root were measured. The results showed significant effects on seed germination and seedling growth of onion. In most germination characteristics, the quadrupole system had a better impact than the bipolar system. For many traits (except for weights), the increase in field intensity degraded the traits. Quadrupole system that applied the magnetic field of 600 μT for 15 minutes, yielded 63% increase in the total seedling weight. Most of the germination traits were not affected by exposure time. Further investigations are required for shorter exposure times compared to used durations in this study.

Keywords: Magnetic field, Onion, Quadrupole system, Seed germination, Seedling growth

Introduction

The seed is a basis for crop production and as the first consumption input has been an undeniable role in the transmission of genetic traits of the product. Even with the abundant use of energy without the use of the proper seed, it cannot be achieved to the maximum yield and optimum performance. Many techniques have been considered to improve germination of seed or its properties such as seed coating (Ranjbar and Kianmehr, 2017), irrigation and nutrient treatments (Feyzollahzadeh *et al.*, 2013), and optimization of threshing operation (Iranmehr, 2014). Stimulation of seeds using magnetic fields is an inexpensive and nonchemical treatment. A magnetic field is an environmental factor for living organisms that affects biological processes in different ways. Living cells contain electrical charges which are produced by free ions or radicals. Magnetic fields can influence cells via interaction with ions and especially ferromagnetic materials, like iron (Rajabbeigi *et al.*, 2013). It may also affect enzyme activity. The influence of the static magnetic field, which is greater than local geomagnetic fields, on seed germination has been the topic of some research. Static or continuous fields were generated by magnets or direct current (DC). The effect of exposing sunflower seeds to static magnetic fields of 125 mT and 250 mT for 1, 10, 20, 60 minutes, 24 hours or in a chronically way was investigated during the germination process. The mean germination time achieved for seeds subjected to treatment was significantly less than control (Carnobell *et al.*, 2005). Tomato seeds were magnetically exposed to magnetic

1- Graduate, Department of Mechanical Engineering of Biosystems, Faculty of Agriculture, University of Jiroft, Jiroft, Iran
2- Assistant Professor, Tuyserkan Faculty of Engineering and Natural Resources, Bu-Ali Sina University, Tuyserkan, Hamedan
3- Assistant Professor, Agriculture Research Institute, Iranian Research Organization for Science and Technology (IROST), Ahmadabad Mostoufi, Tehran, Iran
(*- Corresponding Author Email: m.dowlati@basu.ac.ir)
DOI: 10.22067/jam.v10i1.76370

field strengths (125 or 250 mT) for different exposure time. The results showed a reduction of germination time for magnetic treatments. The germination parameters were lower than control values and the germination rate for treated seeds was higher than control (Martinez *et al.*, 2009). Germination and early growth of wheat and bean were studied under magnetic fields (4 or 7 mT) and osmotic conditions. The application of magnetic fields promoted the germination ratios of seeds (Cakmak *et al.*, 2010). Cucumber seeds were exposed to stationary magnetic field strength from 100 to 250 mT for 1, 2 or 3 h. Germination-percentage and rate of germination increased by 18.5% and 49%, respectively compared to unexposed seeds. The magnetic field of 200 mT for 1 h showed a significant influence on germination parameters (Bhardwaj *et al.*, 2012). Maize seeds were treated by magnetic fields of 50, 100, 150, 200, and 250 mT for 1, 2, 3, and 4 h for all field strengths. Results indicated that the magnetic field significantly enhanced seed performance in terms of percentage of germination, germination speed and seedling length compared to unexposed control. Field application of 200 mT for 1 h exposure gave the best results among the various combinations of field and exposure time (Vashisth & Joshi, 2016). Since the method of magnetic field application can be effective on treatment results, in this study design and implementation of a system was considered to apply a magnetic field to onion seeds and the results were evaluated.

Materials and Methods

Sample preparation

The onion seed used in this experiment was from a yellow short day cultivar named Texas early grano 502. Seeds were disinfected with sodium hypochlorite (1.5%) for two minutes and washed three times with distilled water, and then the onion seeds were macerated with mancozeb fungicide.

Magnetic field application systems

A bipolar system and a quadrupole system were used to apply the magnetic field. Figure 1 shows the system for producing the bipolar magnetic field used in this study (Zamiran *et al.*, 2013). The quadrupole magnetic field system was designed and fabricated (Figure 2).

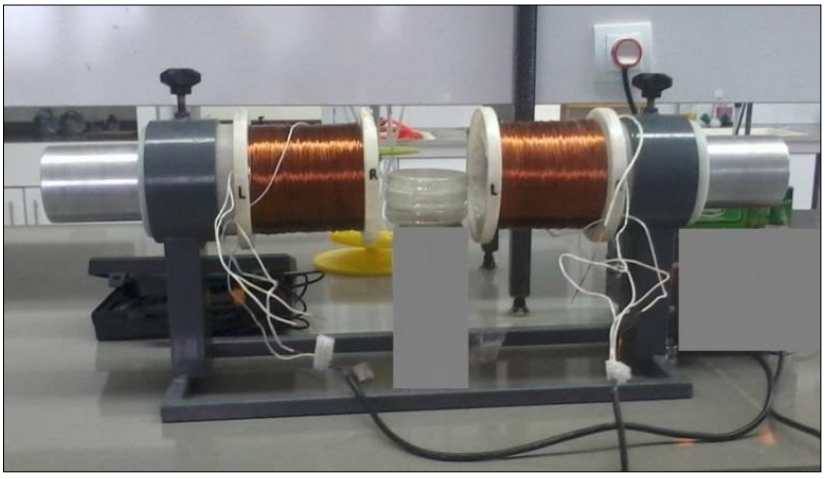

Fig.1. The system for producing the bipolar magnetic field

Design and fabrication of a novel magnetic field system

Quadrupole system consisted of stationary and movable retaining bases for keeping the cores and windings, conductive insulation (made of polytetrafluoroethylene) to avoid contacting the aluminum core with the iron body of the bases, cylindrical coils, central aluminum core, seed position and direct current power supply.

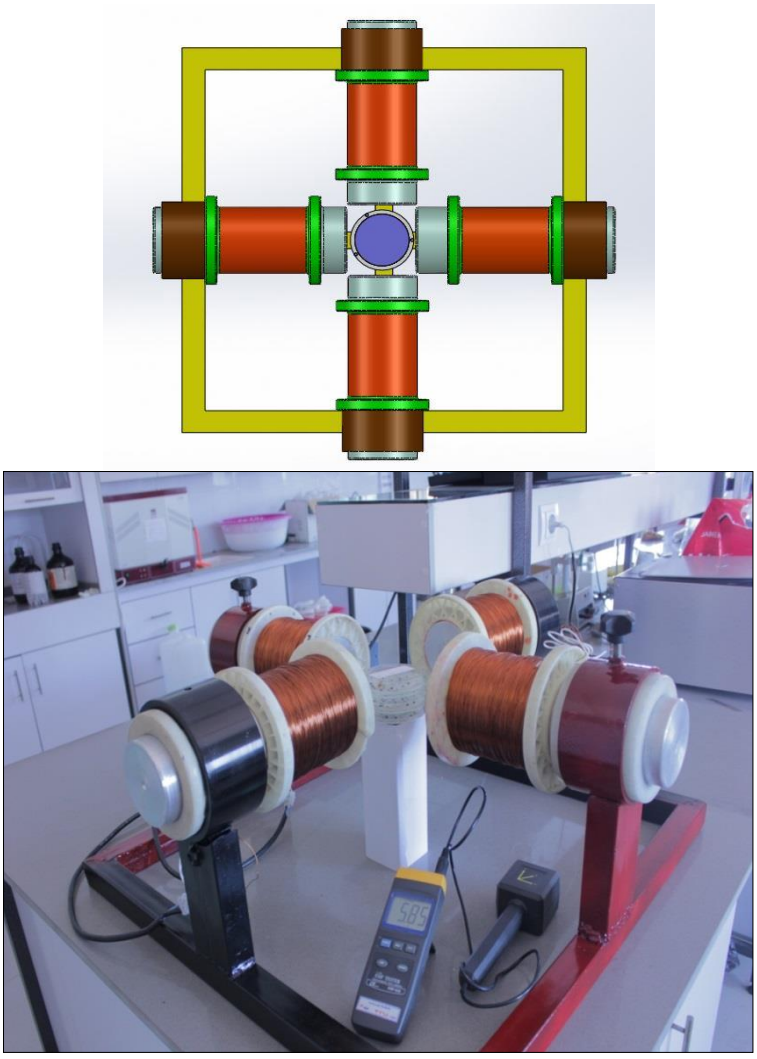

Fig.2. Quadrupole magnetic field system

Lacquer-coated wire (200 micron diameter) was used to form the coils. Each coil consisted of three layers, that is, each coil contains three input wires and three outlet wires. The first layer consisted of 450 rounds, the second layer had 650 rounds and in the third layer or the outer layer 1150 rounds were used. Therefore, the coil had 2250 rounds of copper wire and a resistance of each coil was 31 Ohm. The average diameter and the length of each coil were 105 mm and 128 mm, respectively. The purpose of wrapping coils with three layers was to receive magnetic fields with different intensities from each layer. So layers generated specific field intensity considering the input current. In order to have the minimum field strength, the first layer should be used, which has the smallest wire length as well as second and third layers should be applied to increase the magnetic flux density. If the desired magnetic strength is higher than the field strength of the third layer, it was possible to obtain the maximum field strength from the coil with layers connected in series. In order to improve the magnetic field, a solid aluminum core with a circular cross-section of 88 mm in diameter and a length of 300 mm was used in the middle of each coil. It worth noting that aluminum has paramagnetic properties. The core was easily moved inside the coil and, concerning the paramagnetic properties of aluminum, the backward and forward movement changed the magnetic field so that, as the core moved in the direction of the magnetic field, the intensity of the field was increased. The output current of the power

supply is 12 volts of direct current. The power supply was able to produce four separate lines of 220/12 Volt DC which will be input to each coil and 500 W (Watt) active power. The power supply consisted of four transformers (12 Volt, 6 Amp), converting 220V to 12V. This output current from the transformers was also the AC, which is converted to DC using a rectifier diode bridge. The input current to each coil has the potential to produce a maximum magnetic field with an intensity of 700 μT, which can be changed by increasing the electrical current. The main purpose of using direct current is to have a constant magnetic field, while alternating current causes variable magnetic field. Magnetic flux density generated in each system was measured using a three-axis digital Teslameter (LMF-828 model, Lutron Company, Taiwan). Seeds were subjected to magnetic fields at the induction of 75, 150, 300 and 600 μT for 15, 30, 60 and 120 minutes. Control seeds were kept without magnetic treatment. Treatments were replicated three times and 25 seeds were used for each replication.

Germination test

Seeds were placed on filter paper in Petri dishes. Moisture content was provided by adding distilled water. Petri dishes were sealed with sterilized plastic bags and kept inside the incubator at the temperature of 25 °C. Germination of onion seeds lasted 13 days and the number of germinated seeds was recorded. Germination indices such as percentage, speed and mean time of germination, root and shoot length, fresh and dry weights of shoots and fresh and dry weights of roots were measured. The germination percentage (GP), germination rate (GR), mean germination time (MGT) and seedling vigour index (SVI) were calculated separately using equation (1), (2), (3) and (4):

$$GP=100(N_G/N_T) \quad (1)$$

Where N_G is the number of germinated seeds and N_T is the total number of seeds (Hoseyni and Rezvani Moghadam, 2009).

$$GR=\sum_{i=1}^{n}\frac{Si}{Di} \quad (2)$$

Where S_i is the number of germinated seeds per day, D_i is the number of days, and n is the number of counting days (Maguire, 1962).

$$MGT=\frac{A_1D_1+A_2D_2+\cdots A_nD_n}{A_1+A_2+\cdots A_n} \quad (3)$$

Where A is the number of seeds germinated at time D and n is the total number of days until the last day (Wang and Chang, 2003).

$$SVI = GP\times L \quad (4)$$

Where L is the mean seedling length (cm) and GP is the germination percentage (Aboutalebian *et al.*, 2005).

Five normal seedlings were selected from each petri dish and length of root and shoot and also the weight of fresh root and fresh shoot were measured. The selected seedlings were placed in an electric oven for 48 hours at a temperature of 70 °C to reach a constant weight and then dry weight was obtained.

Statistical analyses were performed using SAS software. Factorial analysis of variance (ANOVA) and Duncan tests were carried out on data.

Results and Discussion

Results of factors affected on onion seed germination parameters were shown in tables 1 and 2.

Table 1- Analysis of variance of magnetic field effect on some onion seed germination traits

Source	df	Mean Square					
		GP	GS	MGT	SVI	Shoot L.	Root L.
Type	1	326.34*	1259.16**	63.19**	12519.52	1127.51**	135.37*
Intensity	3	650.4**	195.26**	0.22	277130.63**	328.04*	212.13**
Time	3	216.84	44.62	0.15	13566.37	128.59	19.74
Type × Intensity	3	171.01	46.10	0.22*	91423.84**	827.90	13.40
Type × Time	3	132.12	9.04	0.07	30743.15	171.01	43.46
Intensity × Time	9	116.55	12.92	0.11	42830.36*	128.35	42.37
Type × Intensity × Time	9	125.97	30.69	0.17*	45423.69*	37.51	61.63

*: significant at the 5% level, **: significant at the 1% level, L.: Length

Table 2- Analysis of variance of magnetic field effect on some onion seed germination traits

Source	df	Mean Square				
		Shoot wet W.	Shoot dry W.	Root wet W.	Root dry W.	Total W.
Type	1	24193.50*	666.76**	4537.50**	63.37**	7776.00
Intensity	3	3785.03	18.79	446.40	6.79*	4656.46
Time	3	4205.42	17.09	1139.60	5.12*	3212.57
Type × Intensity	3	25793.19**	18.79	1283.42	7.68**	24975.53**
Type × Time	3	1277.97	24.82*	1331.28	13.74**	4617.25
Intensity × Time	9	3483.13	17.62*	505.70	2.47	5345.50
Type × Intensity × Time	9	5943.78	13.36	1083.60	1.71	9290.48

*: significant at the 5% level, **: significant at the 1% level, W.: Weight

Table 3- Means comparison of magnetic treatments and control for germination percentage, germination rate and mean germination time of onion seeds

System type	Magnetic flux density(μT)	Exposure time (min)	GP (%)	GR (Seed Day^{-1})	MGT (Day)
Bipolar	75	15	69.33^{abcdef}	24.61^{abcd}	7.57^{defgh}
		30	77.33^{abcd}	26.04^{abc}	7.71^{bcdefg}
		60	73.33^{abcde}	21.90^{abcde}	7.84^{bcdefg}
		120	76.00^{abcd}	27.50^{a}	7.58^{cdefgh}
	150	15	84.00^{a}	25.42^{abc}	7.80^{bcdefg}
		30	80.00^{abc}	26.82^{ab}	7.64^{bcdefg}
		60	70.67^{abcde}	21.96^{abcde}	7.79^{bcdefg}
		120	76.00^{abcd}	21.01^{abcdef}	7.93^{abcdef}
	300	15	73.33^{abcde}	19.63^{cdefg}	8.03^{abcde}
		30	62.67^{cdef}	16.43^{efg}	8.10^{abcd}
		60	65.33^{abcdef}	18.39^{defg}	7.94^{abcdef}
		120	60.00^{def}	19.40^{cdefg}	7.76^{bcdefg}
	600	15	56.00^{ef}	13.94^{g}	8.20^{ab}
		30	70.67^{abcde}	18.53^{defg}	8.00^{abcdef}
		60	62.67^{cdef}	15.86^{fg}	8.20^{ab}
		120	74.67^{abcde}	20.49^{bcdefg}	7.94^{abcdef}
Quadrupole	75	15	79.33^{abc}	20.92^{abcdef}	7.85^{bcdefg}
		30	78.67^{abcd}	21.39^{abcdef}	7.65^{bcdefg}
		60	77.33^{abcd}	21.72^{abcde}	7.35^{gh}
		120	84.00^{a}	21.11^{abcdef}	7.88^{bcdefg}
	150	15	64.67^{bcdef}	20.87^{abcdef}	7.57^{defgh}
		30	72.00^{abcde}	21.13^{abcdef}	7.36^{gh}
		60	79.33^{abc}	21.47^{abcdef}	7.65^{bcdefg}
		120	76.67^{abcd}	20.25^{bcdefg}	7.56^{defgh}
	300	15	66.00^{abcdef}	19.91^{cdefg}	7.79^{bcdefg}
		30	83.33^{ab}	22.04^{abcde}	7.46^{fgh}
		60	62.67^{cdef}	22.74^{abcde}	7.81^{bcdefg}
		120	76.67^{abcd}	20.18^{bcdefg}	7.56^{defgh}
	600	15	52.00^{f}	20.55^{bcdefg}	7.07^{h}
		30	62.67^{cdef}	20.03^{bcdefg}	7.54^{efgh}
		60	65.33^{abcdef}	21.62^{abcdef}	8.12^{abc}
		120	77.33^{abcd}	21.52^{abcdef}	7.66^{bcdefg}
Control	0	0	69.33^{abcdef}	14.07^{g}	8.42^{a}

Effects of treatments on germination percentage, germination rate and mean germination time of onion seeds were presented in Table 3. A significant change was not observed for germination percentage compared to untreated seeds but germination rate was significantly increased. The fastest germination was occurred using the bipolar

system and 75 μT. A significant reduction of mean germination time was observed. One of the possible causes to explain the positive effects of the magnetic field can be paramagnetic properties of atoms found in plant cells. Applying an external magnetic field can spin the atoms in order of the magnetic field. Magnetic properties of molecules and their ability to absorb energy and then changing the magnetic field to transfer energy to other forms of energy as well as other structures in plant cells, leading to activate them (Zeidali *et al.,* 2017).

The results presented in Table 4 showed a significant impact of some magnetic fields on seedling vigour index, length of shoot and root of onion seeds. It seems the quadrupole system with minimum intensity and treatment time results in the highest value among other treatments for these parameters. Length of shoot and root were longer in the quadrupole magnetic treatment and weaker fields.

Table 4- Means comparison of magnetic treatments and control for seedling vigour index, length of shoot and root of onion seeds

System type	Magnetic flux density(μT)	Exposure time (min)	SVI	Shoot length (mm)	Root length (mm)
Bipolar	75	15	833.70^{abcdef}	89.00^{abcdefgh}	30.00^{cde}
		30	964.20 ^{abcde}	83.33^{cdefgh}	42.33^{ab}
		60	909.30 ^{abcdef}	90.67 ^{abcdefg}	33.00^{abcde}
		120	883.90 ^{abcdef}	80.33^{efgh}	35.33^{abcde}
	150	15	1030.40^{abc}	86.67 ^{abcdefgh}	35.33^{abcde}
		30	965.10 ^{abcde}	86.00 ^{abcdefgh}	35.33^{abcde}
		60	908.80 ^{abcdef}	95.00 ^{abcdef}	32.67^{bcde}
		120	822.80 ^{abcdef}	79.33^{fgh}	29.00^{def}
	300	15	885.10 ^{abcdef}	82.67^{defgh}	38.00^{abcd}
		30	718.30^{efg}	86.00 ^{abcdefgh}	29.33^{cdef}
		60	766.20^{cdefg}	88.00 ^{abcdefgh}	28.33^{def}
		120	618.70^{fg}	73.67^{gh}	29.33^{cde}
	600	15	632.40^{fg}	87.33 ^{abcdefgh}	26.00^{ef}
		30	897.10 ^{abcdef}	95.00 ^{abcdef}	32.00^{bcde}
		60	729.90^{defg}	88.00 ^{abcdefgh}	28.33^{def}
		120	854.00 ^{abcdef}	89.33 ^{abcdefgh}	25.67^{ef}
Quadrupole	75	15	1099.90^{a}	104.00^{a}	44.00^{a}
		30	965.60 ^{abcde}	99.67 ^{abcde}	35.67^{abcde}
		60	1018.00 ^{abcd}	103.33^{ab}	38.00^{abcd}
		120	1053.90 ^{abc}	100.33 ^{abcde}	36.33^{abcde}
	150	15	782.00^{cdefg}	96.00 ^{abcdef}	34.00^{abcde}
		30	797.50^{bcdefg}	90.33 ^{abcdefg}	29.00^{def}
		60	1048.90^{abc}	101.00 ^{abcd}	40.67^{abc}
		120	88.40 ^{abcdef}	91.00 ^{abcdefg}	34.67^{abcde}
	300	15	834.40 ^{abcdef}	102.67^{abc}	33.00^{abcde}
		30	1075.30^{ab}	104.00^{a}	35.00^{abcde}
		60	651.70^{fg}	85.00 ^{abcdefgh}	26.00^{ef}
		120	900.80 ^{abcdef}	93.00 ^{abcdefg}	34.00^{abcde}
	600	15	539.90^{g}	84.33 ^{abcdefgh}	28.67^{def}
		30	656.70^{fg}	81.00^{defgh}	33.67^{abcde}
		60	625.90^{fg}	70.67^{h}	31.67^{bcde}
		120	846.50 ^{abcdef}	83.67^{bcdefgh}	33.67^{abcde}
Control	0	0	689.20^{efg}	81.67^{defgh}	18.67^{f}

Means of findings for the fresh and dry weight of shoot and root were compared in Table 5. It was demonstrated that the magnetic treatment can increase these indices. Shoot fresh weight was enhanced by 67% compared to the control using optimum treatment. The magnetic field not only causes the faster penetration of water into the seed but also

affects the speed of enzymatic reactions. Water uptake in the first stage accelerates the seeds swelling and their weight. This may be associated with increased metabolism and more water content in plants (Fischer *et al.*, 2004).

Table 5- Means comparison of magnetic treatments and control for the fresh and dry weight of shoot and root of onion seeds

System type	Magnetic flux density (µT)	Exposure time (min)	Shoot fresh weight (µg)	Root fresh weight (µg)	Shoot dry weight (µg)	Root dry weight (µg)
Bipolar	75	15	378.33^{bcde}	102.33^{abcd}	10.33^{fgh}	5.33^{defgh}
		30	360.33 ^{bcde}	110.67 ^{abcd}	11.33^{efgh}	5.67$^{c\ defgh}$
		60	393.00 ^{bcde}	96.67^{bcd}	12.33^{efgh}	5.00^{efgh}
		120	373.67 ^{bcde}	115.33^{abc}	12.33^{efgh}	4.33^{fgh}
	150	15	392.33 ^{bcde}	87.33^{bcd}	11.67^{efgh}	5.33 ^{defgh}
		30	426.33^{abcde}	92.00^{bcd}	14.00^{cdefg}	5.33 ^{defgh}
		60	392.67 ^{bcde}	96.00^{bcd}	10.67^{fgh}	5.00^{efgh}
		120	358.00 ^{bcde}	83.67^{bcd}	9.00^{gh}	4.33^{fgh}
	300	15	352.67^{cde}	110.67^{abcd}	11.67^{efgh}	5.33 ^{defgh}
		30	349.67^{de}	85.00^{bcd}	13.67^{cdefgh}	5.00^{efgh}
		60	400.67^{abcde}	94.33^{bcd}	12.67^{defgh}	5.33 ^{defgh}
		120	312.00^{e}	88.33^{bcd}	8.33^{h}	4.00^{gh}
	600	15	401.67^{abcde}	85.67^{bcd}	10.67^{fgh}	5.67$^{c\ defgh}$
		30	447.00^{abcde}	104.00^{abcd}	10.67^{fgh}	5.67$^{c\ defgh}$
		60	487.33^{abc}	85.67^{bcd}	11.00^{efgh}	4.67^{efgh}
		120	470.33^{abcd}	127.67^{ab}	16.00^{bcdef}	3.33^{h}
Quadrupole	75	15	398.67^{abcde}	74.00^{cd}	13.67^{cdefgh}	5.33 ^{defgh}
		30	429.33^{abcde}	80.67^{bcd}	15.33^{bcdef}	5.33 ^{defgh}
		60	406.33^{abcde}	77.33^{bcd}	14.33^{cdefg}	4.67^{efgh}
		120	422.33 ^{abcde}	83.67^{bcd}	15.33^{bcdef}	6.67^{bcdef}
	150	15	416.00 ^{abcde}	144.67^{a}	18.00^{abcd}	7.00^{bcde}
		30	406.00 ^{abcde}	78.33^{bcd}	13.67^{cdefgh}	4.33^{fgh}
		60	470.00 ^{abcd}	81.33^{bcd}	20.00^{ab}	8.00^{abc}
		120	405.00 ^{abcde}	81.67^{bcd}	16.67^{bcde}	8.00^{abc}
	300	15	427.00 ^{abcde}	72.33^{cd}	18.00^{abcd}	7.67^{abcd}
		30	469.33 ^{abcd}	72.67^{cd}	18.67^{abc}	6.67^{bcdef}
		60	529.00^{a}	74.67^{cd}	20.00^{ab}	10.00^{a}
		120	424.67 ^{abcde}	78.33^{bcd}	19.00^{abc}	7.67^{abcd}
	600	15	488.67^{ab}	127.00^{ab}	14.33^{cdefg}	5.33^{defgh}
		30	339.00^{de}	74.67^{cd}	12.67^{defgh}	4.67^{efgh}
		60	376.33^{bcde}	72.67^{cd}	22.33^{a}	8.33^{ab}
		120	396.33 ^{abcde}	71.67^{cd}	18.67^{abc}	5.67^{cdefgh}
Control	0	0	317.00^{e}	61.00^{d}	16.67^{bcde}	6.33^{bcdefg}

Comparison of seedling weights is illustrated in Figure 3. Some treatments significantly increased this important germination parameter. Quadrupole system that applied the magnetic field of 600 µT for 15 minutes, yielded 63% increase in total weight.

The magnetic field can have various effects on plant metabolism according to application style, intensity and environmental conditions (Cakmak *et al.*, 2010).

The low-frequency magnetic field (20 mT) was induced to onion seeds at 10, 30 and 60 minutes. For the magnetic treatment of 60 minutes, an increase in energy of germination, germination capacity, and the seedling length was observed. The results were different for two cultivars of onion (Holubowicz *et al.*, 2014). Exposure of dry onion seeds to low frequency non-uniform magnetic fields (160 mT for 15 and 20 min) increased germination compared to unexposed controls. The best finding was found for 160 mT for 15 min (De

Souza *et al.*, 2014). Onion seeds were also pretreated by the static magnetic field (0.03 or 0.06 T) for 30, 60 and 90 minutes. Exposed seeds to 0.06 T with 30 minute gave the maximum values of germination percentage, germination rate, seedling length and seedling dry weight (Hozyan *et al.*, 2015). In present research, weaker magnetic fields were used than many similar studies.

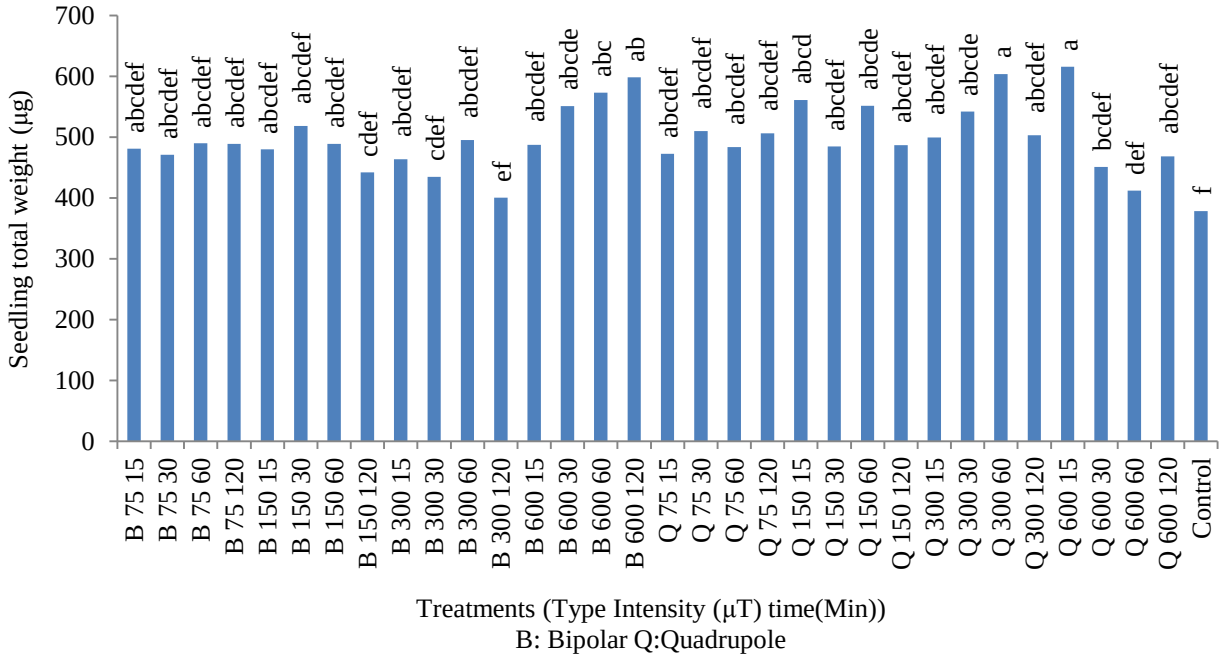

Fig.3. Effect of magnetic treatments on the seedling total weight

Conclusions

It is concluded that the designed system which was optimized to quadrupole has a potential to improve germination seed. Evaluation of the system with onion seed showed significant results. In most germination characteristics, the quadrupole system had better effect than the bipolar system. Generally, in many traits (except for traits related to weight), the increase in field intensity degraded the traits. Most of the germination traits were not affected by exposure time. Therefore short durations are efficient regarding cost and time. Further investigations are suggested for shorter exposure times compared to used durations in this study. Optimum magnetic treatments should be determined for every product. Investigation of the alternative current utilization in this system is also suggested. Meanwhile it may be useful to study the combination of a magnetic field with other treatments. Although the findings were obtained by a laboratory system, it is also possible to develop it in industrial technology.

Acknowledgements

The support of University of Jiroft is appreciated.

References

1. Aboutalebian, M. A., F. Sharifzadeh, M. R. Jahansouz, A. Ahmadi, and M. R. Naghavi. 2005. Effect of osmopriming treatments on speed of emergence, germination percentage, base temperature of germination and seedling vigour index of some wheat cultivars (*Triticum aestivum* L.). Agricultural Research Soil, Water and Plant 5 (1): 67-82.
2. Bhardwaj, J., A. Anand, and S. Nagarajan. 2012. Biochemical and biophysical changes associated with magnetopriming in germinating cucumber seeds, Plant Physiology and Biochemistry 57: 67-73.

3. Cakmak, T., R. Dumlupinar, and S. Erdal. 2010. Acceleration of germination and early growth of wheat and bean seedlings grown under various magnetic field and osmotic conditions. Bioelectromagnetics 31: 120-129.
4. Carbonell, M., E. Martinez, and R. M. Flores. 2005. Influencia de campos magneticos estacionarios de 125mT y 250 mT en la germinacion de semillas de girasol (in Spanish). Ingenieria de Recursos Naturales y del Ambiente 2 (3): 34-39.
5. De Souza, A., D. García, L. Sueiro, and F. Gilart. 2014. Improvement of the seed germination, growth and yield of onion plants by extremely low frequency non-uniform magnetic fields, Scientia Horticulturae 176: 63-69.
6. Feyzollahzadeh, M., A. Nikbakht, and A. Modarres Motlagh. 2013. Investigation of the Effects of Irrigation and Nutrient Treatments on Biophysical and Biomechanical Properties of Safflower Seed. Journal of Agricultural Machinery 3 (1): 58-70. (In Farsi),
7. Fischer, G., M. Tausz, M. Kock, and D. Grill. 2004. Effects of weak 16 Hz magnetic fields on growth parameters of young sunflower and wheat seedlings. Bioelectromagnetics 25 (8): 638-641.
8. Hołubowicz, R., L. Kubisz, M. Gauza, Y. Tong, and D. Hojan-jezierska. 2014. Effect of Low Frequency Magnetic Field (LFMF) on the Germination of Seeds and Selected Useful Characters of Onion (*Allium cepa* L.). Notulae Botanicae Horti Agrobotanici Cluj-Napoca. 42 (1): 168-172.
9. Hoseyni, H., and P. Rezvani Moghadam. 2009. Effect of water and salinity stress in seed germination on Isabgol (*Plantago ovata*). Iranian Journal of Field Crops Research 4 (1): 15-22. (In Farsi).
10. Hozayn, M., A. Amal, A. EL-Mahdy, and H. M. H. Abdel-Rahman. 2015. Effect of magnetic field on germination, seedling growth and cytogenetic of onion (*Allium cepa* L.). African Journal of Agricultural Research 10 (8): 849-857.
11. Imanmehr, A. 2014. Effects of Drum Speed and Feed Rate on Damaged Wheat Grain during Threshing Operation. Journal of Agricultural Machinery 5 (1): 184-190. (In Farsi).
12. Maguire, J. D. 1962. Speed of germination-aid in selection and evaluation for seedling emergence and vigor. Crop Science 2 (2): 176-177.
13. Martinez, E., M. V. Carbonell, Florez, J. M. Amaya, and R. Maqueda. 2009. Germination of tomato seeds (*Lycopersicon esculentum* L.) under magnetic field. International Agro Physics 23: 45-49.
14. Rajabbeigi, E., F. Ghanati, and P. Abdolmaleki. 2013. Physiologic responses of suspension-cultured parsley cells to static magnetic field. Iranian Journal of Plant Biology 5 (15): 59-68. (In Farsi).
15. Ranjbar, F., and M. Kianmehr. 2017. Review of some of Coating Seed Factors in Rotary Pan Coater. Journal of Agricultural Machinery 8 (1): 31-41. (In Farsi).
16. Vashisth, A., and D. K. Joshi. 2016. Growth characteristics of maize seeds exposed to magnetic field. Bioelectromagnetics. DOI: 10.1002/bem.2202.
17. Wang, P., and C. Chang. 2003. Detection of the low-germination-rate resting oospores of Pythium myriotylum from soil by PCR. Letters in Applied Microbiology 36 (3):157-161.
18. Zamiran, A., V. R. Saffari, and M. R. Maleki. 2013. Seed Germination Enhancement of Zinnia (*Zinnia elegans*) Using Electromagnetic Field. Journal of Ornamental Plants 3 (3): 203-214.
19. Zeidali, H., Z. Rostami, F. Darabi, H. Soheyli, Gh. Nabiyouni, and R. Naseri. 2017. Germination and Growth of Wheat and Wild Oat Seedling as Affected by Different Intensities and Times of Magnetic Fields. Biological, Environmental and Agricultural Sciences 2: 86-100.

نشریه ماشین‌های کشاورزی
جلد ۱۰، شماره ۱، نیمسال اول ۱۳۹۹، ص ۱۰-۱

Journal of Agricultural Machinery
Vol. 10, No. 1, Spring- Summer 2020, p. 1-10

طراحی، ساخت و ارزیابی یک سامانه جدید اعمال میدان مغناطیسی به بذر محصولات کشاورزی – مطالعه موردی بذر پیاز

سعید رضایی[۱]، مجید دولتی[۲*]، روزبه عباس زاده[۳]

تاریخ دریافت: ۱۳۹۷/۰۸/۱۱
تاریخ پذیرش: ۱۳۹۸/۰۶/۰۵

چکیده

استفاده از روش‌های غیرشیمیایی یکی از راهکارهای بهبود جوانه‌زنی بذر به‌شمار می‌رود. به‌منظور بررسی اثر اعمال میدان مغناطیسی بر شاخص‌های جوانه‌زنی بذر و رشد گیاهچه پیاز، یک سامانه‌ی میدان مغناطیسی چهار قطبی طراحی و ساخته شد و با سامانه دوقطبی مورد مقایسه قرار گرفت. در سامانه چهارقطبی، هر یک از چهار کلاف سیم پیچ شامل سه‌لایه سیم‌پیچ و یک هسته فلزی است که هسته قابلیت حرکت در درون سیم‌پیچ را دارد. این قابلیت باعث تغییر شدت میدان مغناطیسی، علاوه بر تغییر از طریق تغییر جریان ورودی، خواهد شد. دو آزمایش مستقل با دو سامانه‌ی میدان مغناطیسی به‌صورت فاکتوریل در قالب طرح کاملاً تصادفی با سه تکرار انجام شد. فاکتورها شامل نوع سامانه (دو قطبی و چهار قطبی)، شدت میدان مغناطیسی (۷۵، ۱۵۰، ۳۰۰ و ۶۰۰ میکروتسلا) و مدت زمان اعمال میدان (۱۵، ۳۰، ۶۰ و ۱۲۰ دقیقه) بود. شاخص‌های مورد بررسی عبارت بودند از: درصد جوانه‌زنی، سرعت جوانه‌زنی، متوسط زمان جوانه‌زنی، شاخص بنیه، طول ساقه‌چه، طول ریشه‌چه، وزن تر ساقه‌چه، وزن‌تر ریشه‌چه، وزن تر گیاهچه، وزن خشک ریشه‌چه و وزن خشک ساقه‌چه. به‌طور کلی نتایج نشان داد که میدان مغناطیسی بر روی شاخص‌های جوانه‌زنی و رشد گیاهچه پیاز تاثیر معنی‌دار داشته و سامانه چهارقطبی نسبت به سامانه دوقطبی در بیشتر شاخص‌های مورد مطالعه عملکرد بهتری داشته است. در مورد غالب صفات (به‌جز وزن)، افزایش شدت میدان، منجر به کاهش صفات شد. سیستم چهارقطبی که میدان مغناطیسی ۶۰۰ میکروتسلایی را به مدت ۱۵ دقیقه به بذر اعمال کرد، باعث افزایش ۶۳ درصدی وزن گیاهچه گردید. غالب صفات جوانه‌زنی تحت تأثیر مدت زمان اعمال میدان به بذر قرار نگرفتند. به هرحال بررسی‌های بیشتر در خصوص مدت زمان اعمال میدان نسبت به زمان اعمال شده در این مطالعه ضروری است.

واژه‌های کلیدی: پیاز، جوانه‌زنی بذر، رشد گیاهچه، سامانه چهار قطبی، میدان مغناطیسی

۱- دانش‌آموخته کارشناسی ارشد، گروه مهندسی مکانیک بیوسیستم، دانشکده کشاورزی، دانشگاه جیرفت، جیرفت، ایران
۲- استادیار، دانشکده فنی و منابع طبیعی تویسرکان، دانشگاه بوعلی سینا، همدان، ایران
۳- استادیار، پژوهشکده کشاورزی، سازمان پژوهش‌های علمی و صنعتی ایران، احمدآباد مستوفی، تهران، ایران
(*- نویسنده مسئول: Email: M.dowlati@basu.ac.ir)

DOI: 10.22067/jam.v10i1.76370

Journal of Agricultural Machinery
Vol. 10, No. 1, Spring- Summer 2020, p. 11-21

نشریه ماشین‌های کشاورزی
جلد ۱۰، شماره ۱، نیمسال اول ۱۳۹۹، ص ۲۱-۱۱

An Estimator for Torque and Draft Force Requirements of a New Up-cut Rotary Tiller

I. Ahmadi[1*], M. Beigi[2]

Received: 18-03-2018
Accepted: 26-06-2018

Abstract

The aim of this study is to design, fabricate and evaluate a new type of up-cut rotary tiller and to develop correct formulas to estimate its torque and draft force using the laws of classical mechanics. In order to verify the model, a real-sized prototype of the rotary tiller was tested. It was hypothesized that four processes are involved to create the rotary tiller torque, namely soil cutting, soil lifting, soil-metal friction, and soil velocity. Furthermore, it was assumed that the horizontal components of soil cutting and soil-metal friction forces create the required draft of the machine. Based on these hypothesizes, mathematical formulas were developed to calculate torque, and draft requirements of the machine. To facilitate performing necessary calculations, the developed formulas were entered in a worksheet of the MS Excel software. According to the results of this study, the average experimental draft and torque of the machine tilling a silty clay loam soil were 16.8 N and 12.8 Nm, respectively. Furthermore, the average theoretical draft and torque of the machine were 13 N and 11.8 Nm respectively. These promising results can be considered as the accuracy check of the formulas developed herein.

Keywords: Theoretical modeling, Torque and draft force measurement, Up-cut rotary tiller

Introduction

Imagine a gardener digging and turning over the orchard soil with a shovel. The shovel is a suitable tool in places where the lack of maneuverability is a serious issue. Is there an engine-powered machine that can perform the same? The rotary tiller can be an appropriate option. However, the working depth of a conventional down cut rotary tiller is restricted, and it may have undesirable side effects such as soil re-tilling. The up-cut rotary tiller is an alternative choice to compensate for the above-mentioned drawbacks of the conventional one (Shibusawa, 1993). In order to design a rotary tillage machine, it is important to have a correct understanding of the amount of torque required. To achieve this goal, the majority of researchers measured the torque requirement or specific fuel consumption of a conventional rotary tiller using an experimental procedure (Asland Singh, 2009; Chertkiattipol and Niyamapa, 2010; Matin *et al.*, 2015, Gholami *et al.*, 2017), while few researchers calculated the machine torque theoretically (Bernacki *et al.*, 1972; Ahmadi, 2017). However, the experimental measurement as well as the theoretical calculation of the torque and draft requirements of an up-cut rotary tiller has not received the amount of attention that it deserves.

Therefore, the aim of this study is to design, fabricate and analyze experimentally a new up-cut rotary tiller and to estimate its torque and draft using the laws of classical mechanics.

Materials and Methods

Introducing the machine

The working unit of the machine consists of three main parts: blades, a flange, and a rotating shaft. Each blade is formed from a cutting edge and a blade extension. The blade extension is a curved metal shank with the inner radius of 140 mm, thickness of 20 mm,

1- Assistant Professor of Biosystems Engineering, Department of Plant Production and Genetics Engineering, Isfahan (Khorasgan) Branch, Islamic Azad University, Isfahan, Iran
2- Associate Professor of Biosystems Engineering, Department of Mechanical Engineering, Tiran Branch, Islamic Azad University, Tiran, Iran
(*- Corresponding Author Email: i_ahmadi_m@yahoo.com)
DOI: 10.22067/jam.v10i1.71744

width of 60 mm, and the central angle of 225° (Fig. 1a).

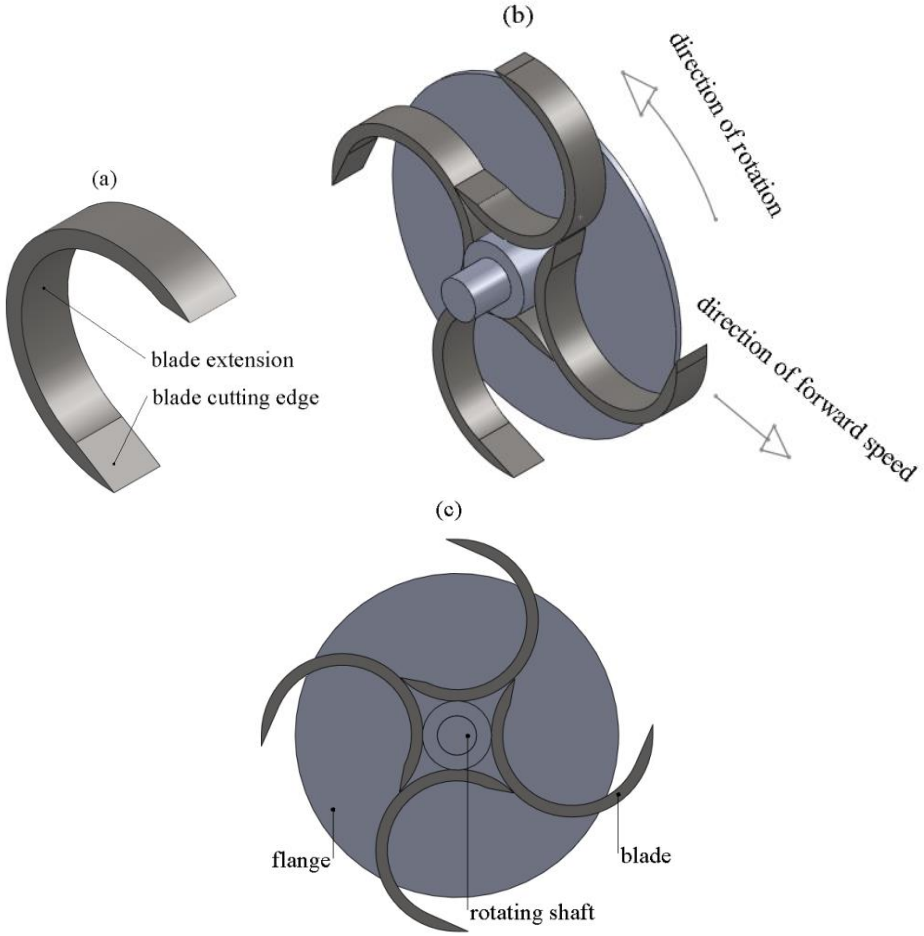

Fig. 1. a) Components of the designed blade, b) 3D, and c) 2D views of the working unit of the tiller

Figs. 1b and 1c depict the method of assembly of the blades on a flange. The end of each blade extension is located tangentially on the back of the blade ahead. During operation, it is expected that the cut soil flows through the blade extension passage as the flange rotates, then the soil is delivered to the back of the next blade extension, which finally discharges it behind the machine.

Introducing the test rig of the machine

After the fabrication of the machine prototype, it was installed on a test rig so that the translational motion of the tiller relative to the ground, as well as the effect of the operation of all blades on the draft force and torque requirements of the machine can be studied. The prototype had a simple manually operated soil bin. Maintaining a fixed speed ratio was the most important point considered for designing the test rig. Fig. 2 shows details of the test rig used herein.

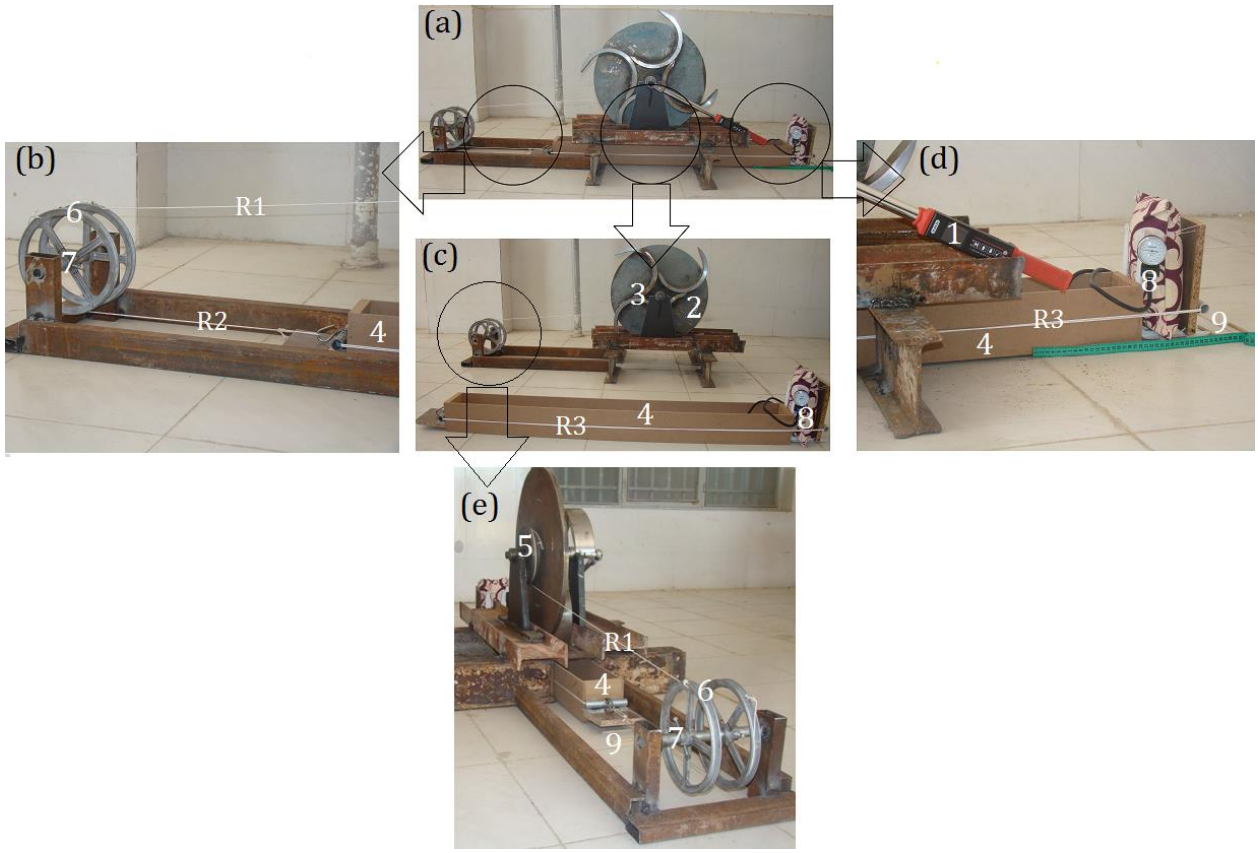

Fig.2. a) Complete assembly, b) magnified view of the front part, c) exploded view, d) magnified view of the rear part of the test rig, and e) the method of motion activation of the soil box. Where digit 1 was used for the digital torque wrench, 2 for the machine shaft and flange, 3 for each of the blades, 4 for the soil box, 5 for the shaft pulley, 6 for the twin pulleys, 7 for the shaft of the twin pulleys, 8 for the pressure sensor and gauge, and 9 for the soil box rollers. Furthermore, R1 was used for the rope that connects the shaft pulley to one of the twin pulleys, R2 for the rope that connects the other twin pulley to the rope R3 and R3 for the rope that surrounds both the pressure sensor and the soil box

The only power source of the test rig is the input torque, which is provided by a manually operated digital torque wrench 1. The resulting rotational motion is transferred through the shaft and flange 2 to the blades 3 of the machine, which were designed to cut the soil of the soil box 4. Pulley 5, which was fixed on the shaft, conveys power to one of the twin pulleys 6 through the rope R1. Because the twin pulleys were fixed to the free-rolling shaft 7, rotation of the first pulley leads to the rotation of the other, which in turn pulls the soil box 4 by means of the rope R2. To measure the required force for the motion of the soil box, a pressure sensor and gauge 8 was utilized (Model: MDF® Calibra Aneroid Premium Professional Sphygmomanometer with the accuracy of ± 3 mmHg without pin stop), which were attached to the soil box using the rope R3. As shown, when the rope R2 pulls the surrounding rope R3, it makes the pressure sensor compressed against the backplane of the soil box 4; therefore, the pressure gauge 8 can measure the horizontal force developed in the soil cutting process. To reduce the friction between the soil box and the ground, free-rolling rollers 9 were used. In this assembly, the value of speed ratio, i.e. the ratio of the peripheral speed of the blade tip to the speed of the soil box, can be altered using

pulleys having different diameters. In the present arrangement of pulleys, the resulting speed ratio was 3.6. Finally, in order to extract the net torque required to cut the soil (T_c) from the total torque measured by the torque wrench 1 (T_t), the imposed torque to the wrench due to the motion of the soil box (T_m) was calculated: The required force for moving the soil box was named by F_m (N), then T_m (Nm) was calculated using the formula $T_m = F_m \times \frac{95}{1000}$, because all of the utilized pulleys had the radius of 95 mm. Finally, T_c can be calculated using the formula $T_c = T_t - T_m$.

An experiment was performed using a remolded silty clay loam soil (Table 1). The average moisture content of the soil was about 10%. Before performing the test, the soil bed was prepared to achieve the desired level of cone penetration resistance i.e. maximum value of about 800 kPa with a cone penetrometer (Model CP20, Agridy Rimikpty. Ltd. Toowoomba, Australia) to a depth of 100 mm. Firstly, the soil was pulverized and water was sprayed on it to achieve the required moisture content. Then, the soil box was filled with the soil in three layers and each layer is leveled and compacted manually to the desired penetration resistance. To ensure uniformity of the soil, preparation of the soil bed was repeated if the penetration resistance values varied significantly from each other.

Table 1- General properties of the soil used for the verification procedure

Texture	Sand (%)	Silt (%)	Clay (%)	pH	EC	C (kPa)	φ(°)	δ(°)	ρ (kg m^{-3})	OMC (%)	Gs
Silty clay loam	18	42	40	6.5	1	10	25	12	1850	1.5	2.74

Estimation of the machine torque

It is hypothesized that, as followed below, four processes are involved to create the machine torque.

Torque requirement due to soil cutting process

To calculate the above-mentioned torque, the kinematics of the blade must be realized. To achieve this goal, the position coordinates of the cutting edge of the working blade were obtained using eq. (1):

$$\begin{cases} x_{wb} = vt + R_b \sin \omega t \\ y_{wb} = -R_b \cos \omega t \end{cases} \quad (1)$$

Note: Definitions of the parameters used in the equations have been given in the Appendix 1.

The geometric path of the working blade (by setting υ = 1 m s^{-1}, ω= 10 rad s^{-1} and R_b= 0.33 m) has been shown in Fig.3a.

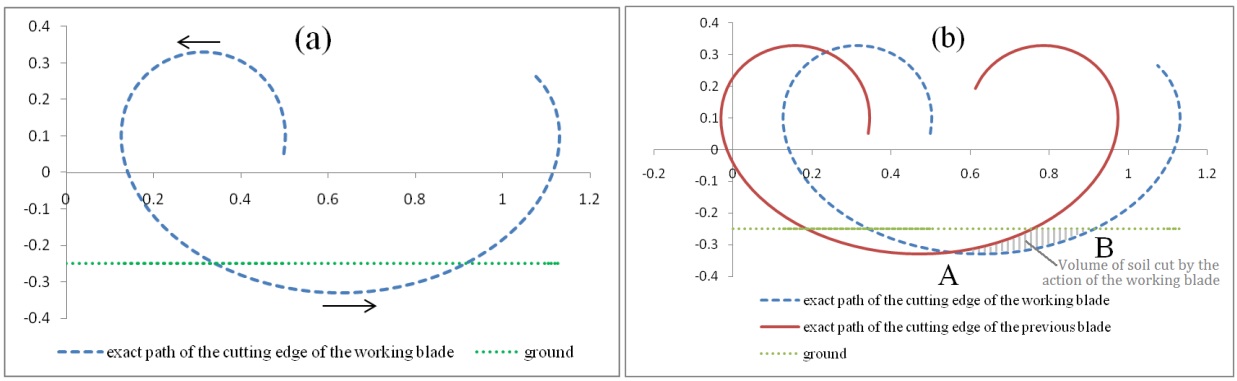

Fig.3. a) The path of the cutting edge of the working blade b) the relative positions of the working and previous blade paths

Since the geometric path of the cutting edge of the previous blade is known (eq.(2)), the volume of soil that is being cut by the working blade will be available.

$$\begin{cases} x_{pb} = vt + R_b \sin(\omega t + \frac{\pi}{2}) \\ y_{pb} = -R_b \cos(\omega t + \frac{\pi}{2}) \end{cases} \quad (2)$$

Simultaneous representation of the cutting edge paths of the working and the previous blades have been depicted in Fig.3b wherein it has been shown that the working blade cuts a narrow layer of soil in its operating cycle. Therefore, the weight (and ultimately the normal force) exerted on the soil failure plane is negligible. In other words, the required shearing force to cut the soil can be calculated using the formula $R_i = cA_i$. To calculate the torque requirement due to R_i using the MS Excel software, the curve AB (having a central angle of about 45°) has been divided into 5 segments (each having a central angle of 9°), and the length of each segment is denoted by $S_i = \sqrt{(x_{wb\,i} - x_{wb\,i-1})^2 + (y_{wb\,i} - y_{wb\,i-1})^2}$, then the area of that segment of the failure plane as well as its corresponding soil shearing resistance can be calculated as $A_i = S_i \times d$ and $R_i = c \times A_i$. Multiplying R_i by $R_b \times \cos(\left|\tan^{-1}\left(\frac{R_b\,\omega \sin \omega t}{v + R_b\,\omega \cos \omega t}\right) - \omega t\right|)$ gives the required instantaneous torque $T_{c\,i}$, and the torque requirement of a blade in one revolution of the rotor due to the soil cutting process (T_C) will be obtained using the following formula: $\frac{\sum T_{c\,i} \times \frac{9\pi}{180}}{2\pi} = \frac{\sum T_{c\,i}}{40}$.

Torque requirement due to soil lifting and soil-metal friction processes

The shape of the blade extension is an arc of a circle. To calculate the torque requirement due to the soil lifting process, it was supposed that the circular arc of the blade extension is divided into 25 segments, each having a central angle of 9°. Moreover, the added soil to the blade extension is accumulated in the lowest segment as the flange rotates. As shown in Fig.4, the working radius of the tiller equals to the distance between the cutting edge of the blade and the center of the rotating shaft $(R_b = r + 2R)$. From the viewpoint of soil motion along the blade extension, the circular arc of the blade extension can be divided into three regions (Fig. 4). The names of the regions are: soil accumulation region (five circular segments, each having a central angle of 9°), soil lifting region (fifteen circular segments, each having a central angle of 9°), and soil discharge region (five circular segments, each having a central angle of 9°).

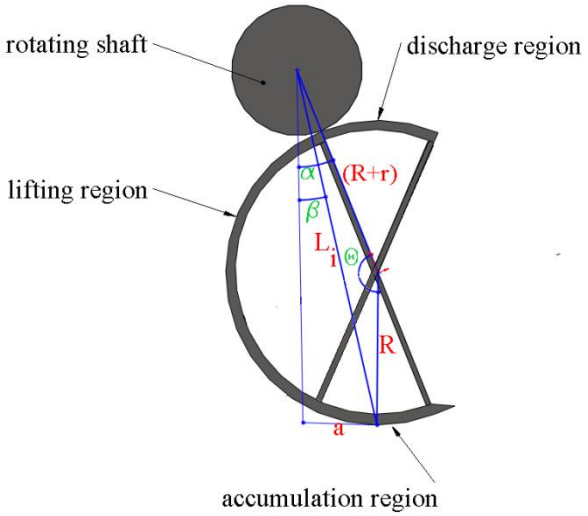

Fig.4. Three regions utilized for the calculation of torque requirement due to soil lifting process

If the position vector of the end of each circular segment (each of 25 circular arcs) is known $(\overrightarrow{L_\iota})$, the instantaneous torque will be available using eq. (3):

$$\overrightarrow{T_{w\iota}} = \overrightarrow{L_\iota} \times \overrightarrow{W_\iota} = \overrightarrow{L_\iota} \times W_i \vec{j} = \overrightarrow{L_\iota} \times (-n\,W_u)\,\vec{j} \quad (3)$$

Where $W_u = \rho_{soil}\ g\ \frac{lb}{2}\ d\ R_b \frac{9\pi}{180}$. Parameter n is an integer with the values of 1, 3, 5, 7, and 9 for the accumulation region segments, 10,9, 7, 5, 3, and 1 for the first six segments of the lifting region and 0 for the rest segments of it and the discharge region segments. Using the parameters shown in Fig.4, the calculating formula of $\overrightarrow{L_\iota}$is as follows(eq. (4)):

$$\begin{cases} |L_i| = \sqrt{R^2 + (R+r)^2 - 2\,R\,(R+r)\cos\theta} \\ a = (R+r)\sin\alpha \\ \beta = \sin^{-1}(\frac{a}{L_i}) \\ \theta = 171°\ to - 45°\ (step\ -9°) \\ \alpha = 9°\ to\ 225°\ (\ step + 9°) \\ \overrightarrow{L_\iota} = |L_i|(\sin\beta\,\vec{\imath} + \cos\beta\,\vec{\jmath}) = L_x\vec{\imath} + L_y\vec{\jmath} \end{cases} \quad (4)$$

The same procedure can be used to calculate the torque requirement due to the soil-metal friction process. The only substitution in eq. (3) is the replacement of $\overrightarrow{W_\iota}$ with $\overrightarrow{F_\iota}$, i.e.,

$$\overrightarrow{T_{F\iota}} = \overrightarrow{L_\iota} \times \overrightarrow{F_\iota} = \overrightarrow{L_\iota} \times F_i\vec{\imath} = \overrightarrow{L_\iota} \times (-\mu\, n\, W_u)\ \vec{\imath} \quad (5)$$

Combining eqs. (3) and (5) gives:

$$\begin{aligned} \overrightarrow{T_{WF\iota}} = \overrightarrow{T_{W\iota}} + \overrightarrow{T_{F\iota}} &= \overrightarrow{L_\iota} \times \left(\overrightarrow{W_\iota} + \overrightarrow{F_\iota}\right) \\ &= \left(L_x\vec{\imath} + L_y\vec{\jmath}\right) \\ &\times \left(W_y\vec{\jmath} + F_x\vec{\imath}\right) \\ &= (L_xW_y - L_yF_x)\vec{k} \end{aligned} \quad (6)$$

Finally, the torque requirement due to combined soil lifting and soil-metal friction processes in one revolution of each blade can be obtained using eq. (7):

$$\overrightarrow{T_{WF}} = \frac{\sum(\overrightarrow{T_{WF\iota}}\frac{9\pi}{180})}{2\pi} = \frac{\sum\overrightarrow{T_{WF\iota}}}{40} \quad (7)$$

Required dynamic torque

To calculate dynamic torque, the angular impulse and momentum method can be utilized. Eq. (8) demonstrates the formula. This formula is written for one of the above-mentioned 25 segments. Furthermore, suppose that the position vector $(\overrightarrow{L_\iota})$ and the soil mass (m_i) are constant values during the soil movement in each of 9° segments.

$$\begin{aligned} \overrightarrow{L_\iota} \times m_i\overrightarrow{V_{\iota-1}} + \overrightarrow{T_{D\iota}}\,dt &= \overrightarrow{L_\iota} \times m_i\overrightarrow{V_\iota} \xrightarrow{yields} \overrightarrow{T_{D\iota}}\,dt \\ &= \overrightarrow{L_\iota} \times m_i(\overrightarrow{V_\iota} - \overrightarrow{V_{\iota-1}}) \\ &\xrightarrow{yields} \overrightarrow{T_{D\iota}} \\ &= \frac{m_i\overrightarrow{L_\iota} \times (\overrightarrow{V_\iota} - \overrightarrow{V_{\iota-1}})}{dt} \end{aligned} \quad (8)$$

In eq. (8), $\overrightarrow{V_\iota}$ is the absolute value of soil velocity at the end of each circular segment, and dt is equal to $\frac{\frac{9\,\pi}{180}}{\omega}$. To calculate $\overrightarrow{V_\iota}$, the absolute position vector of soil at the end of each segment must be available (eq. (9)):

$$\begin{cases} \overrightarrow{X_\iota} = (vt + |L_i|\sin\omega t)\vec{\imath} \\ \overrightarrow{Y_\iota} = -|L_i|\cos\omega t\,\vec{\jmath} \end{cases} \quad (9)$$

The first derivative of eq. (9) leads to the absolute velocity of soil at the end of each circular segment, i.e.:

$$\begin{cases} \overrightarrow{V_{x\iota}} = (v + |L_i|\omega\cos\omega t)\vec{\imath} \\ \overrightarrow{V_{y\iota}} = |L_i|\omega\sin\omega t\,\vec{\jmath} \end{cases} \quad (10)$$

Applying the specifications of the vector product, the value of $\overrightarrow{T_{D\iota}}$ can be calculated using eq. (11):

$$\overrightarrow{T_{D\iota}} = \frac{m_i(L_x\vec{\imath}+L_y\vec{\jmath})\times[\,(V_{x\,i}-V_{x\,i-1})\vec{\imath}+(V_{y\,i}-V_{y\,i-1})\vec{\jmath}]}{dt} = \frac{m_i\,(L_x(V_{y\,i}-V_{y\,i-1})-L_y(V_{x\,i}-V_{x\,i-1}))}{dt}\vec{k} \quad (11)$$

Finally, the required dynamic torque in one revolution of a blade can be calculated as follows:

$$\overrightarrow{T_D} = \frac{\sum\overrightarrow{T_{D\iota}}}{40} \quad (12)$$

Now, since all of the torque requirements in one revolution of a blade are known (i.e., $\overrightarrow{T_C}, \overrightarrow{T_{WF}}, and\ \overrightarrow{T_D}$), the total torque of a blade $(\vec{T})$ can be calculated by summing them. Furthermore, the total torque of a flange $(\overrightarrow{T_F})$ and the total torque of the tiller $(\overrightarrow{T_T})$ can be obtained as follows:

$$\begin{cases} \overrightarrow{T_F} = N_b\vec{T} \\ \overrightarrow{T_T} = N_f\overrightarrow{T_F} \end{cases} \quad (13)$$

To facilitate performing calculations, the formulas developed herein were entered in a worksheet of the MS Excel software, where you can alter the values of five independent

parameters and observe the updated results and charts by pressing the Enter key (refer to the supplementary file).

Estimation of the machine draft theoretically

In order to estimate the draft force of the machine theoretically, horizontal components of soil cutting force and soil-metal friction force were calculated and summed. It should be noted that since the soil weight is directed down and the values of inertial force and moment of the cut soil are negligible in comparison with the corresponding items of the machine, the effect of soil weight and speed on the machine draft were neglected. The procedure for calculating the two components of the draft is summarized here:

• Dividing the time span from the instant when the rotating blade meets the soil to the instant when it reaches to the ground surface into five equally sized segments, and calculating the corresponding length of soil that is cut during each of them (S_i).

• Calculating the horizontal component of soil cutting force i.e. $F_{cxi} = c \times S_i \times d \times \cos(\left|\tan^{-1}\left(\frac{R_b\,\omega \sin \omega t}{v+R_b\,\omega \cos \omega t}\right) - \omega t\right|)$, and the horizontal component of soil-metal friction force i.e. $F_{fxi} = \mu\, n\, W_u$ for each time segment.

• Summing F_{cxi}s and F_{fxi}s to calculate SF_{cx} and SF_{fx}.

• Multiplying SF_{cx} and SF_{fx} by $\frac{\frac{9\pi}{180}}{2\pi} = \frac{1}{40}$ to achieve average values of soil cutting force and soil-metal friction force.

Results and Discussion

Comparison of torque and draft curves of a single blade

Fig.5a shows the distribution of the theoretically obtained soil cutting-induced and the soil motion-induced torque curves of a blade over one revolution of the tiller shaft. The soil motion-induced torque consists of soil lifting, friction, and dynamic torques, and the sum of soil cutting and soil motion-induced torques composes the machine torque. The theoretical curves were obtained by entering the following values as the model input parameters: $c = 10\ kPa, v = 0.01\ m\ s^{-1}, \omega = 0.1\ rad\ s^{-1}, R = 0.14\ m, r = 0.05\ m, d = 0.04\ m, \mu = 0.2, and\ \rho = 1850\ kg\ m^{-3}$. The theoretical soil-cutting-induced torque was about 9 Nm on part AB of the curve, which is exactly over the soil-cutting period. Then, it falls to zero and remains zero on part CD, where the working blade is not in contact with the soil. Finally, when the blade encounters the soil at the beginning of the next rotation of the blade, the curve jumps up to reach point E. On the other hand, the variation of the soil motion-induced torque starts from zero at F, where the working blade just touches the soil. Since there is no mass on the blade extension at F, all components of the soil motion-induced torque are zero at this point. The curve goes up from F to reach the largest value of about 6 Nm at G ($\alpha \cong 55^{\circ}$), and then it falls down and intersects the horizontal axis at H ($\alpha \cong 100^{\circ}$). The soil motion-induced torque remains zero between points H and I ($\alpha \cong 100^{\circ} - 360^{\circ}$) because the blade extension does not carry any soil in this range.

Figs. 5b and 5c depict the distribution of theoretical as well as experimental curves of the machine torque and the draft force of a blade over one revolution of the tiller shaft, respectively. The proximity of theoretical curves to the experimental ones can be considered as the verification of the developed formulas. As shown, both of the torque curves have zero values after rotation of the tiller shaft through the angle of 90°. This observation can be explained from this point that after rotation of the shaft through this rotation angle, almost all of the cut soil dropped from the blade surface; therefore, because the mass of soil supported by the blade was negligible, its corresponding soil motion-induced torque had zero values, too. In order to explain why the draft curves have zero values after the tiller shaft rotated about 50°, it is necessary to consider that the draft force is created from the interaction between the blade and the uncut soil. Because the blade is in contact with the uncut soil only in the first 50° of the shaft rotation, it is expected to have zero values for the draft force after this rotation angle.

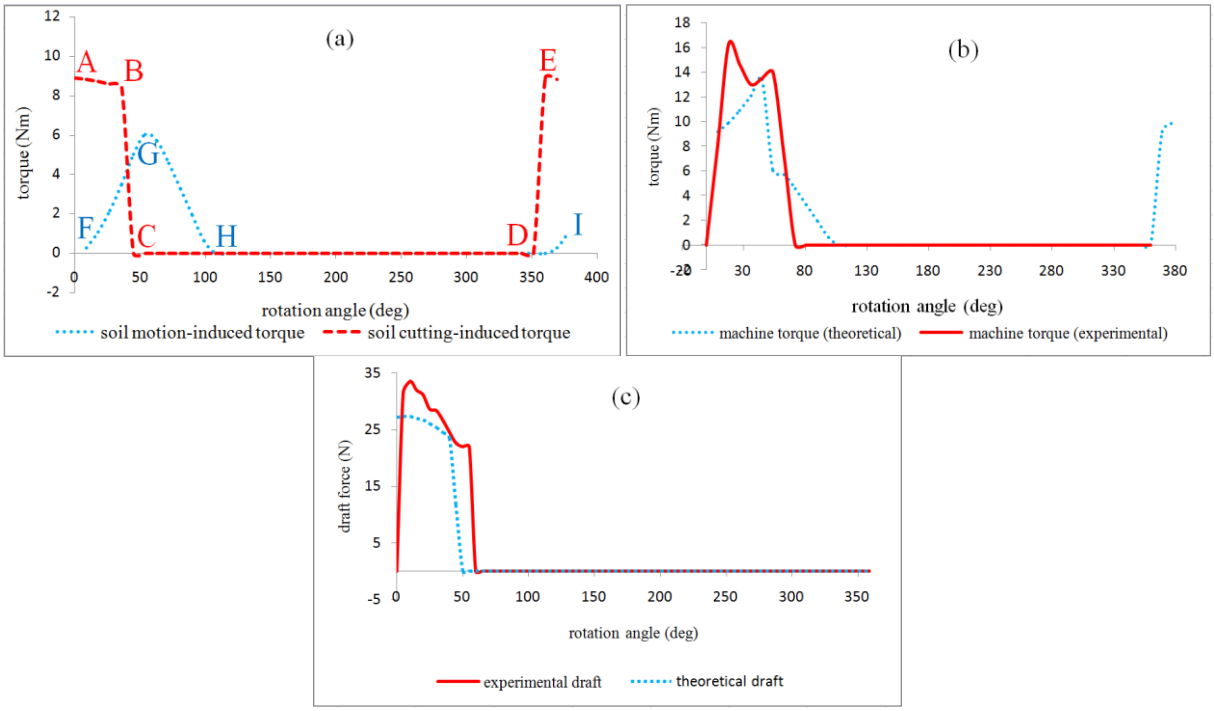

Fig.5. Comparison of a) theoretically estimated soil cutting and soil motion-induced torque curves b) theoretical and experimental curves of the machine torque, and c) theoretical and experimental draft curves of a blade

Furthermore, the average theoretical machine torque of a blade is around 2.95 Nm and the average experimental machine torque is about 3.2 Nm. Moreover the average theoretical draft force of a blade is around 3.25 N and the average experimental draft force is about 4.2 N. The difference between the average theoretical and experimental torques as well as draft forces may be due to dissimilarity in the working conditions of the modeled and real machines, the difference in the properties of the study soil, and the effect of unconsidered or neglected processes for the development of the theoretical formulas.

Effect of all blades on the torque requirements of the machine

Fig.6 shows the variation of the total, draft-induced and machine torques as a function of the angular position of the tiller shaft.

An important result obtained from Figure 6 regarding the design of the tiller is that in order to have a durable machine, the number of the tiller blades should be doubled because there are angular spans in the charts where the torque requirement is zero. These angular spans, which are exactly matched with the time spans when no blade is in contact with the soil, make the curves to have a periodic up and down variation. This means that the torque requirement of the machine have a periodic nature, which leads to the vibration of the machine and ultimately makes the tiller to fail sooner. However, if the number of the tiller blades is doubled, the valleys of curves will be filled, which means that the machine will work with fewer vibrations. In order to double the number of blades without affecting the configuration of them, the new blade gang, having the same arrangement as the first, should be installed on the other side of the tiller flange. Moreover, each blade of the new gang should be welded to the flange exactly halfway of each circular arc between the two adjacent blades of the first gang.

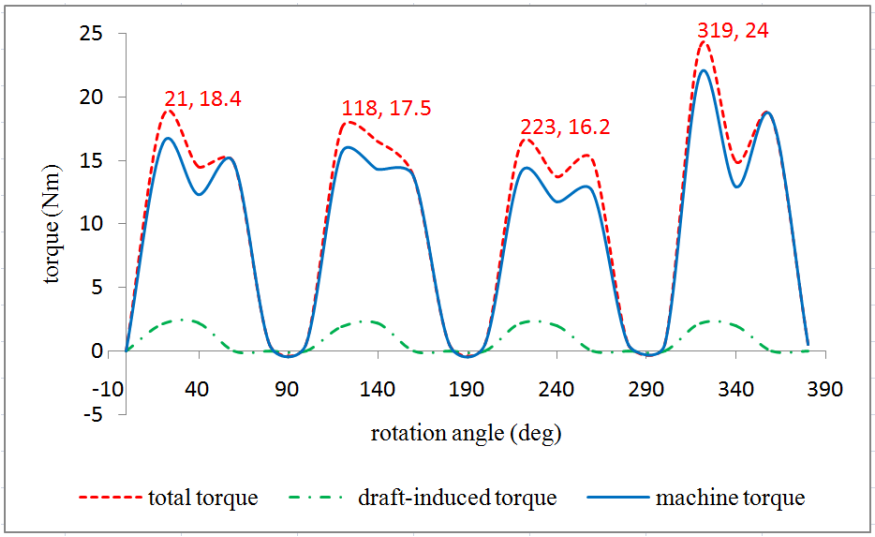

Fig. 6. Experimentally measured torque curves of the machine over one revolution of the tiller shaft

Conclusions

In this study, the soil engaging components of a new up-cut rotary tiller were designed and fabricated and the torque and draft force requirements of the machine were formulated using the laws of classical mechanics. The comparison of the calculated theoretical torque and draft force with the experimental ones had promising results that can be considered as the verification of the formulas developed herein (From a quantitative viewpoint, the average experimental draft and torque of the machine tilling a silty clay loam soil were 16.8 N and 12.8 Nm, respectively). Furthermore, the average theoretical draft and torque of the machine were 13 N and 11.8 Nm respectively. The outputs obtained from the formulas (driving torque of the machine and required draft force of it) can be used to design the transmission system of the machine.

Acknowledgment

The authors are grateful to the anonymous reviewers who devoted their valuable time to inspect this manuscript.

References

1. Ahmadi, I. 2017. A torque calculator for rotary tiller using the laws of classical mechanics. Soil & Tillage Research 165: 137-143.
2. Asl, J.H., and S. Singh. 2009. Optimization and evaluation of rotary tiller blades: computer solution of mathematical relations. Soil & Tillage Research106: 1-7.
3. Bernacki, H., J. Haman, and Cz. Kanafojski. 1972. Agricultural machines, theory and construction. Scientific publications foreign co-operation center of the CISTEI. Warsaw.
4. Chertkiattipol, S., and T. Niyamapa. 2010. Variations of torque and specific tilling energy for different rotary blades. International Agricultural Engineering Journal 19 (3): 1-14.
5. Gholami, H., D. Kalantari, and M. Rajabi Vandechali. 2017. Testing and evaluation of a rototiller with new ridged blades. Journal of Agricultural Machinery 7 (1): 26-36. (In Farsi).
6. Matin, M.A., J. M. Fielke, and J. M. A. Desbiolles. 2015. Torque and energy characteristics for strip-tillage cultivation when cutting furrows using three designs of rotary blade. Biosystems Engineering 129: 329-340.
7. Shibusawa, S. 1993. Reverse rotational rotary tiller for reduced power requirement in deep tillage. Journal of Terramechanics 30 (3): 205-217.

Appendix 1-Definition of the parameters used in the theoretical formulas

Item	Definition (unit)
L_i	Distance between the end point of the i-th segment of the blade extension and the center of rotor (m)
N_b, N_f	Number of blades per flange and number of flanges (-)
R_i	Shearing resistance of soil located close to the i-th segment of the blade path through the soil (N)
$S_i \ and \ A_i$	Length (m) and area (m^2) of the i-th segment of the blade path
T_{ci}	Torque supplied for cutting the soil located close to the i-th segment of the blade path through the soil (Nm)
T_{wi}, $T_{Fi}, T_{WFi}, and \ T_{Di}$	Torques supplied respectively to the soil lifting, overcoming the soil-metal friction, combined soil lifting and overcoming the soil-metal friction, and dynamic motion of the soil located close to the i-th segment of the blade extension (Nm)
V_i	Absolute velocity of the soil located close to the i-th segment of the blade extension (m s^{-1})
$W_i \ and \ F_i$	The weight of, and the friction force exerted on the soil located close to the i-th segment of the blade extension (N)
W_u	The weight of soil that enters to the first segment of the blade extension (N)
X_i, Y_i	The X and the Y components of the absolute position of the soil located close to the i-th segment of the blade extension (m)
$\vec{\imath}, \vec{\jmath}$	Unit vectors along the x and the y axes, respectively
m_i	The mass of the soil located close to the i-th segment of the blade extension (kg)
x_{wb}, y_{wb}	The x and the y position coordinates of the cutting edge of the working blade (mm)
x_{pb}, y_{pb}	The x and the y position coordinates of the cutting edge of the previous blade (mm)
c	Soil cohesion (kPa)
d	Blade width (m)
lb	Bite length of the blade (m)
$r, R, and \ R_b$	The rotating shaft radius, the blade extension radius, and the distance between the cutting edge of the blade and the rotating shaft center, respectively (m)
t	Time (s)
v	Forward speed of the machine (m s^{-1})
μ	Coefficient of soil-metal friction (-)
ω	Angular velocity of the rotor (rad s^{-1})

نشریه ماشین‌های کشاورزی
جلد ۱۰، شماره ۱، نیمسال اول ۱۳۹۹، ص ۲۱-۱۱

Journal of Agricultural Machinery
Vol. 10, No. 1, Spring- Summer 2020, p. 11-21

تخمینگر گشتاور و مقاومت کششی روتیواتور چرخش معکوس جدید

ایمان احمدی[1*]، محسن بیگی[2]

تاریخ دریافت: ۱۳۹۶/۱۲/۲۷
تاریخ پذیرش: ۱۳۹۷/۰۴/۰۵

چکیده

هدف از پژوهش حاضر طراحی، ساخت و ارزیابی یک نمونه جدید از روتیواتور چرخش معکوس، همچنین توسعه فرمول‌های صحیح برای تخمین نیازهای گشتاوری و نیرویی آن با استفاده از قوانین مکانیک کلاسیک است. به‌منظور تایید مدل، نمونه اولیه دستگاه مورد آزمون قرار گرفت. فرض شد که چهار فرآیند در ایجاد گشتاور مورد نیاز ماشین دخالت دارند که عبارتند از: برش خاک، بالا برده شدن خاک، اصطکاک بین خاک و فلز و سرعت خاک. از سوی دیگر فرض گردید که مؤلفه افقی نیروی برش و اصطکاک بین خاک و فلز در ایجاد مقاومت کششی مورد نیاز ماشین نقش دارند. بر مبنای این فرض‌ها، فرمول‌های ریاضی برای تخمین نیازهای گشتاوری و مقاومت کششی ماشین توسعه داده شد. برای تسهیل در انجام محاسبات، فرمول‌ها وارد نرم‌افزار اکسل شد. بر مبنای نتایج این پژوهش مقاومت کششی و گشتاور متوسط اندازه‌گیری شده برای خاک‌ورزی خاک دارای بافت لوم رسی سیلت‌دار به‌ترتیب برابر با ۱۶/۸ نیوتن و ۱۲/۸ نیوتن‌متر به‌دست آمد. به‌علاوه مقاومت کششی و گشتاور متوسط تخمین زده شده به‌ترتیب برابر با ۱۳ نیوتن و ۱۱/۸ نیوتن‌متر به‌دست آمد. شباهت مقادیر تخمین زده شده به مقادیر اندازه‌گیری شده بیانگر صحت فرمول‌های توسعه‌یافته در این پژوهش می‌باشد.

واژه‌های کلیدی: اندازه‌گیری گشتاور و مقاومت کششی، گاوآهن دوار چرخش معکوس، مدل‌سازی تئوری

۱- استادیار مکانیک بیوسیستم، گروه مهندسی تولید و ژنتیک گیاهی، دانشگاه آزاد اسلامی، واحد اصفهان (خوراسگان)، اصفهان، ایران
۲- دانشیار مکانیک بیوسیستم، گروه مهندسی مکانیک، دانشگاه آزاد اسلامی، واحد تیران، تیران، ایران
(*- نویسنده مسئول: Email: i_ahmadi_m@yahoo.com)

DOI: 10.22067/jam.v10i1.71744

Journal of Agricultural Machinery
Vol. 10, No. 1, Spring- Summer 2020, p. 23-35

نشریه ماشین‌های کشاورزی
جلد ۱۰، شماره ۱، نیمسال اول ۱۳۹۹، ص ۳۵-۲۳

Feasibility of Drone Imagery for Monitoring Performance of a Modified Drill in a Conservation Farming System

Z. Kavoosi[1*], M. H. Raoufat[2]

Received: 07-03-2018
Accepted: 25-08-2018

Abstract

In this paper, performance of a no-till corn planter in a soil covered with previous wheat residue was evaluated. Three levels of crop residue cover (CRC): 30, 45 and 60%, two planting schemes; on-bed and in-furrow and two forward speed: (4 and 8 km h^{-1}) were considered as treatments. The field was evaluated by ground and air observations. The purpose of this study was to investigate the capability of aerial images captured by an unmanned aerial vehicle (UAV) in identifying the distances between corn seedlings and as a result, assessing the quality of planter performance. Collected data from ground and aerial imagery were used to calculate seed establishment indices including multiple index, miss index, quality of feed index, precision index and also emergence rate index (ERI), for each plot. Images captured from10 m altitude (4.5 mm $pixel^{-1}$) could give satisfactory results in relation to our objectives. Our results show that acceptable correlations existed between terrestrial and aerial seedlings spacing data sets ($0.94<R<0.98$) suggesting the aerial imagery is a good choice for evaluating the seed establishment and estimating ERI. Aerial imagery data source underestimated quality of feed and precision indices, overestimated miss index and could not provide processed data range needed for computing multiple index due to low image resolution, weeds presence within crop rows and overlapping of leaves.

Keywords: Aerial imagery, Crop residue cover (CRC), Seed establishment indices, Unmanned aerial vehicle (UAV)

Introduction

Farming practices have undergone huge changes to cope with increasing demands for more food and safeguarding environment (Zheng *et al.*, 2012). A considerable number of studies have been conducted to explore advantages and best management practices including soil preparation, previous residue management and planting into partially covered soils. Conservation farming techniques are often associated with previous surface crop residue management. Keeping certain amount of previous residue helps retaining some soil moisture and reducing soil erosion through increased water infiltration into soil, in addition this practice provides more carbon source needed for maintaining a proper C/N ratio (Naresh *et al.*, 2016). On the other hand farming practices such as conservation tillage helps to reduce energy needed for crop production thus cheaper farming can be realized. Some farmers avoid to adopt conservation farming due to possibility of poor stand establishment which might ultimately reduce crop yield. Available conventional planters fail to place seeds into soils which are less tilled. The adverse effects of planting into residue covered soils have been emphasized by Swan *et al.* (1994) and Fallahi and Raoufat (2008). Inadequate seeding depth, low uniformity in seed spacing, variation in seed placement depth and decrease in crop yield are a few adverse effects reported by above researchers.

Planter attachments such as coulters are valuable tools for cutting the residue and help achieving proper seeding depth, on the other hand, row-cleaners clear the seeding row from residue and clods helping a good drill and seed placement. These attachments are necessary tools for a successful planting into a partially residue covered soils where conventional planters fail to penetrate into the top soil.

1 and 2- Graduate PhD student and Professor, respectively. Dept. of Biosystems Engineering, Shiraz University, Shiraz, Iran
(*- Corresponding Author Email: Zahra84_kavoosi@yahoo.com)
DOI: 10.22067/jam.v10i1.71498

Raoufat and Matbooei (2007) concluded that using row cleaner in farms with 50% crop residue cover at a forward speed of 7 km h^{-1} resulted in the best plant establishment, uniformity in seed spacing and desirable values of emergence rate, miss, quality of feed and precision indices. Dadi and Raoufat (2012) found that using a winged chisel furrow opener preceded by a row cleaner equipped with treader wheels arrangement removes appreciable amounts of residue on the planting row in a conservation farming system. They observed better cleaning of crop residue at higher forward speeds, but this caused an increase in miss index that was not desirable.

As the conservation farming is extending throughout the world certain tillage and planting systems have been developed including no-till planters. These planters, place seeds into covered or partially covered residue soils. The performance of the planter shall be monitored by measuring seedling spacings. Currently, data acquisition from farms relies on manual field-data collection, survey responses, and agricultural censuses, but it is extremely difficult to acquire the data systematically and continuously over large areas using these methods. Alternatively, remote sensing techniques have the potential to survey different practices in farms inexpensively and efficiently in a systematic, timely and cost-effective manner (Zheng *et al.*, 2014; Rostami and Afzali Gorouh, 2017). Satellites and aircrafts have been widely employed to monitor crop growth, estimate crop yield and also for site specific management applications. In spite of few advantages, acquiring images from satellites and air crafts is expensive and not easy for farmers and researchers to access. Low quality of acquired images from satellite and air crafts, effect of weather conditions on imagery and adverse effects of satellite sensor characteristic is other limiting factors. As an alternative, unmanned aerial vehicles (UAVs) have been used for aerial imagery and has found applications in crop monitoring and management (Jannoura *et al.*, 2015; Xiang and Tain, 2011). The UAVs are able to fly at lower altitudes as compared to airplanes and satellites. They can capture ultrahigh resolution images and therefore have been recently used to capture images of objects such as small plants and patches (Xiang and Tian, 2011). The flight preparation time for UAVs is low and imagery can be scheduled even on cloudy days therefore the UAVs image acquisition system is more flexible. The costs of imagery and data acquisition for the UAVs are lower compared to satellites and other available aircrafts, commercial cameras having various degrees of image resolution and configuration have been marketed which can be mounted on UAVs as desired giving the operators and researchers more flexibility (Sankaran *et al.*, 2015). Many researchers have concluded that commercial cameras are powerful parts of data acquisition systems for UAVs especially when green vegetation is to be monitored both from air and land. In summary low cost and high resolution of the UAVs equipped with proper image capture and acquisition hardware makes this a good choice for assessing green vegetative cover such as broadly and wheat on farms (Torres-Sanchez *et al.*, 2014).

Precision agriculture is one of the areas which has adopted UAV for the last 12 years. For instance, biomass and nitrogen status of corn, alfalfa and soybean crops have been estimated by unmanned helicopters equipped with camera and image acquisition systems by Hunt, Cavigelli, Daughtry, McMurtrey, and Walthall in 2005. In similar studies unmanned radio controlled helicopters used to acquire thermal and narrow band multispectral images to estimate biophysical parameters correlated with leaf area index, water stress and chlorophyll content (Berni, Zarco-Tejada, Suarez, and Fereres, 2009). In another study remote sensing technology was used to estimate grain yield and total aerial biomass of a rice crop (Swain, Thomson, and Jayasuriya, 2010). Having aerial images, they established regression equation between measured parameters and normalized difference vegetation index (NDVI) given by images and obtained regression coefficients of 0.72 and

0.76 for grain yield and aerial biomass, respectively. In an investigation conducted by Aguera, Carvajal, and Saiz (2011) an acceptable correlation was established between applied nitrogen to sunflower and NDTI extracted from images captured by a quadcopter at a height of 70 m above the crop (Vega *et al.*, 2015).

In another research performed by Zhang *et al.*, 2018, the distances between corn seedlings (2-3 fully expanded leaves) were calculated by using the images captured by a Phantom 3 Professional flying at five altitudes: 1, 2, 3, 4 and 5m. They developed a method by training an algorithm in an indoor facility with plastic corn plants. Then, the method was scaled up and tested in a field with maize plant spacing that exhibiting natural variation. Their major problem was the presence of weeds specially weeds growing within crop rows. They could achieve reliable results at an altitude of 5m. In summary they concluded that it is possible to precisely quantify the distance between corn plants.

Varela *et al.* (2018) aimed to develop a reliable, timely, and unbiased method for counting corn plants based on ultra-high-resolution imagery acquired from unmanned aerial systems (UAS) to automatically scout fields and apply it to real field conditions. Their data processing included five steps: (1) images were converted into excess greenness (ExG)-vegetation index, (2) row detection and contours were delineated, (3) geometric descriptors were built from contours, (4) classifier training, and (5) classifier testing. Their results showed that for successful model implementation, plants should have between two to three leaves when images are collected (to avoid overlapping) and best workflow performance was reached at 2.4 mm resolution corresponding to 10 m of altitude.

Because planting space is still a critical parameter for crop growth models, it is critical to focus on how to measure plant to plant distances in a row. The UAV systems represent a powerful tool that can be used to collect high-resolution real-time images of cropping systems, and thereby support the calculation of plant interval distances. In this study, our objective was to investigate the ability of a low cost drone; DJI Phantom 3 Professional[1] equipped with a commercial RGB camera for monitoring performance of a corn planter in a conservation farming system. Two important issues in conservation farming are the specification of the tilling machine (if used) and of the planter. Adequate literature is available on specifications of the planters suitable for placing seeds in partially residue covered soils (Raoufat and Mahmoodie, 2005; Bahrani *et al.*, 2007; Dadi and Raoufat, 2012; Nejadi and Raoufat, 2013) considering recommendations by above researchers, it is decided to use a newly manufactured no-till planter made by Tarashkadeh Company[2].

Materials and Methods

I: Experimental site

Our research was conducted in one of the Experimental Stations of College of Agriculture, Shiraz University, Shiraz, Iran (29°44′2″N, 52°35′33″E upper left point and 29°43′59.6″N, 52°35′40″E lower right point). The selected farm was covered with fresh previous irrigated wheat residue averaging 8000 kg ha^{-1}.

II: Plots preparation

In subsequent operations, the previous crop residue was reduced and adjusted to the three desired levels considered for this study. First the loose straw discharged from combine was baled out from the field and only 3500 kg ha^{-1} was left (equivalent to 60% CRC) and considered as R1. The remaining fallen residues were removed out and residue was adjusted to 1700 kg ha^{-1} (equivalent to 45% CRC) forming the second level R2. For preparing the third level, (R3) the remaining crop residue was grazed and established at 620 kg ha^{-1} (equivalent to 30% CRC). This level corresponds to minimum residue level recommended for conservation farming (CTIC, 2010). To prepare a field having various scenery of seed placement, seeds were

1- Dà-Jiāng Innovations Science and Technology Co, Shenzhen, China

2- www.Tarashkadeh.com

planted at two forward speeds of 4 and 8 kmh^{-1} on plots having residue cover levels of 30, 45 and 60 %. The conventional local practice of planting on-bed and in-furrow was also considered. Therefore, a total of 12 treatments in 3 replications was considered for our study. The statistical design was split-split plot arranged as a complete block design, main plots were crop residue, sub plots were planting scheme and sub-sub plots were planter forward speed. Each plot was measured 4×30 m^2. The corn was a hybrid single cross 704 with emergence rate of 92% and purity of 98%. Corn was planted in plots by a no-till planter made by Tarashkade Company. Each unit of the four-row planter included a plain coulter and a wave coulter. The former assisted in placing fertilizer and the latter assisted in pulverizing a narrow band ready for falling seeds. The row spacing was adjusted to 60 cm and theoretical seed spacing of 15.5 cm. Sowing date was July, 31th 2016 and on the next day first irrigation was done. After irrigation, the plots were closely monitored for any seedling emergence.

III: Data collection

Measurements in each plot were the number of seeds emerged daily and the distance between consecutive seedlings. Newly emerged seedlings were counted every day in a 6 meters length in the middle of each row in each plot. Counting continues until no changes was seen in the number of newly emerged seedlings. The measurements were taken both on the ground and by the drone. For terrestrial measurements on the August 20th 2016, a measuring tape was placed on each row and distances between consecutive seedlings were measured and recorded. Drone images were captured from each plot at 14 different altitudes (4, 6, 8,…and 30m) on the 20th and the 27th August 2016. Pixel resolution of images captured at different altitudes and different time intervals after planting (20 and 27 days after planting), were examined to find the best altitude and timing for drone imagery. Only the images captured at 10 meter height (4.5 mm $pixel^{-1}$) could give satisfactory results in relation to our objectives. It should be noted that although resolution for imagery at lower altitudes was better but captured scenery was small. On the other hand, given the condition of the plot, imagery at altitudes more than 10 m height could not give satisfactory pixel information for detecting single corn seedlings. As images captured at earlier stages of corn growth had less leaves overlapping problem so the first drone imagery taken on the 20th August was selected for further analysis.

IV: Data processing

Due to presence of heavy residues, weeds, shadow and leaves overlapping it was impossible to analyze images using written code programs like Matlab[1], therefore the analysis was continued semi manually with the help of ImageJ[2] and Excel[3] programs. Fig.1 shows a part of aerial image of a plot with the least residue level (30% CRC), planted on-bed at 8 km h^{-1}, having the least problem of weed and leaves overlapping taken on the 20th August 2016.

For measuring distances between corn seedlings a rectangular marker of 1×0.22 m^2 in yellow color (for calibration purpose) was placed in each plot so that the hovering drone camera could capture images of each specific plot and the marker laid on it. For each plot, the captured image from a 10m height was retrieved in ImageJ program and as demonstrated in Fig.2 the marker length was calculated by using the tools “straight” and “measure” commands. Then the distance between adjacent seedlings was measured in the same way. Camera distortion was not a problem as measurements were performed for each plot separately and the equivalent seedling spacing was calculated by using the length of the yellow marker in the plot image. In the next step measured distances from ImageJ were moved to spreadsheet (Excel 2013) and converted to real distances in centimeters by equation (1).

1- Matrix Laboratory

2- National Institutes of Health, USA, http://imagej.nih.gov/ij

3- Microsoft Corporation

$$Seedling\ spacing\ (cm) = \frac{seedling\ spacing\ (pixel)}{length\ of\ marker\ (pixel)} * 100(cm) \quad (1)$$

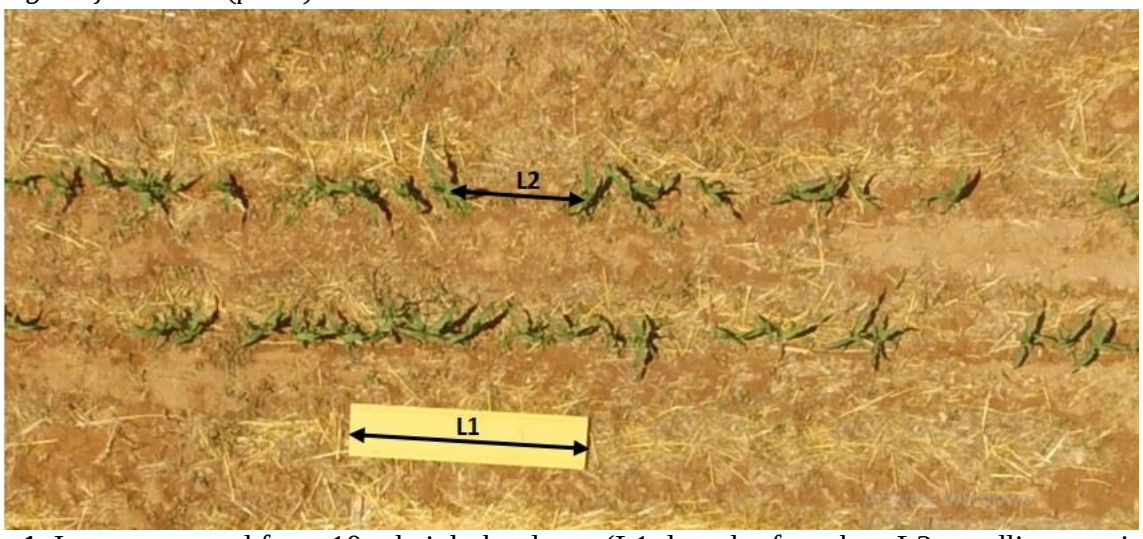

Fig.1. Image captured from 10m height by drone (L1: length of marker, L2: seedling spacing)

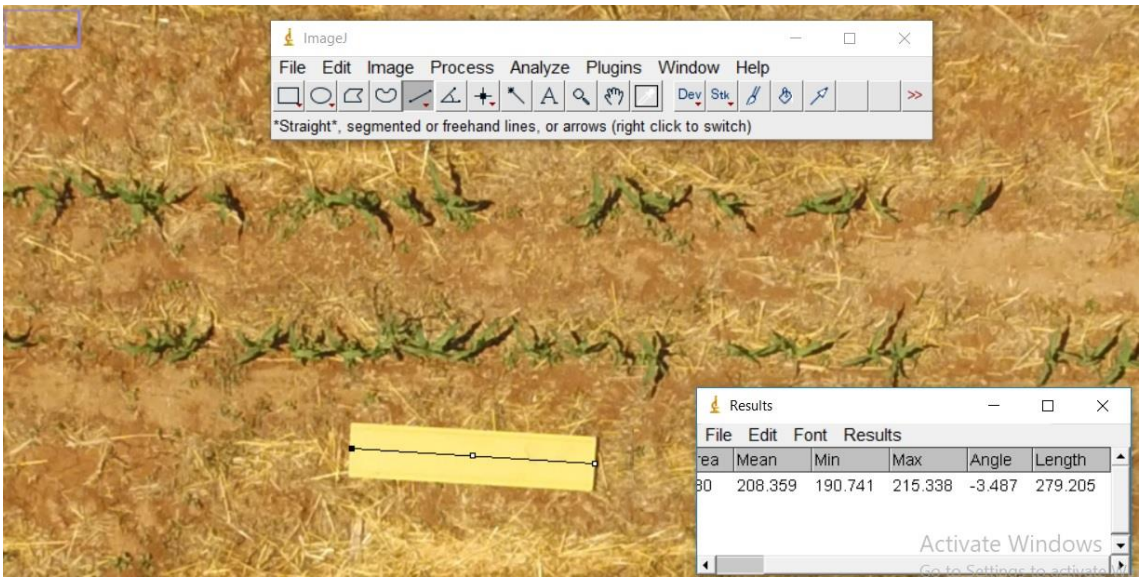

Fig.2. Measuring seedling spacing in ImageJ

For terrestrial measurements a measuring tape was placed in each row and consecutive distances between seedlings were measured and recorded. At this stage two sets of data were at hand, one gathered manually and one concluded from drone imagery. In the next step, the existence of a linear correlation between these two sets of data was investigated. In addition, multiple index, miss index, quality of feed index and precision index were calculated. In the following section these indices are briefly introduced.

Multiple index: The theoretical spacing is the distance between seedlings assuming that there were no skips, multiples, or variability and is based on the manufacturer's specifications. It will theoretically be equal to the mode of distribution of spacing. The multiple index D is the percentage of spacing that are less than or equal to half of the theoretical spacing. That is:

$D = \frac{n_1}{N} \times 100$

Where, n_1 is the number of spacing that are more than zero but no more than half times the theoretical spacing; and N is the total number of distances measured. Smaller values of D indicate better performance (Kachman and Smith, 1995).

Quality of feed index: The quality of feed index A is the percentage of spacing that are more than half but no more than 1.5 times the theoretical spacing. That is:

$A = \frac{n_2}{N} \times 100$

Where, n_2 is the number of spacing that are more than half but no more than 1.5 times the theoretical spacing; and N is the total number of distances measured. Larger values of A indicate better performance than smaller values. In other words, the quality of feed index is a measure of how often the spacing are close to the theoretical spacing (Kachman and Smith, 1995).

Miss index: The miss index M is the percentage of spacing greater than 1.5 times the theoretical spacing. That is:

$M = \frac{n_3}{N} \times 100$

Where, n_3 is the number of spacing that are more than 1.5 times the theoretical spacing; and N is the total number of distances measured. Smaller values of M indicate better performance than larger values (Kachman and Smith, 1995).

Precision: Precision, C is a measure of the variability in spacing between plants after accounting for variability due to both multiples and skips. A practical upper limit is 29%. Smaller values of C indicate better performance than larger values. The precision is the coefficient of variation of spacing that are classified as singles. That is:

$C = \frac{S_2}{X_{ref}} \times 100$

Where, S_2 is the sample standard deviation of spacing that are more than half but no more than 1.5 times the theoretical spacing. And x_{ref} is the theoretical spacing of plants (Kachman and Smith, 1995).

Emergence Rate Index (ERI): For each treatment an ERI was determined by counting the number of plants emerged from a mid-6 m length of rows for several days after planting (DAP) using the following equation introduced by Erbach (1982):

$ERI = \sum_{n=1}^{x} \frac{EMG_n - EMG_{n-1}}{DAP_n}$

Where, n is the nth emergence observation, EMG_n is the percentage of seeds planted emerged on the day of the nth emergence observation, EMG_{n-1} is the percentage of seeds planted emerged on the day of the (n-1)th emergence observation equal to 0 when n=1 and DAP_n is the number of days after planting when the nth emergence observation was taken. In this study counts were made on 7, 10, 12, 14 days after planting and stopped when no further increase in emerged counts was observed.

Results and Discussion

I. General relationship between two sets of data

Data on seedlings spacing after emergence gathered manually and corresponding data on seedlings spacing is obtained from drone imagery were retrieved in Excel program, the relationship between these two sets of data was examined and their correlation coefficient: R related to their linear relationships was calculated (Table 1). This table shows that there is a good relationship between ground data and aerial ones and therefore, it is possible to use drones to evaluate the seedling emergence and indices of seed stand establishment.

As mentioned in the previous paragraph the first drone imagery was accomplished on the same day when ground measurements were taken. Seven days later aerial imagery was repeated to look for the existence of any change in imagery results. Correlation coefficients between the ground and aerial data for the two sets are reported in Table 1. It shows that ground and aerial observations are well correlated and therefore aerial imagery has the potential to replace the tedious ground measurements. Furthermore this table shows that there is no significant difference between the two data sets and therefore we can

conclude that do not need to rush for aerial imagery. However it should be pointed out that the timing interval between planting date and aerial data collection should not be so long as weeds and accelerated leaf growth hinder aerial imagery and reduce the accuracy of results.

Table 1- Correlation coefficient R between terrestrial and aerial seedling spacing data

Plot	R (Terrestrial 20-8-2016 vs. Drone 20-8-2016)	R (Terrestrial 20-8-2016 vs. Drone 27-8-2016)
R1P1V1	0.97	0.97
R1P1V2	0.97	0.96
R1P2V1	0.95	0.95
R1P2V2	0.96	0.98
R2P1V1	0.96	0.95
R2P1V2	0.96	0.94
R2P2V1	0.95	0.95
R2P2V2	0.97	0.95
R3P1V1	0.98	0.95
R3P1V2	0.96	0.97
R3P2V1	0.94	0.94
R3P2V2	0.97	0.95

R1= 60% CRC; R2=45% CRC; R3=30% CRC; P1= on-bed; P2= in-furrow; V1=4km h^{-1}; V2=8km h^{-1}

It should be noted that the present study was aimed to the asses capability of aerial imagery on a local farm covered with high residue and considerable weeds. The full automatic analysis of images is not possible for such farm. Other researchers, including Zhang *et al.*, 2018 and Varela *et al.*, 2018 have worked in fields having considerably less residue and weeds, hence they have been able to proceed in a more automatic approach.

The statistical analysis of data gathered manually and from aerial imagery, for these indices related to seed placement showed that the amount of CRC, planting scheme and forward speed of planter had no significant effect on indices related to seed placement, therefore it can be concluded that the no-till planter used, performed satisfactorily.

Table 2 shows that none of the indices have been significantly affected by the sources of variation for both terrestrial and aerial data sources. In other words stand establishment indices can be estimated using aerial imagery data sources with no significant loss of accuracy.

II. Planter performance indices

In the next step means of four indices of multiple index, quality of feed index, miss index and precision index from terrestrial and aerial sources have been compared. The deviation between the indices calculated by drone data and the ones calculated by terrestrial data is shown in Table 3.

Table 2- Analysis of variance of seed establishment indices for ground and aerial data

Source of variation	df	Multiple index		Quality of feed index		Miss index		Precision index	
		Terrestrial	drone	Terrestrial	drone	Terrestrial	drone	Terrestrial	drone
		F	F	F	F	F	F	F	F
Replication	2	0.30^{ns}	0.25^{ns}	2.02^{ns}	0.08^{ns}	3.40^{ns}	0.08^{ns}	0.19^{ns}	1.89^{ns}
Residue (R)	2	1.16^{ns}	1.35^{ns}	0.85^{ns}	0.22^{ns}	0.80^{ns}	0.16^{ns}	0.16^{ns}	0.44^{ns}
Position (P)	1	2.05^{ns}	1.38^{ns}	4.43^{ns}	0.07^{ns}	3.78^{ns}	0.20^{ns}	0.71^{ns}	0^{ns}
Velocity (V)	1	3.94^{ns}	5.38^{ns}	5.61^{ns}	1.23^{ns}	3.35^{ns}	0.53^{ns}	0.68^{ns}	0.15^{ns}
RP	2	0.18^{ns}	1.43^{ns}	0.30^{ns}	0.66^{ns}	0.38^{ns}	0.40^{ns}	1.01^{ns}	1.03^{ns}
RV	2	0.57^{ns}	1.35^{ns}	1.70^{ns}	1.32^{ns}	1.76^{ns}	0.91^{ns}	0.02^{ns}	2.06^{ns}
PV	1	0.71^{ns}	1.38^{ns}	0.01^{ns}	2.26^{ns}	0.91^{ns}	1.69^{ns}	1.44^{ns}	1.22^{ns}
RPV	2	1.09^{ns}	1.43^{ns}	0.04^{ns}	2.67^{ns}	1.48^{ns}	2.07^{ns}	0.14^{ns}	0.08^{ns}
Error	12								

^{ns} means no significant difference at P≤0.01

Table 3- Comparison of means of seed establishment indices for ground and aerial data

Plot	Index, %	Terrestrial 20-8-2016	Drone 20-8-2016	Deviation I	Drone 27-8-2016	Deviation II
R1P1V1	Multiple index	6.68	0.00*	+6.68	0.00*	+6.68
	Quality of feed index	79.74	74.56	+5.18	60.48	+19.26
	Miss index	13.57	25.43	-11.86	39.52	-25.95
	Precision index	25.89	22.42	+3.47	18.03	+7.86
R1P1V2	Multiple index	9.51	3.84	+5.67	0.00*	+9.51
	Quality of feed index	68.15	52	+16.15	49.05	+19.1
	Miss index	22.34	44.16	-21.82	50.95	-28.61
	Precision index	26.52	24.96	+1.56	19.31	+7.21
R1P2V1	Multiple index	7.67	0.00*	+7.67	0.00*	+7.67
	Quality of feed index	74.95	63.22	+11.73	53.19	+21.76
	Miss index	17.37	36.78	-19.41	46.81	-29.44
	Precision index	24.39	21.69	+2.7	15.50	+8.89
R1P2V2	Multiple index	12.88	0.00*	+12.88	0.00*	+12.88
	Quality of feed index	65.94	72.98	-7.04	58.25	+7.69
	Miss index	21.36	28.14	-6.78	40.65	-19.29
	Precision index	26.38	19.93	+6.45	20.05	+6.33
R2P1V1	Multiple index	7.57	0.00*	+7.57	0.00*	+7.57
	Quality of feed index	76.71	66.97	+9.74	48.98	+27.73
	Miss index	15.71	33.03	-17.32	51.01	-35.3
	Precision index	23.67	21.25	+2.42	14.10	+9.57
R2P1V2	Multiple index	9.95	0.00*	+9.95	0.00*	+9.95
	Quality of feed index	78.01	73.61	+4.4	47.86	+30.15
	Miss index	12.04	26.39	-14.35	52.14	-40.1
	Precision index	23.15	18.99	+4.16	21.54	+1.61
R2P2V1	Multiple index	12.82	0.00*	+12.82	0.00*	+12.82
	Quality of feed index	68.67	64.64	+4.03	52.42	+16.25
	Miss index	18.51	35.36	-16.85	47.58	-29.07
	Precision index	25.53	22.96	+2.57	17.44	+8.09
R2P2V2	Multiple index	12.18	0.00*	+12.18	0.00*	+12.18
	Quality of feed index	68.65	65.89	+2.76	59.60	+9.05
	Miss index	19.51	34.11	-14.6	37.06	-17.55
	Precision index	27.64	19.01	+8.63	19.16	+8.48
R3P1V1	Multiple index	6.60	0.00*	6.60	0.00*	+6.60
	Quality of feed index	83.89	73.83	10.06	56.94	+26.95
	miss index	9.49	26.17	-16.68	43.06	-33.57
	precision index	25.69	17.32	+8.37	17.74	+7.95
R3P1V2	multiple index	7.15	1.80	+5.35	0.00*	+7.15
	quality of feed index	73.73	63.54	+10.19	50.39	+23.34
	Miss index	19.12	34.65	-15.53	49.61	-30.49
	Precision index	24.27	23.86	+0.41	16.43	+7.84
R3P2V1	Multiple index	3.33	0.00*	+3.33	0.00*	+3.33
	Quality of feed index	78.44	71.39	+7.05	54.52	+23.92
	Miss index	18.22	30.16	-11.94	45.48	-27.26
	Precision index	24.08	21.71	+2.37	16.32	+7.76
R3P2V2	Multiple index	12.97	1.85	+11.12	0.00*	+12.97
	Quality of feed index	69.14	63.89	+5.25	61.18	+7.96
	Miss index	17.89	34.26	-16.37	38.81	-20.92
	Precision index	27.05	24.13	+2.92	16.09	+10.96

*: Aerial imagery partially failed to provide data needed for computing this index

R1= 60% CRC; R2=45% CRC; R3=30% CRC; P1= on-bed; P2= in-furrow; V1=4km h^{-1}; V2=8km h^{-1}

Examination of Table 3 shows that aerial imagery partially failed to provide data needed for computing multiple index. As can be seen from this table for most of the indices studied (except multiple index) data collected from drone imagery could give values more or less equal to those from ground data, however these values are either underestimated or overestimated as compared to the control (indices computed from ground data). To examine the extent of difference between each index as computed by ground or aerial data sources, drone index data were deducted from its corresponding values (columns 5 and 7 Table 3). Careful inspection of data reported in columns 5 and 7 indicates that for miss index drone imagery gives higher values and for other two indices (quality of feed index and precision) the drone imagery gives lower values. Fortunately for all treatments similar conclusions could be drawn.

III. Emergence Rate Index

Analysis of variance of data on ERI indicates that only residue levels and planting position affect this index (Table 4). Further analysis was performed (Table 5) to seek for any difference between treatments and their interactions. The comparison showed that amounts of CRC and two planting schemes; on-bed and in-furrow had significant effect on rate of corn emergence and this maybe be due to the ability of CRC in maintaining soil moisture and also presence of more water in furrows. Speed had no significant effect on this index confirming the ability of the modified corn planter to perform well at various forward speeds.

Table 4- Analysis of Variance of ERI

Source of variation	df	Sum of Squares (SS)	Mean Square (MS)	F
Replication	2	45.78	22.89	1.12^{ns}
Residue	2	336	168	8.24^{**}
Position	1	297.9	297.9	14.61^{**}
Velocity	1	46.04	46.04	2.26^{ns}
RP	2	7.34	3.67	0.18^{ns}
RV	2	1.99	0.99	0.05^{ns}
PV	1	6.25	6.25	0.31^{ns}
RPV	2	0.97	0.48	0.02^{ns}
Error	12	244.70	20.39	
Total	35	1278.36		

** Significant difference at P≤0.01

Table 5- Duncan's multiple range test for ERI%

Plot	ERI% mean	Overall effect of residue × planting position	Overall effect of residue level
R1P1V1	19.37^{abc}	19.84^{ab}	22.34^{a}
R1P1V2	20.32^{abc}		
R1P2V1	23.10^{ab}	24.84^{a}	
R1P2V2	26.59^{a}		
R2P1V1	14.60^{bc}	15.79^{bc}	18.41^{a}
R2P1V2	16.98^{abc}		
R2P2V1	19.37^{abc}	21.03^{ab}	
R2P2V2	22.70^{ab}		
R3P1V1	10.87^{c}	11.35^{c}	14.86^{a}
R3P1V2	11.83^{c}		
R3P2V1	17.14^{abc}	18.37^{abc}	
R3P2V2	19.60^{abc}		

a b c: Means with the same letter are not significantly different at P≤0.01

R1=untouched; R2= raked and baled out; R3= well grazed; P1= on-bed; P2= in-furrow; V1= 4 km h^{-1}; V2= 8 kmh^{-1}

Means of ERI% have been statistically compared in Table 5. This table shows that treatment R1P2V2 corresponds to the maximum ERI% in our study. While the

minimum ERI was noticed for treatment R3P1V1. Table 5 shows that as speed is changed from V1 to V2 there is a considerable increase in percent ERI throughout all processed data. Although significant difference exists between all six data points in this table it can be seen that as we move our planting position from on-bed scheme to in-furrow scheme increasing change occurs in our ERI values. Although not necessarily in a significant manner. Overall effects of residue levels on ERI in our study has also been dealt with in Table 5. Although not significant, a decreasing effect was noticed for decreasing the residue level. As speed increases from V1 to V2 there is a considerable increase in ERI throughout all 12 plots (Fallahi and Raoufat, 2008; Dadi and Raoufat, 2012; Nejadi and Raoufat, 2013).

Conclusions

An acceptable linear correlation with $0.94<R<0.98$ existed between seedling spacing, obtained from terrestrial and aerial measurements. Therefore it can be concluded that drone imagery can be used as a reliable tool for monitoring planter performance in the residue covered fields. This study results are in line with those of Zhang *et al.* (2018) and Varela *et al.* (2018). We obtained satisfactory results from experimental sites covered with considerable previous residues. It should be mentioned that the experimental site of Zhang *et al.* (2018) and Varela *et al.* (2018) was clear of ample residue experienced in this study. The study showed that none of the establishment indices have been significantly affected by the sources of variation for both terrestrial and aerial data sources, therefore stand establishment indices can be estimated using aerial imagery data sources with no significant loss of accuracy. It could be seen that for most of the indices (except multiple index), data collected from drone imagery gives values which slightly underestimated or overestimated indices as compared to the control (indices computed from ground data); for miss index drone imagery gives higher values and for other two indices (quality of feed index and precision) the drone imagery gives lower values. Fortunately for all treatments similar conclusions could be drawn. The CRC and planting scheme had significant effects on ERI, which is logical because seed emergence needs optimum temperature and humidity and presence of crop residue retains soil water and keeps soil temperature suitable for seed emergence. In-furrow planting and planting on higher levels of residue resulted in conditions which were more favorable for higher ERI. The maximum and minimum ERI were noticed for treatment having residue level of 60% planted in-furrow at forward speed of 8 kmh^{-1}(R1P2V2) and treatment having residue level of 30% planted on-bed at 4 kmh^{-1}(R3P1V1), respectively. It is recommended that for better results aerial imagery be confined to days seedlings have 2-3 fully expanded leaves and the field sprayed for eradicating weeds. However employing state-of-the-art cameras and existence of less residue are a plus.

Acknowledgement

Authors would like to express their gratitude to the Research Council, Shiraz University, Shiraz, Iran for providing the necessary funds and support for conducting this study.

References

1. Aguera, F., F. Carvajal, and M. Saiz. 2011. Measuring sunflower nitrogen status from an unmanned aerial vehicle-based system and on the ground device. In International Archives of the Photogrammetry, Remote Sensing and Spatial Information Sciences, XXXVIII-1/C22. ISPRS ICWG I/V UAV-g2011 (unmanned aerial vehicle in geomatics) conference, Zurich, Switzerland.
2. Bahrani, M. J., M. H. Raoufat, and H. Ghadiri. 2007. Influence of wheat residue management on irrigated corn grain production in a reduced tillage system. Soil & Tillage Research 94: 305-309.

3. Berni, J. A. J., P. J. Zarco-Tejada, L. Suarez, and E. Fereres. 2009. Thermal and narrowband multispectral remote sensing for vegetation monitoring from an unmanned aerial vehicle. IEEE Transactions on Geoscience and Remote Sensing 47: 722-738.
4. CTIC. Crop Residue Management Survey System; Conservation Technology Information Center: West Lafayette, IN, USA, 2009. Available at: http://www.crmsurvey.org. Accessed 26 January 2010.
5. Dadi, V., and M. H. Raoufat. 2012. Comparative performance of six planter attachments in two residue management corn production systems. Spanish Journal of Agricultural Research 10 (4): 950-958.
6. Erbach, D. C. 1982. Tillage for continuous corn and corn-soybean rotation. Transactions of ASAE 25: 906-911.
7. Fallahi. S., and M. H. Raoufat. 2008. Row-cleaner planter attachments in a conservation tillage system: a comparative study. Soil Tillage Research 98: 27-34.
8. Hunt, E. R., M. Cavigelli, C. S. T. Daughtry, J. E. McMurtrey, and C. L. Walthall. 2005. Evaluation of digital photography from model aircraft for remote sensing of crop biomass and nitrogen status. Precision Agriculture 6: 359-378.
9. Jannoura, R., K. Brinkmann, D. Uteau, C. Bruns, and R. G. Joergensen. 2015. Monitoring of crop biomass using true color aerial photographs taken from a remote controlled hexacopter. Biosystems Engineering 129: 341-351.
10. Kachman, S. D., and J. A. Smith. 1995. Alternative measures of accuracy in plant spacing for planters using single seed metering. Transactions of the ASAE 38 (2): 379-387. http://agris.fao.org/agris.
11. Naresh, R. K., R. K. Ashish Dwivedi, R. S. Gupta, S. S. Rathore, S. P. Dhaliwal, P. Kumar, R. Kumar, S. Vikrant, S. Vineet, and S. Onkar. 2016. Influence of Conservation Agriculture Practices on Physical, Chemical and Biological Properties of Soil and Soil Organic Carbon Dynamics in the Subtropical Climatic Conditions: A Review. Journal of Pure and Applied Microbiology 10 (2): 1061-1080.
12. Nejadi, J., and M. H. Raoufat, 2013. Field performance of a pneumatic row crop planter equipped with active toothed coulter for direct planting of corn in wheat residue. Spanish Journal of Agricultural Research 11 (2): 327-334.
13. Raoufat, M. H., and R. A. Mahmoodieh. 2005. Stand Establishment Responses of Maize to Seedbed Residue, Seed Drill Coulters and Primary Tillage Systems. Biosystems Engineering 90 (3): 261-269.
14. Raoufat, M. H., and A. Matbooei. 2007. Row cleaners enhance reduced tillage planting of corn in Iran. Soil Tillage Research 93: 152-161.
15. Rostami, M. A., and H. Afzali Gorouh. 2017. Remote sensing of residue management in farms using Landsat 8 sensor imagery. Journal of Agricultural Machinery 7 (2): 388-400. (In Farsi).
16. Sankaran, S., L. R. Khot, C. Z. Espinoza, S. Jarolmasjed, V. R. Sathuvalli, G. J. Vandemark, P. N. Miklas, A. H. Carter, M. O. Pumphrey, N. R. Knowles, and M. J. Pavek. 2015. Low-altitude, high-resolution aerial imaging systems for row and field crop phenotyping: A review. European Journal of Agronomy 70: 112-123.
17. Swain, K. C., S. J. Thomson, and H. P. W. Jayasuriya. 2010. Adoption of an unmanned helicopter for low-altitude remote sensing to estimate yield and total biomass of a rice crop. Transactions of the ASABE 53: 21-27.
18. Torres-Sanchez, J., J. M. Pena, A. I. Castro, and F. Lopez-Granados. 2014. Multi-temporal mapping of the vegetation fraction in early-season wheat fields using images from UAV. Computers and Electronics in Agriculture 103: 104-113.
19. Varela, S., P. R. Dhodda, W. H. Hsu, P. V. V. Prasad, Y. Assefa, N. R. Peralta, T. Griffin, A. Sharda, A. Ferguson, and I. A. Ciampitti. 2018. Early-Season Stand Count Determination in

Corn via Integration of Imagery from Unmanned Aerial Systems (UAS) and Supervised Learning Techniques. Remote Sensing 10, 343.
20. Vega, F. A., F. C. Ramirez, M. P. Saiz, and F. O. Rosua. 2015. Multi-temporal imaging using an unmanned aerial vehicle for monitoring a sunflower crop. Biosystems Engineering 132: 19-27.
21. Xiang, H., and L. Tian. 2011. Development of a low cost agricultural remote sensing system based on an autonomous unmanned aerial vehicle (UAV). Biosystems Engineering 108: 174-190.
22. Zhang, J., B. Basso, R. F. Price, G. Putman, and G. Shuai. 2018. Estimating plant distance in maize using Unmanned Aerial Vehicle (UAV). PLOS ONE 13 (4): e0195223. https://doi.org/10.1371/journal.pone.0195223.
23. Zheng, B., J. B. Campbell, G. Serbin, and J. M. Galbraith. 2014. Remote sensing of crop residue and tillage practices: Present capabilities and future prospects. Soil & Tillage Research 138: 26-34.
24. Zheng, B., J. B. Campbell, and K. M. de Beurs. 2012. Remote sensing of crop residue cover using multi-temporal Landsat imagery. Remote Sensing of Environment 117: 177-183.

نشریه ماشین‌های کشاورزی
جلد ۱۰، شماره ۱، نیمسال اول ۱۳۹۹، ص ۳۵-۲۳

Journal of Agricultural Machinery
Vol. 10, No. 1, Spring- Summer 2020, p. 23-35

امکان‌سنجی پایش عملکرد یک کارنده‌ی اصلاح شده در سیستم کشاورزی حفاظتی با استفاده از تصاویر هواپیماهای بدون سرنشین

زهرا کاوسی[۱*]، محمد حسین رئوفت[۲]

تاریخ دریافت: ۱۳۹۶/۱۲/۱۶
تاریخ پذیرش: ۱۳۹۷/۰۶/۰۳

چکیده

در این مقاله، عملکرد یک کارنده کشت مستقیم ذرت در زمین پوشیده از بقایای گندم (سه سطح پوشش بقایای ۳۰، ۴۵ و۶۰ درصد، دو طرح کاشت روی پشته و داخل جوی، سرعت کاشت ۴ و ۸ کیلومتر بر ساعت) از طریق مشاهدات زمینی و هوایی ارزیابی شد. هدف از این مطالعه بررسی توانایی تصاویر گرفته شده توسط پرنده‌ی بدون سرنشین برای تشخیص فواصل بین بوته‌های ذرت و در نتیجه ارزیابی کیفیت عملکرد کارنده بود. داده‌های جمع‌آوری شده از زمین و تصاویر هوایی برای محاسبه شاخص‌های استقرار بذر شامل شاخص‌های چندتایی، نکاشت، کیفیت تغذیه، دقت و همچنین شاخص سرعت جوانه‌زنی برای هر پلات، استفاده شد. تصاویر اخذ شده از ارتفاع ۱۰ متری (۴/۵ میلی‌متر بر پیکسل) نتایج خوبی با توجه به اهداف ما داشت. نتایج نشان داد که همبستگی قابل قبولی (ضریب همبستگی بین ۰/۹۴ تا ۰/۹۸) میان داده‌های زمینی و هوایی فاصله بین بوته‌های ذرت وجود دارد و می‌توان نتیجه گرفت که تصویربرداری هوایی انتخاب مناسبی برای ارزیابی استقرار بذر و تخمین سرعت جوانه‌زنی می‌باشد. داده‌های تصاویر هوایی مقادیر شاخص های کیفیت تغذیه و دقت را کمتر و مقادیر شاخص نکاشت را بیشتر از نتایج داده‌های زمینی تخمین زد و نتوانست داده‌های لازم برای محاسبه شاخص چندتایی را به‌دلیل دقت پایین تصاویر، حضور علف‌های هرز مابین ردیف محصول و هم‌پوشانی برگ‌ها فراهم کند.

واژه‌های کلیدی: پرنده بدون سرنشین، پوشش سطحی بقایا، تصویربرداری هوایی، شاخص‌های استقرار بذر

۱- دانش‌آموخته دکتری، گروه مهندسی بیوسیستم، دانشگاه شیراز، شیراز، ایران
۲- استاد، گروه مهندسی بیوسیستم، دانشگاه شیراز، شیراز، ایران
(*- نویسنده مسئول: Email: Zahra84_kavoosi@yahoo.com)

DOI: 10.22067/jam.v10i1.71498

Journal of Agricultural Machinery
Vol. 10, No. 1, Spring- Summer 2020, p. 37-48

نشریه ماشین‌های کشاورزی
جلد ۱۰، شماره ۱، نیمسال اول ۱۳۹۹، ص ۴۸-۳۷

Early Detection of Fire Blight Disease of Pome Fruit Trees Using Visible-NIR Spectrometry and Dimensionality Reduction Methods

N. Bagheri[1*], H. Mohamadi-Monavar[2]

Received: 07-04-2018
Accepted: 15-08-2018

Abstract

Fire Blight (FB) is the most destructive bacterial disease of pome fruit trees around the world. In recent years, spectrometry has been shown to be an accurate and real-time sensing technology for plant disease detection. So, the main objective of this research is early detecting FB of pear trees by using Visible-Near-infrared spectrometry. To get this goal, the reflectance spectra of healthy leaves (ND), non-symptomatic (NS), and symptomatic diseased leaves (SY) were captured in the visible–NIR spectral regions. In order to keep the important information of spectra and reduce the dimension of data, three linear and non-linear manifold-based learning techniques were applied such as, Principal Component Analysis (PCA), Sammon mapping and Multilayer auto-encoder (MAE). The output of manifold-based learning techniques was used as an input of the SIMCA (Soft independent modeling by class analogy) classification model to discriminate NS and ND leaves. Based on the results, the best classification accuracy obtained by using PCA on the 1st derivative spectra, with accuracy of 95.8%, 89.3%, and 91.6% for ND, NS, and SY samples, respectively. These results support the capability of manifold-based learning techniques for early detection of FB via spectrometry method.

Keywords: Early detection, Fire blight, Precision agriculture, Remote sensing, Vis/NIR Spectrometry

Introduction

At least 10% of global food production is lost due to plant disease (Zhang *et al.*, 2012). Fire blight (FB) is the most destructive bacterial disease of apple (*Malus domestica*), pear (*Pyrus communis*) and more generally of Maloideae, a subfamily of the Rosaceae. The causal agent is the necrogenic Gram-negative bacterium Erwinia amylovora (Ea). This pathogen enters the plant through natural openings such as the apoplast of parenchyma cells and colonize nectarthodes or through wounds on succulent aerial parts. Once inside the susceptible host plant, the bacteria multiply mainly in actively growing shoots inducing the progressive necrosis of the infected plant tissues. In resistant host plants or in non-host plants, bacteria cause a local cell death (hypersensitive-like reaction) and are unable to further colonize the plant tissue (Gaucher *et al.*, 2013). To decrease product losses, fast and timely identification of FB disease is very important (Bagheri *et al.*, 2018). Scouting is normally used as a method for FB detection, which is time consuming and laborious. Thus, an accurate and real-time sensing technology for improvement of plant disease detection is necessary (Futch *et al.*, 2009). Nowadays, spectrometry in the Visible and Near-Infrared (NIR) spectral ranges shows good potential for detection of plant disease and stress (Sankaran *et al.*, 2010; Bagheri *et al.*, 2018). So, various researchers (Delalieux *et al.*, 2007; Purcell *et al.*, 2009; Spinelli *et al.*, 2006; Yang *et al.*, 2007) have used spectral reflectance-based techniques for plant disease detection (Purcell *et al.*, 2009). Bravo *et al.* (2003) and Moshou *et al.* (2004) developed a ground-based spectral data collecting system for disease detection in winter wheat fields, which achieved a classification accuracy of over 90% (Bravo *et al.*, 2003; Moshou *et al.*, 2004). Naidu *et al.* (2009) applied visible infrared spectrometry (350-2500 nm) for detecting

1- Assistant Professor, Agricultural Engineering Research Institute, Agricultural Research, Education and Extension Organization (AREEO), Karaj, Iran
2- Assistant Professor, Department of Biosystem Engineering, Faculty of Agriculture, Bu-ali Sina University, Hamadan, Iran
(*- Corresponding Author Email: n.bagheri@areeo.ac.ir)
DOI: 10.22067/jam.v10i1.71911

grapevine leafroll disease. It was reported that the classification accuracy based on stepwise discriminant analysis ranged from %73 to %81 depending on the features (vegetative indices) used for detecting infected (symptomatic and non-symptomatic) and healthy leaves (Naidu *et al.*, 2009). Lui *et al.* (2010) applied neural network and PCA (Principle Component Analysis) techniques to discriminate different fungal infection levels in rice panicles with a portable spectroradiometer in the laboratory (350 to 2500 nm). Results indicated that it is possible to discriminate different fungal infection levels of rice panicles under laboratory conditions using spectrometry data (Lui *et al.*, 2010). Zhang *et al.* (2012) detected powdery mildew of wheat via a spectroradiometer in a laboratory. Based on the results, the PLSR (Partial Least Square Regression) model with a coefficient of determination (R^2) of 0.80 was good for estimating disease severity and FLDA (Fisher Linear Discriminant Analysis) with accuracy over 90% was produced for the heavily-damaged leaves. Mahlein *et al.* (2013) developed specific spectral disease indices for detection of three leaf diseases, Cercospora leaf spot, sugar beet rust and powdery mildew in sugar beet plants. The classification results for discrimination of healthy leaves from infected with Cercospora leaf spot, sugar beet rust and powdery mildew leaves were obtained as 92%, 87%, and 85%, respectively (Mahlein *et al.*, 2013). Yuan *et al.* (2013) analyzed spectral data of winter wheat leaves for detection of yellow rust disease. The spectral differences showed a stronger response in 380-650 nm for both healthy and diseased leaves at the leaf scale. Phadikar *et al* (2013) classified different types of rice diseases by extracting features from the infected regions of the rice plant images. To reduce complexity of the classifier, important features were selected using rough set theory (RST) to minimize the loss of information. Finally, using selected features, a rule base classifier was built that covered all the diseased rice plant images and provided superior result compare to traditional classifiers. Finally, ten-fold cross validation was performed to measure the efficiency of the proposed method, which showed superiority over other methods (Phadikar *et al.*, 2013). Barbedo *et al.* (2015) presented an algorithm for automatic detection of *Fusarium* head blight in wheat kernels using hyperspectral imaging. With classification accuracy above 91%, the developed algorithm was robust to factors such as shape, orientation, shadowing and clustering of kernels. Huang *et al* (2015) proposed a new method for grading panicle blast based on hyperspectral imaging. The method was based on the concept of the ‘‘bag of textons”, which defines a ‘‘bag of spectra words” (BoSW) model for hyperspectral image data representation. The results indicated that the proposed method could effectively grade panicle blast with classification accuracies of up to 81.4% for six-class grading and 96.4% for two-class grading in the validation datasets (Huang *et al.*, 2015).

Based on literature review, no research has carried out yet for early detection of FB by spectral data. Because of the necessity of developing a system for early detection of FB disease, in the present research, Visible-NIR spectrometry method was used as a non-destructive method for detection of FB in pear trees during growing. For dimensionality reduction, several spectral preprocessing techniques and three manifold-based learning methods were applied on the spectra for more accurate detection of NS infected leaves. In order to extract an identification algorithm, the performance of preprocessed reflectance spectra and the dimensionality reduction methods were evaluated in affected trees at early stages.

Materials and Methods

Pear leave samples

Pear leaves of healthy and infected trees were collected from a 5 ha pear tree orchard at Damavand city of Tehran Province in Iran on May 2016. Collecting leaves was carried out under clear sky conditions between 10:00 am to 14:00 pm. 34 healthy trees (ND), 50 symptomatic infected trees (SY) and 22 non-

symptomatic infected trees (NS) were selected (Fig.1).

After collecting leaves, samples were packed with different plastic bags and transported immediately to a nearby indoor laboratory for spectral measurements. All leaves were tested in the laboratory by Selective Culture Method to confirm presence of *Erwinia amylovora* bacteria in samples. In this laboratory test, all samples were washed in tap water.

ND

NS

SY

Fig.1. Images of ND, NS, and SY trees

Infected tissues were surface sterilized by immersion in 10% household bleach for 3 min and rinsed twice in sterile distilled water (SDW) for a few minutes. Leaf samples were each macerated in a few drops of SDW in a sterile glass Petri dish using a sterile scalpel and forceps. Thirty minutes after maceration, 30 μ L of macerated tissue were streaked onto King's medium agar B (KB). The plates were then incubated at 27°C for 2-3 days and observed daily for bacterial growth. Suspected colonies of *Erwinia amylovora* (white,

circular, mucoid, and curved) were selected and further purified on KB agar at 27°C (King *et al.*, 1954).

Spectral data acquisition

A portable high-resolution fiber-optic spectrometer (Avaspec 3648, Netherland) in the range of 200 to 1100 nm with a resolution of 0.05-20 nm was used to collect the spectral reflectance data of pear leaves under laboratory conditions. The dark spectrum was obtained by turning off the light source (Dep UV, 78W / 0.75A, Dimension: 315 x 165 x 140 mm/weight: 5 kg AVAntes. Netherland) and covering the tip of the fiber-optics reflectance probe (7 fibers 200 mm or 400 mm core, 6 light-fibers, 1 read fiber, N.A.= 0.22. Standard 2 m length, splitting point in the middle. AVAntes. Netherland) completely. The reference spectrum ($R_{reference}$) was measured by turning the light source on and placing the probe in the front of a reference tile. Then the sample spectrum (R_{sample}) was measured to calculate the relative spectrum by following equation:

$$R_{relatuve} = \frac{R_{sample} - R_{dark}}{R_{reference} - R_{dark}} \times 100 \qquad (1)$$

Due to the high level of noise in the 200-400 nm and 1000-1100 nm, further analysis was performed only on the spectral data in the range of 400-1000 nm. The spectral measurements were taken 5 times for each sample. Data of ND, SY, and NS leaf samples was collected and recorded. The absorbance at a certain wavelength (λ) was calculated as [log (1/Reflectance)] at this wavelength (λ) based on Beer Lambert law.

Chemo metric analysis

All data analysis and feature extraction were performed in MATLAB (version 2011b, Math work, Inc. USA). Preprocessing methods and plot visualizations of features were carried out in Unscrambler Software (Version X10; CAMO Software, Oslo, Norway). For each sample, three measurements with two replications were carried out and mean value was obtained for each concentration. Two of the most commonly used scatter-correction techniques in spectroscopy, Multiplicative Scatter Correction (MSC) (Geladi *et al.*, 1985) and Standard Normal Variate (SNV) (Barnes *et al.*, 1989) were used. MSC aims to reduce the scattering effects by fitting each spectrum to a reference spectrum, which usually corresponds to the mean spectrum of the data set. Each spectrum is fitted by linear least square regression. The first derivative filtering based on Savitzky-Golay was used to remove offsets (Savitzky and Golay, 1964). SIMCA classification accuracy of these preprocessing methods is shown in Table 1. To detect ND, NS and SY, samples, spectral variables extracted from the pre-processed spectra were used directly as inputs of classification algorithms. Mentioned manifold-based learning techniques were applied to reduce the magnitude of the high-dimensional spectral variables space in order to improve the performance of the classifier (Tian, 2010).

Most of the time, measured data have high-dimensional vectors while terse and precise manifold data is required (Ghodsi, 2006). Therefore, it is necessary to protect the least vital parameters that describe all data information and manifold learning methods and also remove additional data. Hereon, three more common unsupervised dimensionality reduction methods were used: Principal Component Analysis (PCA) (Jolliffe, 2002), Sammon mapping (Sammon, 1969), and Multilayer auto-encoders (MAE) (Demers and Cottrell, 1993). The number of features were applied for these dimensionality reduction methods was between four to seven. In order to establish the same condition, four features were selected.

Multilayer auto-encoders are feed-forward neural networks with an odd number of hidden layers (Demers and Cottrell, 1993) which share weights between the top and bottom layers (although asymmetric network structures may be employed as well). In PCA, the data transformation is linear, while Sammon mapping and MAE are non-linear methods. PCA is one of the classical methods in dimensional reduction. PCA is also known as the Karhunen Loève transform, or singular value decomposition (SVD). The key idea of PCA is to find the low-dimensional linear subspace which captures the maximum

proportion of the variation within the data. According to Lorente *et al*. (2015) and Lee and Verleysen (2007) research, PCA and Sammon mapping were suitable for the small data sets used in this work, since the simplest models of manifold learning methods are more acceptable for small data sets with high-dimensionality (Lee and Verleysen, 2007; Lorente *et al.*, 2015). Furthermore, MAE as a nonlinear method was applied to support the results of two other manifold leaning techniques. The application of MAE in plant disease detection has not been reported yet, while neural networks are more common (Laurindo *et al.*, 2017; Liu *et al.*, 2010). The goal of SIMCA as a classification method is to get an organization rule for a set of *m* known groups, thus it is used to distinguish *m* classes where the similarity within a class is emphasized (Vanden Braden and Hubert, 2005). In SIMCA algorithm, the format of training samples was described by dimensionality reduction techniques (PCA, Sammon mapping and MAE) for each class. The original SIMCA and modifications by Hawkins (Mahalanobis distance) and Gnanadesikan methods were compared with respect to classification accuracy and their robustness towards the number of PCs selected to describe the different classes. SIMCA modified with the Mahalanobis distance method was found to be a good alternative to the original SIMCA which seems to be more robust for finding outliers when the exact number of PCs for building the model is not known (De Maesschalck *et al.*, 1999).

Leave one out cross-validation (LOOCV) was performed to evaluate and compare the performance of the classification models. 80 percent of data was used for calibration and 20 percent of data was used for validation. Five iterations were applied and 20% of data left out each time. A mean confusion matrix was created as an average of all iterations. For evaluating the classification performance, overall accuracy was computed for each classification model from its associated mean confusion matrix (Fleiss, 1981).

Results and Discussion

Development of classification models

According to the algorithm of SIMCA, all acquired data were classified into healthy and diseased classes. The combination of spectral ranges (visible-short NIR), the pre-processing methods (no pre-processing, SG, MSC and SNV), and the dimensionality reduction techniques (PCA, Sammon mapping and MAE) were evaluated with regards to their classification performance in detecting NS leaves. The results of the SIMCA classifier on the visible–NIR spectra with applying the different preprocessing techniques and three dimensionality reduction methods show in Table 1. The accuracy of SIMCA and other linear classification methods has confirmed early bruises detection of apples in different regions of spectra (Baranowski *et al.*, 2012) and pistachios classification (Vitale *et al.*, 2013). The most accurate SIMCA model was the PCA manifold, with 95.8% accuracy on the derivative spectra. As a whole, the 1st derivative spectra showed the most accurate classification results in comparison with MSC and SNV methods. According to Lorente *et al*. (2015) research, the best classification results belonged to the raw spectra without preprocessing with small differences to SNV and MSC methods (Lorente *et al.*, 2015). This is because the scatter-correction methods only remove the structural and physical variations of spectra, while they save the absorption properties related to the chemical components in the spectra. It should be noted that the 1st derivative preprocessing method was not evaluated with them. In consequence, MSC and SNV probably removed some important information for FB detection from the spectral measurements, as both try to fit spectra to the mean of spectrum. The total accuracy of dimensional reduction methods was almost higher than each class. Since the maximum number of samples belong to SY, then this group had the most weight in the total result. In order to display the classification of NS group, the cooman's plot was also drawn in every dual group. The vertical and horizontal axis of cooman's plot showed two classes and the SIMCA critical distance (0.95) from each

class. In this study, ND, SY and NS data placed in class1, class2 and class3, respectively. Cooman's plot has four parts. The data which is belong to two classes was placed in the lower left square. It means there is just a small distance from both models, while out of ranges' data dispersed in the upper right square. Fig 2 shows the cooman's plot of different sample groups with SIMCA model. For example in Fig. 2a, samples in the horizontal rectangle belong to class2 and the vertical rectangle on the left shows samples of class1. According to Fig. 2, NS samples had more confliction with SY in three studied data reduction methods (c, f and h) whereas ND and SY separated obviously. However, interference was rarely seen between NS and ND (Fig. 2b, e and g). According to Table 1, the 1st derivative preprocessed spectra had the better results in comparison with other methods. Therefore cooman's plot was drawn based on SG. The performance of cooman's plot was also approved by full differentiation of aroma components of wild strawberries (Negri *et al.*, 2015).

Table 1- SIMCA classification accuracy of non-preprocessing and some preprocessing methods for dimensionality reduction techniques in Visible-NIR region (%)

Dimensionality reduction techniques	Classes	Classification accuracy (%)			
		Raw data	1st derivative	SNV	MSC
PCA	ND	90.3	95.8	92.7	93.1
	NS	86.9	89.3	85.7	88.4
	SY	93.1	91.6	94.0	91.6
	Total	96.4	98.0	97.4	96.94
Sammon mapping	ND	85.9	92.0	88.2	91.3
	NS	81.4	83.9	81.5	83.3
	SY	90.5	90.6	91.7	89.1
	Total	92.4	95.0	93.8	93.94
MAE	ND	88.5	94.7	90.9	92.2
	NS	83.9	89.3	83.8	86.5
	SY	92.6	90.4	92.0	89.7
	Total	94.8	97.0	95.3	95.2

Partial Least Square (PLS)

PLS as a full spectrum method was employed for the analysis of FB in pear leaves. The calibration model was developed in order to evaluate test data. Then the first polynomial equation was predicted. PLS regression model using calibration and validation data of raw, SG, SNV and MSC spectra is shown in Fig. 3. The same accuracy was recorded between actual and predicted data for detection of palm oil adulteration in lard (Basri *et al.*, 2017), and between predicted and reference values of tocopherol content in olive oil (Cayuela and Garcia, 2017). Based on the coefficient determination of PLS regression (Fig. 3), the calibration and validation of a PCA classifier on SNV and MSC spectra, was fitted in comparison with nonlinear techniques. According to the results of Table 1, 1st derivative and MSC are more accurate preprocessing methods. Three dimensionality reduction techniques and two preprocessing methods, including 1st derivative and MSC was combined in order to distinguish NS leaves (Table. 2). The results are almost close in studying manifold learning based methods, whereas PCA prediction was more accurate. Lorente *et al* (2015) showed similar results on citrus (Lorente *et al.*, 2015). Based on the result, combination of MSC and PCA showed a better predictive model in comparison with Sammon mapping and MAE. In the most cases, the models for three types of dimensionality reduction techniques are completely strength and accurate because they were able to distinguish the NS leaves as members of SY class.

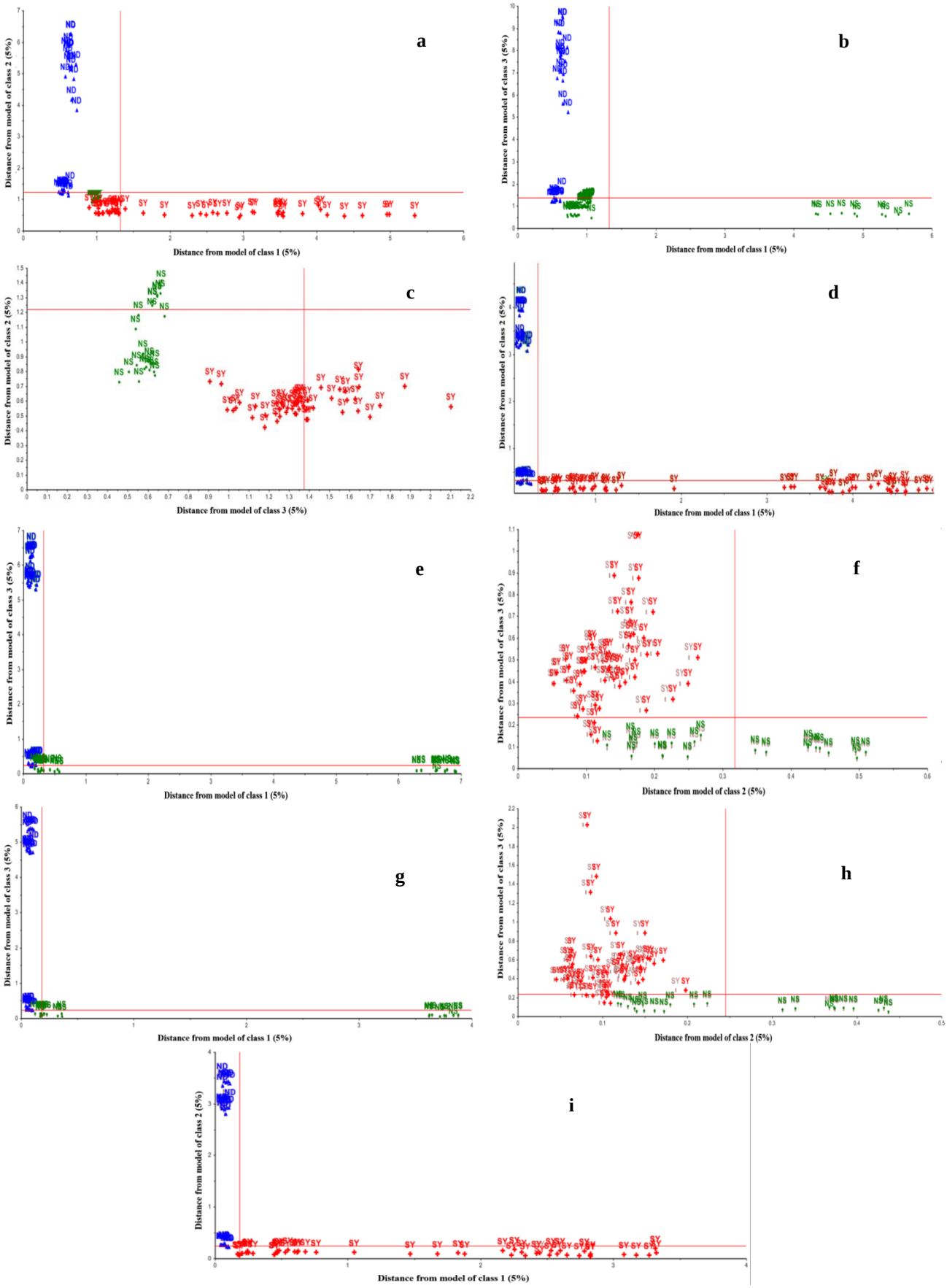

Fig.2. Coomans plot of SIMCA model which a, b and c related to PCA, d, e and f showed the Sammon Mapping results and g, h and i depicted MAE analysis

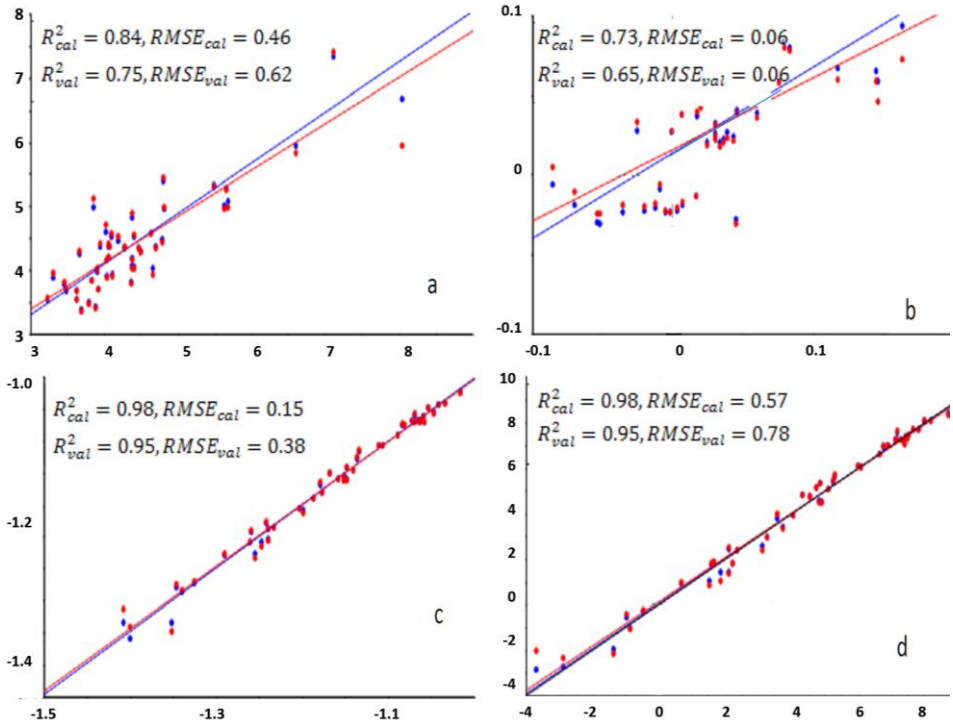

Fig.3. PLS regression model using calibration and validation data of a. raw, b. SG, c. SNV and d. MSC spectra

Table 2- Prediction percent of NS as Diseased or Healthy leaves

		PCA		Sammon mapping		MAE	
		Diseased	**NS**	**Diseased**	**NS**	**Diseased**	**NS**
1st derivative	**Diseased**	96.0	76.5	89.0	55.5	95.0	61.2
	NS	2.7	22.3	11.0	42.1	3.1	36.8
MSC	**diseased**	98.0	75.9	94.0	62.2	97.0	71.4
	NS	2.0	24:0	5.0	32.9	1.6	29.0

Conclusions

In the present research, the ability of spectrometry method for detection of FB disease of pear trees was assessed. For this purpose, the visible and NIR spectra of pear trees' leaves were obtained with a spectrometer (200-1100 nm). In order to eliminate any inappropriate information, several spectral pre-processing techniques (1st derivative SG, MSC and SNV) were then adjusted on the spectra. In order to detect non-symptomatic FB affected leaves in early stage, some manifold-based learning methods (PCA, Sammon mapping and MAE) were applied to transform the high-dimensional spectral data into significant representations of low-dimensional spectral data.

According to the results, the maximum NS classification accuracy (89.3%) was obtained by employing PCA and MAE on the derivative spectra. In the case of visible-NIR spectra, the second NS classification accuracy (88.4%) was acquired by employing PCA on the MSC correction spectra. From these results, it can be concluded that, the linear manifold learning technique for dimensionality reduction (PCA) is more accurate than the non-linear technique (Sammon mapping and MAE). Furthermore, it should be noticed that the 1st derivative SG showed the most accurate classification results than the MSC and then SNV preprocessed spectra and also ND was discriminant from NS and SY in significant level of 5%. As reported by these results, the present research plans the

structure of an automatic commercial system based on dimensionality reduction and classifier methods for early detection of FB in near future.

References

1. Bagheri, N. Mohamadi-Monavar, H. Azizi, A. Ghasemi, A. 2018. Detection of Fire Blight disease in pear trees by hyperspectral data. European Journal of Remote Sensing 51 (1): 1-10.
2. Baranowski, P., W. Mazurek, J. Wozniak, and U. Majewska. 2012. Detection of early bruises of apple using hyperspectral and thermal imaging. Food Engineering 110: 345-355.
3. Barbedo, J. G. A., C. S. Tibola, and J. M. C. Fernandes. 2015. Detecting Fusarium head blight in wheat kernels using hyperspectral imaging. Biosystems Engineering 131: 65-76.
4. Barnes, R. J., M. S. Dhanoa, and S. J. Lister. 1989. Standard normal variate transformation and de-trending of near-infrared diffuse reflectance spectra. Applied Spectroscopy 43: 772-777.
5. Basri, K. N., M. N. Hussain, J. Bakar, Z. Sharif, M. F. Abdul-Khir, and A. S. Zoolfakar. 2017. Classification and quantification of palm oil adulteration via portable NIR spectroscopy. Spectrochimica Acta Part A: Molecular and Biomolecular Spectroscopy 173: 335-342.
6. Bravo, C., D. Moshou, J. West, A. McCartney, and H. Ramon. 2003. Early disease detection in wheat fields using spectral reflectance. Biosystems Engineering 84 (2): 137-145.
7. Cayuela, J. A., and J. F. Garcia. 2017. Sorting olive oil based on alpha-tocopherol and total tocopherol content using near-infrared spectroscopy (NIRS) analysis. Food Engineering: 1-10.
8. Delalieux, S., J. Van Aardt, W. Keulemans, E. Schrevens, and P. Coppin. 2007. Detection of biotic stress (*Venturia inaequalis*) in apple trees using hyperspectral data: non-parametric statistical approaches and physiological implications. European Journal of Agronomy 27 (1): 130-143.
9. DeMers, D., and G. Cottrell. 1993. Non-linear dimensionality reduction. In Advances in Neural Information Processing Systems, 5: pages 580-587, San Mateo, CA, USA, 1993. Morgan Kaufmann.
10. De Maesschalck, R., A. Candolfi, D. L. Massart, and S. Heuerding. 1999. Decision criteria for soft independent odeling of class analogy applied to near infrared data, Chemometrics and Intelligent Laboratory Systems 47: 65-77. DOI: 10.1016/S0169-7439(98)00159-2.
11. Fleiss, J. L. 1981. Statistical Methods for Rates and Proportions, second ed. Wiley-Interscience.
12. Futch, S. H., S. Weingarten, and M. Irey. 2009. Determining greening infection levels using multiple survey methods in Florida citrus. Proceedings of Florida State Horticulture Society 122: 152-157.
13. Gaucher, M., T. D. Bernonville, S. Guyot, J. F. Dat, and M. N. Brisset. 2013. Same ammo, different weapons: Enzymatic extracts from two apple genotypes with contrasted susceptibilities to fire blight (*Erwinia amylovora*) differentially convert phloridzin and phloretin in vitro, Plant Physiology and Biochemistry 72: 178-189.
14. Geladi, P., D. MacDougall, and H. Martens. 1985. Linearization and scatter-correction for near-infrared reflectance spectra of meat. Applied Spectroscopy 39: 491-500.
15. Ghodsi, A. 2006. Dimensionality Reduction "A Short Tutorial", Department of Statistics and Actuarial Science, University of Waterloo, Ontario, Canada.
16. Huang, S., L. Qi, X. Ma, K. Xue, W. Wang, and X. Zhu. 2015. Hyperspectral image analysis based on BoSW model for rice panicle blast grading. Computers and Electronics in Agriculture 118: 167-17.
17. Jolliffe, I. T. 2002. Principal Component Analysis, second ed. Springer, New York, USA.
18. King E. O., M. K. Ward, and D. E. Raney. 1954. Two simple media for the demonstration of pyocyanin and fluorescein. Journal of Laboratory and Clinical Medicine 44: 301-307.

19. Laurindo, B. S., R. D. F. Laurindo, A. M. Azevedo, F. T. Delazari, J. C. Zanuncio, and D. J. Henriques da Silva. 2017. Optimization of the number of evaluations for early blight disease in tomato accessions using artificial neural networks, Scientia Horticulturae 218: 171-176.
20. Lee, J. A., and M. Verleysen. 2007. Nonlinear Dimensionality Reduction. Springer, New York, USA.
21. Liu, Z. Y., H. F. Wu, and J. F. Huang. 2010. Application of neural networks to discriminate fungal infection levels in rice panicles using hyperspectral reflectance and principal components analysis. Computers and Electronics in Agriculture 72: 99-106.
22. Lorente, D., P. Escandell-Montero, S. Cubero, J. Gomez-Sanchis, and J. Blasco. 2015. Visible-NIR reflectance spectroscopy and manifold learning methods applied to the detection of fungal infections on citrus fruit. Food Engineering 163: 17-24.
23. Mahlein, A. K., T. Rumpf, P. Welke, H. W. Dehne, L. Plümer, U. Steiner, and E. C. Oerke. 2013. Development of spectral indices for detecting and identifying plant diseases. Remote Sensing of Environment 128: 21-30.
24. Mohammadi Moghaddam, T., S. M. A. Razavi, M. Taghizadeh, A. Sazgarnia, and B. Pradhan. 2015. Vis-NIR hyperspectral imaging and multivariate analysis for prediction of the moisture content and hardness of Pistachio kernels roasted in different conditions. Journal of Agricultural Machinery 5 (2): 281-291. (In Farsi).
25. Moshou, D., C. Bravo, J. West, S. Wahlen, A. McCartney, and H. Ramon. 2004. Automatic detection of 'yellow rust' in wheat using reflectance measurements and neural networks. Computers and Electronics in Agriculture 44 (3): 173-188.
26. Naidu, R. A., E. M. Perry, F. J. Pierce, and T. Mekuria. 2009. The potential of spectral reflectance technique for the detection of Grapevine leafroll-associated virus-3 in two red-berried wine grape cultivars. Computers and Electronics in Agriculture 66: 38-45.
27. Negri, A., D. Allegra, L. Simoni, F. Rusconi, C. Tonelli, L. Espan, and M. Galbiati. 2015. Comparative analysis of fruit aroma pattern in the domesticated wild strawberries "Profumata di Tortona" (F. moschata) and "Regina delle Valli" (F. vesca), Frontiers in Plant Science 6: 1-13.
28. Phadikar, S., J. Sil, and A. K. Das. 2013. Rice diseases classification using feature selection and rule generation techniques. Computers and Electronics in Agriculture 90: 76-86.
29. Purcell, D. E., M. G. O' Shea, R. A. Johnson, and S. Kokot. 2009. Near-infrared spectroscopy for the prediction of disease rating for Fiji leaf gall in sugarcane clones. Applied Spectroscopy 63 (4): 450-457.
30. Sammon, J. W. 1969. A nonlinear mapping for data structure analysis. IEEE Transactions on Computers 18: 401-409.
31. Sankaran, S., A. Mishra, R. Ehsani, and C. Davis. 2010. A review of advanced techniques for detecting plant diseases. Computers and Electronics in Agriculture 72 (1): 1-13.
32. Savitzky, A., and M. J. E. Golay. 1964. Smoothing and differentiation of data by simplified least square procedures. Analytical Chemistry 36 (8): 1627-1639.
33. Spinelli, F., M. Noferini, and G. Costa. 2006. Near infrared spectroscopy (NIRs): Perspective of fire blight detection in asymptomatic plant material. Proceeding of 10th International Workshop on Fire Blight. Acta Hort 704: 87-90.
34. Tian, T. S. 2010. Dimensionality Reduction for Classification with High-Dimensional Data. PhD thesis, VDM Verlag, Saarbrücken, Germany.
35. Vanden Branden, K., and M. Hubert. 2005. Robust classification in high dimensions based on the SIMCA method, Chemom. Intell. Lab. Syst. 79: 10-21 available at: http://dx.doi.org/10.1016/j.chemolab.2005.03.002.

36. Vitale, F., M. Bevilacqua, R. Bucci, A. D. Magri, A. L. Magri, and F. Marini. 2013. A rapid and non-invasive method for authenticating the origin of pistachio samples by NIR spectroscopy and chemometrics.
37. Yang, C. M., C. H. Cheng, and R. K. Chen. 2007. Changes in spectral characteristics of rice canopy infested with brown planthopper and leaffolder. Crop Science 47: 329-335.
38. Yuan, L., J. C. Zhang, K. Wang, R. W. Loraamm, W. J. Huang, J. H. Wang, and J. L. Zhao. 2013. Analysis of spectral difference between the foreside and backside of leaves in yellow rust disease detection for winter wheat. Precision Agriculture, published online, 7 May 2013.
39. Zhang, J. C., R. L. Pu, J. H. Wang, W. J. Huang, L. Yuan, and J. H. Luo. 2012. Detecting powdery mildew of winter wheat using leaf level hyperspectral measurements. Computers and Electronics in Agriculture 85: 2-13.

نشریه ماشین‌های کشاورزی
جلد ۱۰، شماره ۱، نیمسال اول ۱۳۹۹، ص ۴۸-۳۷

Journal of Agricultural Machinery
Vol. 10, No. 1, Spring- Summer 2020, p. 37-48

تشخیص زودهنگام بیماری آتشک درختان میوه دانه‌دار با استفاده از طیف‌سنجی مرئی- مادون قرمز و نزدیک و روش‌های کاهش ابعاد

نیکروز باقری[1*]، حسنا محمدی منور[2]

تاریخ دریافت: ۱۳۹۷/۰۱/۱۸
تاریخ پذیرش: ۱۳۹۷/۰۵/۲۴

چکیده

بیماری آتشک یکی از مخرّب‌ترین بیماری باکتریایی درختان میوه دانه‌داردر سراسر جهان است. در سال‌های اخیر، طیف‌سنجی به‌عنوان یک روش دقیق و زمان واقعی برای تشخیص بیماری‌های گیاهی شناخته شده است. بنابراین، هدف اصلی این پژوهش تشخیص بیماری آتشک درختان گلابی در مراحل اولیه آلودگی با استفاده از طیف‌سنجی مرئی و مادون قرمز نزدیک است. برای دستیابی به این هدف، طیف بازتابی برگ‌های سالم، برگ‌های شبه‌بیمار و برگ‌های بیمار در محدوده طیفی نور مرئی و مادون قرمز نزدیک اندازه‌گیری شد. به منظور حفظ اطلاعات مهم طیفی و همچنین کاهش ابعاد داده‌ها، روش‌های مختلف خطی و غیرخطی مانند تجزیه و تحلیل PCA، نقشه‌برداری سامون و روش اتوکودر چندلایه (MAE) مورد استفاده قرار گرفت. خروجی روش‌های مذکور به‌عنوان ورودی برای روش طبقه‌بندی SIMCA با هدف تفکیک برگ سالم، بیمار و شبه‌بیمار به‌کار رفت. بر اساس نتایج، بهترین طبقه‌بندی با استفاده از روش PCA در طیف مشتقی، با دقت ۹۵/۸، ۸۹/۳ و ۹۱/۶ درصد به‌ترتیب برای نمونه‌های سالم، شبه‌بیمار و بیمار به‌دست آمد. این نتایج توانایی روش‌های یادگیری چندمنظوره را برای تشخیص زودهنگام بیماری آتشک با استفاده از طیف‌سنجی تأیید می‌کند.

واژه‌های کلیدی: بیماری آتشک، تشخیص زودهنگام، سنجش از دور، طیف‌سنجی مرئی/مادون‌قرمزنزدیک، کشاورزی دقیق

۱- استادیار پژوهش، مؤسسه تحقیقات فنی و مهندسی کشاورزی، سازمان تحقیقات، آموزش و ترویج کشاورزی، کرج، ایران
۲- عضو هیئت علمی، گروه مهندسی بیوسیستم، دانشکده مهندسی کشاورزی، دانشگاه بوعلی سینا، همدان، ایران
(*- نویسنده مسئول: Email: n.bagheri@areeo.ac.ir)

DOI: 10.22067/jam.v10i1.71911

Journal of Agricultural Machinery
Vol. 10, No. 1, Spring- Summer 2020, p. 49-58

نشریه ماشین‌های کشاورزی
جلد ۱۰، شماره ۱، نیمسال اول ۱۳۹۹، ص ۵۸-۴۹

Comparison of the Laser Backscattering and Digital Imaging Techniques on Detection of α-Solanine in Potatoes

S. Babazadeh[1], P. Ahmadi Moghaddam[2*], A. Sabatyan[3], F. Sharifian[4]

Received: 19-03-2019
Accepted: 11-09-2019

Abstract

The overall objective of this research is to check the abilities of two non-destructive techniques, the digital imaging (DI) and laser light backscattering imaging (LLBI), on detection of α-solanine toxicant in potatoes. Potato samples were classified in healthy and toxic categories based on the amount of α-solanine. For quantifying α-solanine in potato tubers, high-performance liquid chromatography (HPLC) has been used. The results of classification showed that single layer perceptron neural networks can classify potatoes with the accuracies of 94.28% and 98.66% by DI and LLBI systems (Donald cultivar), respectively. It can be said that LLBI systems might take precedent over DI systems due to their high accuracy, rapidity, and industrial capability.

Keywords: Backscattering imaging, Digital imaging, Glycoalkaloids, Liquid chromatography, Quality inspection

Introduction

Food safety is a key factor in the food and agriculture industries, because consumers prefer to purchase qualitative and reasonable products (Wu and Sun, 2013b). Potato (*Solanum tuberosum* L.), is one of the most important food crops of the world (Ji *et al.*, 2012), which can solve the poverty problem in all the world due to its valuable nutrients. So it can guarantee the food security of today and tomorrow generations (FAO, 2008). Unlike wheat and beans, some vegetables such as onion, garlic, and potato lose their nutritional values when sprouted (Tavakoli and Najafzadeh, 2015) and therefore, toxic compounds would be produced in the sprouts, flowers, and skin of potato tubers. Hence, the recognition of these toxic compounds that appear in green color at the skin of potato samples is necessary due to food safety and quality inspection of potatoes.

Potato tubers may consist of high levels of α-solanine and α-chaconine. These are two glycoalkaloids that can occur with each other and are issued under a unique heading, "solanine". Light exposure of potato tubers is inevitable at different stages of harvest and post-harvest periods that leads to physiological changes in tubers. These changes are due to chlorophyll synthesis and toxic glycoalkaloids in all the surrounded layers of potato tubers. Accumulations of these toxic compounds lead to economic losses. Since the suggested safety amount of glycoalkaloids is about 200 mg kg^{-1} (fresh weight) of potato (FAO/WHO, 2003), efforts should be made to decrease these toxins in potatoes to minimize possible values, especially for people who use them a lot. It is notable that this issue is more important for children.

Currently, different apparatuses are widely used to detect solanine in potatoes, tomatoes, and eggplants, which however are time-consuming, tedious, costly, and destructive. These methods are gas chromatography, liquid chromatography, spectrophotometry, etc. Therefore, it is critical and necessary to apply accurate, rapid, reliable, efficient, and non-invasive alternatives to evaluate the quantity and quality-related attributes of food products (Espinoza *et al.*, 2014). Recently, optical sensors have been studied as potential tools due to the non-destructive inspection of food safety (Wu and Sun, 2013a). Geng *et al.*

1, 2 and 4- Ph.D. Candidate, Associate Professor and Assistant Professor, respectively, Department of Mechanical Engineering of Biosystems, Faculty of Agriculture, Urmia University, Urmia, Iran
3- Associate Professor, Department of Physics, Faculty of Sciences, Urmia University, Urmia, Iran
(* Corresponding Author Email: p.ahmadi@urmia.ac.ir)
DOI: 10.22067/jam.v10i1.79800

(2019) reported a technique for separating clods and stones from potatoes using laser backscattering imaging. The recognition results showed that the best wavelength for separation with the high accuracy of 98% was at 850 nm (Geng *et al.*, 2019). Maestresalas *et al.* (2016) study developed a system of hyper-spectral imaging to recognize potatoes that have been affected by black-spot. In Ji *et al.* (2019) study, intact potatoes were separated from defective ones using hyper-spectral imaging and were classified using support vector machine with the accuracy of 90%. Ye *et al.* (2018) detected and classified major bruised potatoes by hyper-spectral imaging.

In this paper, the abilities of two non-invasive techniques, which are the digital imaging (DI) and laser light backscattering imaging (LLBI), have been studied on detection of only α-solanine in potato tubers. For this purpose, algorithms were developed for both techniques and compared with each other.

Material and Methods

Sample preparation

Potato tubers of 'Donald' and 'Ceasar' cultivars were bought in late June and November 2016 from a market in Urmia, Iran (70 and 100 homogenous samples of 'Donald' and 'Ceasar' cultivars, respectively). Then, potato samples were kept in the dark and cool (4±2 ºC) room until doing the experiments, because light exposure and high temperature can induce the potato tubers and increase the formation of these glycoalkaloids in them. Finally, potato tubers have been washed with water and dried.

Two dimensional (2-D) imaging systems

The imaging was done in two different environments for RGB digital imaging and laser light backscattering imaging methods, one under white LED bubble into the imaging chamber and the other under laser light in absolutely dark room.

Imaging set-ups

Digital imaging chamber

Image preparation of potato tubers was performed in an imaging chamber with the dimensions of 55×40×25 cm. It has consisted of the white LED bubbles per each side and a cavity for locating the camera lenses at the top. A digital camera equipped with a CCD sensor (Sony Cyber-Shot, Model DSC-W200, Japan) was used for this purpose.

Optical set-up

A laser imaging system has been used to this study. It included the following tools; a CMOS camera (Sony Cyber-Shot, Model DSC-HX9V, Japan), a semiconductor laser at 635 nm (3 mW power, the diameter of 2 mm for beam spot), two polarized filters, a cubic beam splitter, and a potato holder. The camera was assembled perpendicular toward the laser light, and the backscattering light was recorded by a camera (Fig.1).

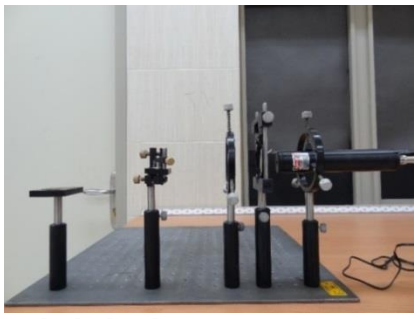

Fig.1. The laser light backscattering imaging optical set-up

Acquiring digital images

The images were captured by the CCD digital camera from both sides of potato with 3264×2448 pixels resolution in RGB color space. 140 and 200 images were taken from potato tubers of cv. 'Donald' and 'Ceasar', respectively. Additionally, different regions of potatoes were in the exposure of the laser light. Therefore, images have been acquired by the CMOS camera with the resolution of

4608×3456 pixels in RGB space. In LLBI method, 210 and 300 images were captured from the surface of potato tubers of cv. 'Donald' and 'Ceasar', respectively.

Digital image processing

RGB Digital imaging processes

After transferring the images to a personal computer (PC), processing operations were done by MATLAB software as following:

- Distinguishing potato tubers from the backgrounds (*DPB*) by equations 1 and 2:

$DPB = 1.7G - R - B$ (cv. Donald) (1)

$DPB = B - G + 0.5R$ (cv. Ceasar) (2)

- Calculating the total area of potato on binary image (showed as *A*)
- Extracting the green parts of potato by *XOR* function
- Acquiring the area of the extracted region (showed as *C*)
- Calculating the percentage of green parts in total parts of potato by equation 3:

$$S = \frac{C}{A} \times 100 \quad (3)$$

- Multiplying the binary image of extracted green regions by *R*, *G*, and *B* components
- Averaging the values of *R*, *G*, and *B* components for green regions.

Some morphological features such as the percentage of green parts of potato in total parts of potato and mean values of R, G, and B components for green parts were extracted. Fig.2 shows the processing levels of the images. Since some features such as the conditions of environment and the instrument can influence the RGB measurements of a digital camera, the calibration of the device is necessary. For this reason, Minolta colorimeter (Konica Minolta Chroma Meter, Model CR-400, Japan) has been used in $L^*a^*b^*$ color space.

LLBI processing

After taking the backscattering images, processing operations were done using MATLAB software. Acquired Laser parameters for each image were backscattered area (A_{635}), the amplitude (a_1), and half-width (c_1) coefficients of Gaussian curves. Fig.3 shows the intensity diagrams of scattering light in red channels of the images for both groups of potatoes.

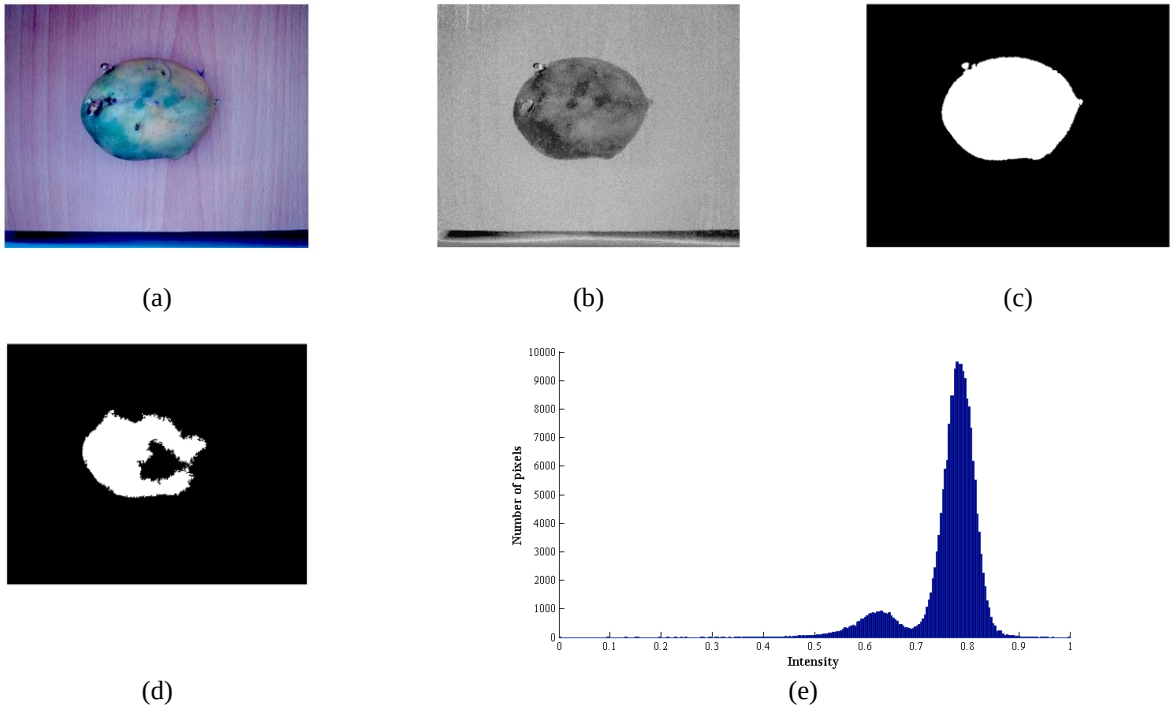

Fig.2. The processing stages of images (cv. 'Ceasar'); (a) the original image, (b) gray- level image, (c) binary image, (d) extracted green region, (e) histogram for separating potato tubers from background

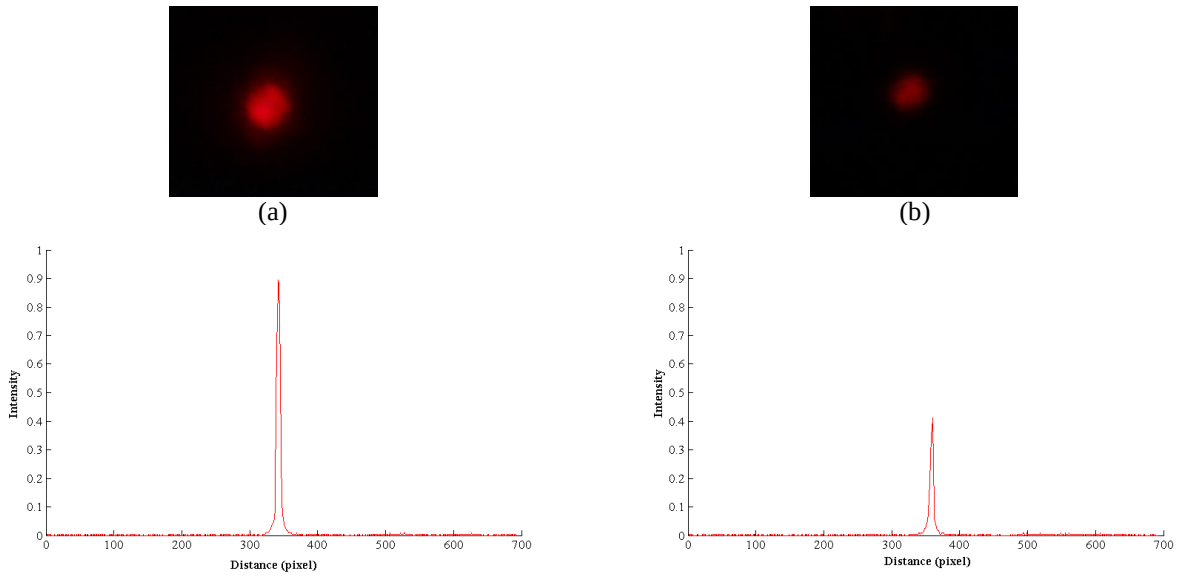

Fig.3. (a & b) The backscattered images for healthy and toxic potatoes, respectively, (c & d) the intensity diagrams of scattering light in red channels for healthy and toxic potatoes, respectively (cv. 'Donald')

Destructive test for measuring solanine

A chemical and destructive analysis is needed to quantify glycoalkaloids in potato samples, including high-performance liquid chromatography (HPLC) system. Based on Rytel (2012) study, the ratio between α-chaconine and α-solanine has been concluded about 65 to 35, so the acceptable level of α-solanine in tubers is 70 mg kg^{-1} fresh weight of potato. Therefore, potatoes would be categorized based on this quantity. For this purpose, HPLC instrument (Smartline series, Knauer Co., Germany) was used and α-solanine was separated during the elution with the mobile phase at the flowing rate of 1.5 mL/min. Then, α-solanine was determined by a UV detector at 207 nm, and the amount of α-solanine in samples was measured by comparing it with the peak area of standard chromatogram at the retention time of 2.6 min.

Table ***1*** shows the chromatography analysis of potato samples in some tubers.

Table 1- HPLC analysis of potato tubers (cv. 'Donald & Ceasar')

Potato classification	cv. 'Donald' α- solanine (mg kg^{-1} of fresh potato)	cv. 'Ceasar' α- solanine (mg kg^{-1} of fresh potato)
Healthy	44.5	39.81
	61.93	50.45
	64.55	68.98
Toxic	83.60	70.15
	93.43	88.76
	113.98	107.69

Classification of potatoes by artificial neural networks (ANNs)

The artificial neural networks classified potatoes into healthy and toxic categories based on the extracted features. The

Levenberg-Marquardt network was trained with 70 percent of the data. This network depends on improving the descent gradient and mean square error (MSE) (Kaveh *et al.*, 2019). For applying error back-propagation network, differentiating of transfer function is important. Therefore, the hyperbolic tangent sigmoid function was applied as a transfer function in a single layer perceptron neural network (SLPN).

Results and Discussion

Digital camera calibration

The results demonstrated that relationships between the digital camera and colorimeter data were linear and correlation coefficients for L^*, a^*, and b^* values were 0.917, 0.948, and 0.903, respectively (Fig.4).

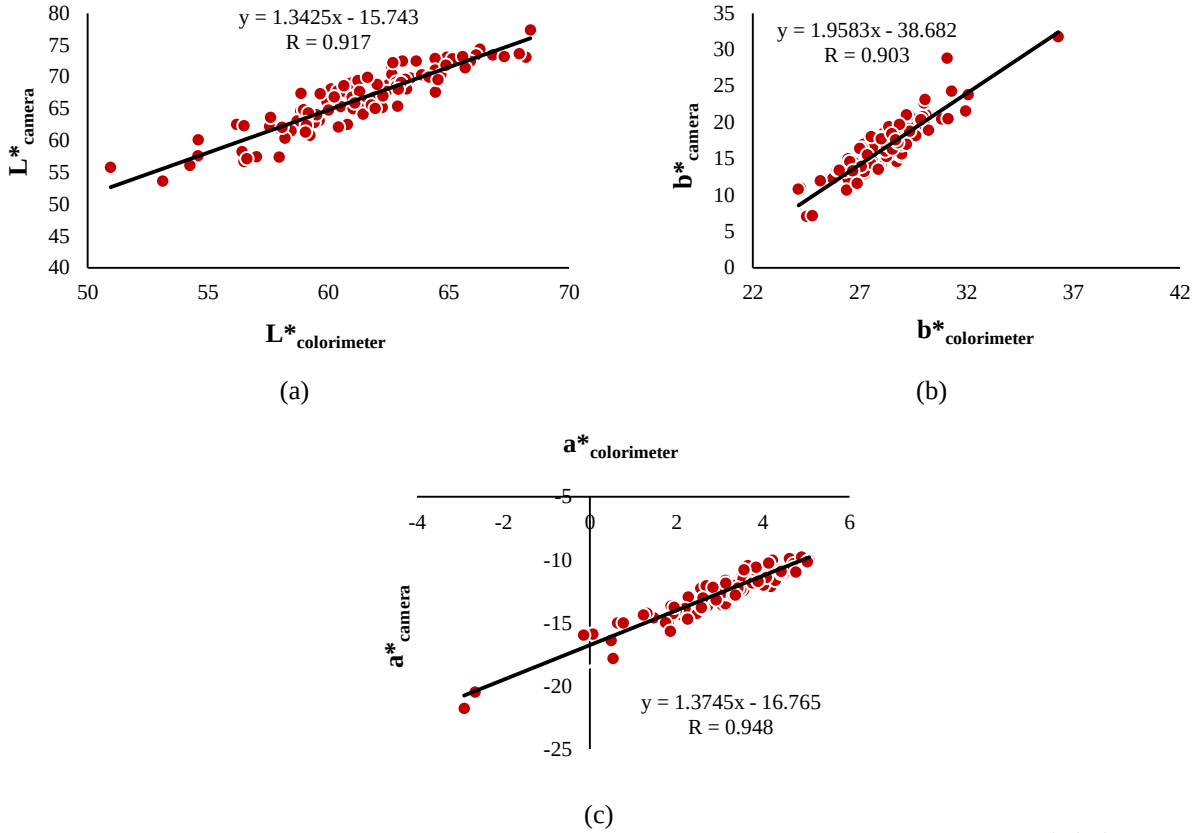

Fig.4. Correlation diagrams between Minolta colorimeter and digital camera in $L^*a^*b^*$ space

Classification of potatoes using digital images

The potato tubers were classified into two categories, healthy and toxic, based on four extracted characteristics using ANNs. These features such as the percentage of green parts of potato in total parts of potato and mean values of R, G, and B components of green parts were the inputs in topography of the designed ANNs. The best performance in ANNs was achieved when the numbers of neurons were six based on MSE of 0.019543 for cv. 'Donald' and five with the MSE of 0.00023482 for cv. 'Ceasar' (Fig.5). The accuracies for these topographies were reported to be 94.28% and 98.88% for cv. 'Donald' and 'Ceasar', respectively. The main reason for achieving the high accuracies is determining the different relations for each cultivar to separate the potato tubers from the background. Extracting the threshold relations was based on trial and error that this method is quite difficult for all cultivars of potatoes in on-line applications. Fig.6 demonstrates a sample of confusion matrixes of LED-excitation imaging system for cv. 'Ceasar'.

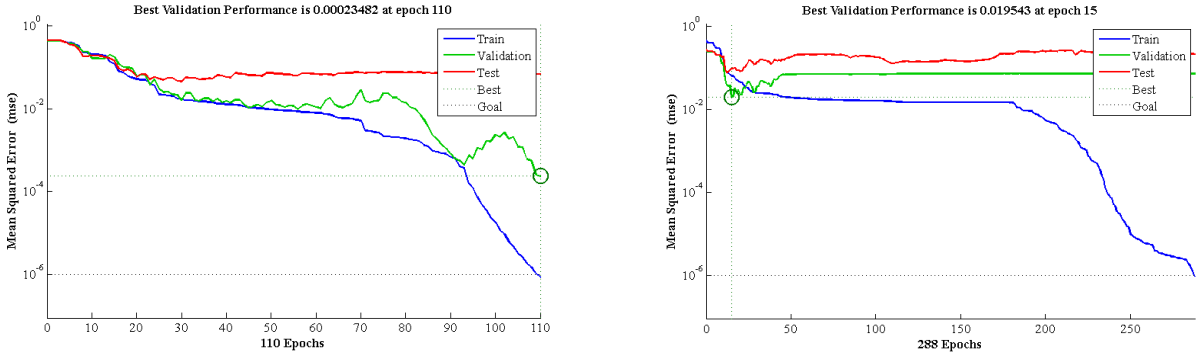

(a) (b)

Fig.5. The performance diagram in DI system; a) 'Ceasar', and b) 'Donald' cultivars

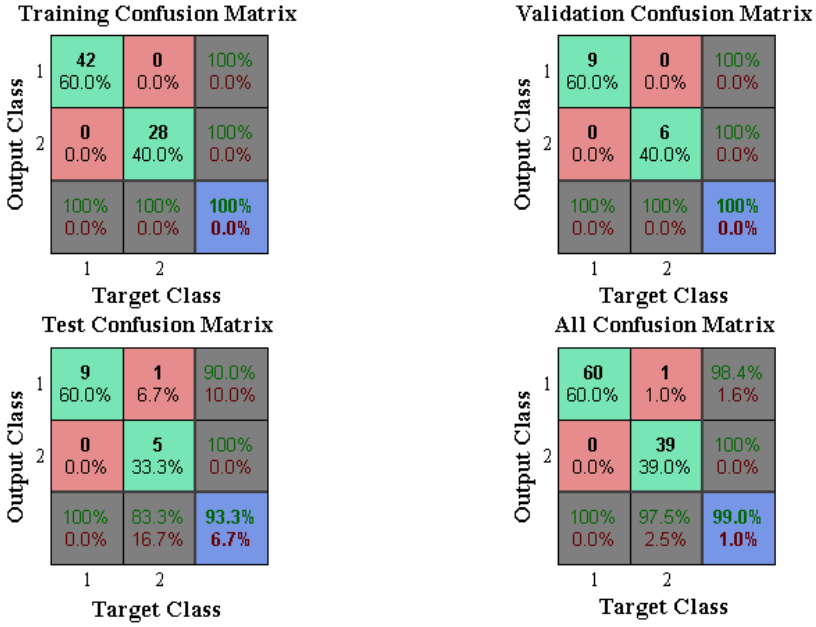

Fig.6. A sample of confusion matrixes for the digital imaging system (cv. 'Ceasar')

Classification of potatoes by LLBI images

In this technique, three features that have been mentioned before were the inputs of designed ANNs. The ANNs accuracy values for cv. 'Donald' and 'Ceasar' were 98.66% and 99.16%, respectively. The performance diagram for LLBI system is shown in Fig.7. Here is the reason that how changes in the amount of solanine can affect the backscattering area of laser in potato tubers. Solanine appears in green color at the surface of the potato. When the laser beam in the wavelength of red region encounters with the tuber, it can cause a deduction in the backscattered area. Hence, changes in backscattering area lead to variations in amplitude and half-width parameters in the Gaussian curves, thus the amount of solanine can be predicted using of these parameters.

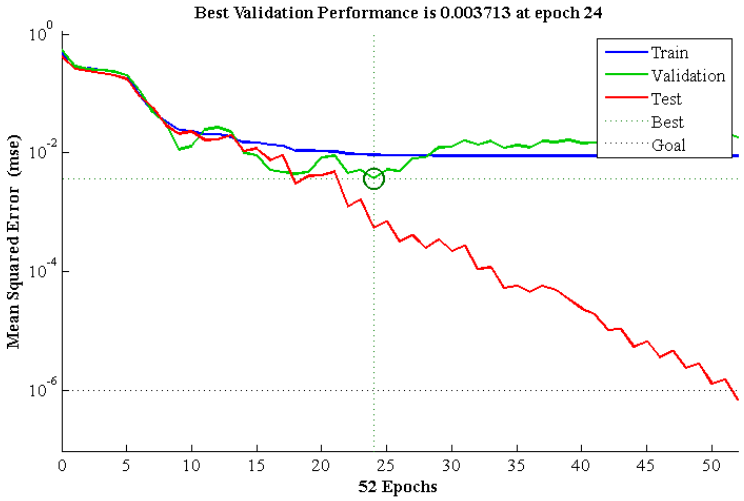

Fig.7. The performance diagram of LLBI system for cv. 'Ceasar'

Comparison of two non-invasive techniques

In this research, two varieties of potato tubers have been studied using two imaging (DI and LLBI) systems. In the DI system, the accuracy of the network in 'Donald' cultivar was fewer than 'Ceasar' tubers. The reason can be described based on this fact that 'Donald' tubers had brighter skin than 'Ceasar' potatoes. Therefore, the algorithm has been mistaken in the calculation of area in some samples. As well as, the classification algorithm in 'Ceasar' cultivar was better than 'Donald' tubers in the LLBI system. The comparison of results in both cultivars shows that the accuracies of networks in 'Ceasar' potato tubers were higher than 'Donald' samples due to the textural properties of potato samples, because 'Donald' variety is a spring cultivar of potato that has an easily-to-cut and soft skin. During the time, there can be occurred enzymatic browning phenomena surround the bruised regions and can cause errors. However, 'Ceasar' samples have a thicker skin in comparison with another variety and they do not have the problem of scabbing.

In general, LLBI system was more accurate than DI system in both cultivars, but there were some advantages and disadvantages of each ones. In DI systems, the reflectance of light in the imaging chamber can influence the results, so finding the best relationship between R, G, and B components for separating the considered region from the background is difficult. Moreover, the algorithm needs more neurons to have a good classification. Therefore, this causes the complexity in the structure and topography of the designed ANN. However, the structure of ANN in LLBI systems was simple, especially in cv. 'Donald' with just three neurons. In this case, the study should be done in an absolutely dark environment that is difficult for human beings to work in these situations, but it is suitable for industrial and optical devices that decreases the errors resulting from the environmental noises. It can be stated that LLBI system has this opportunity to be commercialized.

Recently, these non-invasive methods for detection of glycoalkaloids in potato tubers have been employed. There are few studies about the determination of solanine with the image processing method. Ebrahimi *et al.* (2011) reported that the average error of image processing for estimating the greening areas of potatoes was 5.26% just for 25 images without doing any reference test to be sure about the real quantities of glycoalkaloids. In the current research, there was a widespread data with a less amount of error that shows the reliability of the used technique. In addition, HPLC technique was necessary to confirm the image processing data that other studies did not do it at all. In Tavakoli and Najafzadeh (2015) study, the authors used the image processing

method for recognizing just the sprouts without reporting any accuracy for their work. Gao *et al.* (2018) used hyper-spectral imaging for identifying the sprouted potatoes from the others with the accuracy of 95.3%. In the case of LLBI, there is not any study by other researchers to use it for detecting solanine, but this technique has been used in many areas such as measuring the moisture content and shrinkage of agricultural products after drying (Udomkun *et al.*, 2014), soluble solid content, and firmness of products (Mollazade *et al.*, 2013).

Conclusions

In this research, α-solanine could be detected by digital imaging and laser light backscattering imaging techniques in potato tubers. So, both methods can be successfully used in the food industry. In LLBI technique, it can be applicable in cultivars with smooth surfaces. But in the digital imaging system, different relations are needed for different cultivars of potatoes separation from the background. Although, LLBI technique is used in a dark environment, it can be said that LLBI systems might take precedent over LED imaging systems due to their high accuracy, rapidity, and industrial capability. There is little information about laser backscattering imaging and more studies are needed to check the effects of some morphological parameters on LLBI systems.

Acknowledgment

The authors would like to acknowledge Prof. Dr. K. Farhadi (Department of Chemistry, Urmia University, Urmia, Iran), for his collaboration on this project.

References

1. Espinoza, M. A., G. Istamboulie, A. Chira, T. Noguer, M. Stoytcheva, and J. L. Marty. 2014. Detection of glycoalkaloids using disposable biosensors based on genetically modified enzymes. Analytical Biochemistry. Article in press. DOI: 10.1016/j.ab.2014.04.005.
2. FAOSTAT. 2008. International year of the potato. New light on a hidden treasure. An end-of-year review. Rome.
3. FAO/WHO. 2003. Joint FAO/WHO expert committee on food additives. Sixty-first meeting. Summary and conclusions. 52: 22. Retrieved from ftp://ftp.fao.org/es/esn/jecfa/jecfa61sc.pdf.
4. Ji, X., L. Rivers, Z. Zielinski, M. Xu, E. MacDougall, J. Stephen, and J. Zhang. 2012. Quantitative analysis of phenolic components and glycoalkaloids from 20 potato clones and in vitro evaluation of antioxidant, cholesterol uptake, and neuroprotective activities. Food Chemistry 133 (4): 1177-1187.
5. Kaveh, M., Y. Abbaspour-Gilandeh, R. Amiri Chayjan, and R. Mohammadigol. 2019. Comparison of mathematical modeling, artificial neural networks and fuzzy logic for predicting the moisture ratio of garlic and shallot in a fluidized bed dryer. Journal of Agricultural Machinery 9 (1): 99-112. (In Farsi).
6. E. Rytel. 2012. Changes in the Levels of Glycoalkaloids and Nitrates after the Dehydration of Cooked Potatoes. American Journal of Potato Research 89 (6): 501-507.
7. Tavakoli, M., and M. Najafzadeh. 2015. Application of the image processing techniques for separating sprouted potatoes in the sorting line. Journal of Applied Environmental and Biological Sciences 4 (11S): 223-227.
8. Wu, D., and D. W. Sun. 2013a. Advanced applications of hyperspectral imaging technology for food quality and safety analysis and assessment: A review- Part I: Fundamentals. Innovative Food Science and Emerging Technologies 19: 01-14.
9. Wu, D., and D. W. Sun. 2013b. Advanced applications of hyperspectral imaging technology for food quality and safety analysis and assessment: A review- Part II: Applications. Innovative Food Science and Emerging Technologies 19: 15-28.
10. Gao, Y., Q. Li, X. Rao, and Y. Ying. 2018. Precautionary analysis of sprouting potato eyes using hyperspectral imaging technology. International Journal of Agricultural and Biological

Engineering 11 (2): 153-157.
11. Ebrahimi, E., K. Mollazade, and A. Arefi. 2011. Detection of greening in potatoes using image processing techniques. Journal of American Science 7 (3): 243-247.
12. Udomkun, P., M. Nagle, B. Mahayothee, and J. Müller. 2014. Laser-based imaging system for non-invasive monitoring of quality changes of papaya during drying. Food Control 42: 225-233.
13. Mollazade, K., M. Omid, F. A. Tab, Y. R. Kalaj, S. S. Mohtasebi, and M. Zude. 2013. Analysis of texture-based features for predicting mechanical properties of horticultural products by laser light backscattering imaging. Computers and Electronics in Agriculture 98: 34-45.
14. Geng, J., L. Xiao, X. He, and X. Rao. 2019. Discrimination of clods and stones from potatoes using laser backscattering imaging technique. Computers and Electronics in Agriculture 160: 108-116.
15. Maestresalas, A. L., J. C. Keresztes, M. Goodarzi, S. Arazuri, C. Jaren, and W. Saeys. 2016. Non-destructive detection of blackspot in potatoes by Vis-NIR and SWIR hyperspectral imaging. Food Control. Article in press. DOI: 10.1016/j.foodcont.2016.06.001.
16. Ji, Y., L. Sun, Y. Li, J. Li, S. Liu, X. Xie, and X. Yuantong. 2019. Non-destructive classification of defective potatoes based on hyperspectral imaging and support vector machine. Infrared Physics and Technology. Article in press. DOI: 10.1016/j.infrared.2019.04.007.
17. Ye, D., L. Sun, W. Tan, W. Che, and M. Yang. 2018. Detecting and classifying minor bruised potato based on hyperspectral imaging. Chemometrics and Intelligent Laboratory Systems. Article in press. DOI: 10.1016/j.chemolab.2018.04.002.

نشریه ماشین‌های کشاورزی
جلد ۱۰، شماره ۱، نیمسال اول ۱۳۹۹، ص ۵۸-۴۹

Journal of Agricultural Machinery
Vol. 10, No. 1, Spring- Summer 2020, p. 49-58

مقایسه‌ی روش‌های پس‌پراکنشی لیزر و تصویربرداری دیجیتال روی تشخیص آلفا- سولانین در سیب‌زمینی

سعیده بابازاده[۱]، پرویز احمدی مقدم[۲*]، آرش ثباتیان[۳]، فاروق شریفیان[۴]

تاریخ دریافت: ۱۳۹۷/۱۲/۲۸
تاریخ پذیرش: ۱۳۹۸/۰۶/۲۰

چکیده

هدف اصلی این تحقیق، بررسی توانایی‌های دو روش غیر مخرّب، تصویربرداری دیجیتال (DI) و تصویربرداری پس‌پراکنشی نور لیزر (LLBI)، روی تشخیص سم آلفا- سولانین در سیب‌زمینی است. نمونه‌های سیب‌زمینی در گروه‌های سالم و سمّی براساس مقدار آلفا- سولانین موجود دسته‌بندی شدند. کروماتوگرافی مایع با عملکرد بالا (HPLC) برای تعیین مقدار آلفا- سولانین موجود در غده‌های سیب‌زمینیی استفاده گردید. نتایج طبقه‌بندی نشان داد که شبکه عصبی پرسپترون تک لایه می‌تواند سیب‌زمینی‌ها را با دقّت ۹۴/۲۸٪ و ۹۸/۶۶٪ به ترتیب توسط سیستم‌های تصویربرداری دیجیتال و پس پراکنشی لیزر (رقم دونالد) طبقه‌بندی نماید. می‌توان گفت که سیستم‌های پس‌پراکنشی لیزر ممکن است از سیستم‌های تصویربرداری دیجیتال به دلیل دقّت و سرعت بالای آن و همچنین قابلیت صنعتی شدن آن سبقت گیرد.

واژه‌های کلیدی: بررسی کیفیت، تصویربرداری پس‌پراکنشی، تصویربرداری دیجیتال، کروماتوگرافی مایع، گلیکوآلکالوئیدها

۱- دانشجوی دکتری، گروه مهندسی مکانیک بیوسیستم، دانشکده کشاورزی، دانشگاه ارومیه، ارومیه، ایران
۲- دانشیار، گروه مهندسی مکانیک بیوسیستم، دانشکده کشاورزی، دانشگاه ارومیه، ارومیه، ایران
۳- دانشیار، گروه فیزیک، دانشکده علوم، دانشگاه ارومیه، ارومیه، ایران
۴- استادیار، گروه مهندسی مکانیک بیوسیستم، دانشکده کشاورزی، دانشگاه ارومیه، ارومیه، ایران
(*- نویسنده مسئول: Email: p.ahmadi@urmia.ac.ir)

DOI: 10.22067/jam.v10i1.79800

Journal of Agricultural Machinery
Vol. 10, No. 1, Spring- Summer 2020, p. 59-72

نشریه ماشین‌های کشاورزی
جلد ۱۰، شماره ۱، نیمسال اول ۱۳۹۹، ص ۷۲-۵۹

Optimization of Refinement Operations of Sugarcane Harvester Hydraulic Oil

H. Nematpour Malek Abad[1], M. J. Sheikhdavoodi[2*], I. Hazbavi[3], A. Marzban[4]

Received: 11-10-2018
Accepted: 02-01-2019

Abstract

The purpose of this study was to model and optimize the offline refinement operations of sugarcane harvester hydraulic oil using RSM. For this purpose, the effects of independent variables of operating hours (250, 500 and 750 hours), Twin Dip Filter Mesh (7, 9 and 11 microns) and hydraulic oil refining times (0, 1 and 2) on variables of water contamination, uncleanness level (NAS), silicon (Si), viscosity (Vis) and oil acid number (TAN) were evaluated. The results indicated that all models were suitable for water contamination, uncleanness level (NAS), silicon (Si), viscosity (Vis) and oil acid number (TAN) for describing experimental data. In addition, the desirability function showed that the optimum conditions for the offline refinement operations of the hydraulic oil of the sugar cane harvester included 728.61 operating hours, the 7-micron filter mesh, and the two refining times of the oil. Under this condition, the amount of water contamination, the uncleanness level (particles 5 to 15 micrometers), Vis, Si, and TAN were equal to 187.63 ppm, 234000, 5.91 ppm, 66.34 centistokes and 0.65 (mg KOH g^{-1}), respectively.

Keywords: Offline Refinement of Hydraulic Oil, Optimization, Response Surface Method, Sugarcane harvester

Introduction

One of the important items in mechanical equipment and in general agricultural machines is the entry of contaminations including water, fuel, silica, chips, soot particles, etc. into hydraulic systems and engine oils. All mechanical equipment that uses oil for lubrication or power transmission, are always affected by the quality of the oil. In fact, Contamination is the enemy of hydraulic systems and other mechanical systems under lubrication which passes through sensitive parts or the environment via lubricant and causes damage to them. Oil contamination in mechanical systems causes major problems such as machine failure, undesired repairs, loss of oil life, etc., which directly affects the efficiency of the equipment and consequently the efficiency of the production and causes unforeseen costs. Using clean oils, removing and controlling contaminants will have many benefits including minimizing equipment failure, reducing operational and repair costs, increasing the operational efficiency of the equipment and increasing the lifespan of the oil. Types of contamination of oils include physical and chemical contaminants. The physical contaminant is the same as solid particles with oil, the most important consequence of which is mechanical erosion. Chemical contaminants generally include water, some metals such as copper and materials produced via oil usage. Therefore, there are two solutions to prevent such problems. First, evacuate all oil from the system and substitute with fresh oil or by filtration, separate particles from contaminated oil (Masoudi, 2011; Ranjbar *et al.*, 2003; Saghafi, 2008). Cargol (2005) identified most of the internal problems of machines by analyzing oil, and mentioned that doing these tests is effective for initial troubleshooting and performance enhancement. Macnian *et al.* (2006) in a study determined the time of detection and the degree of failure using oil analysis on diesel engines and the fuzzy logic.

1- PhD Graduate of agricultural mechanization, Department of Biosystems Engineering, Shahid Chamran University of Ahvaz, Iran
2- Professor, Department of Biosystems Engineering, Shahid Chamran University of Ahvaz, Iran
3- Assistant Professor, Department of Biosystems Engineering, Lorestan University, Khorramabad, Iran
4- Associate Professor, Agricultural Sciences and Natural Resources University of Khuzestan, Mollasani, Iran
(*- Corresponding Author Email: javad1950@gmail.com)
DOI: 10.22067/jam.v10i1.75912

This would prevent the car from breaking down, failure and suspension. Macinan *et al.* (2003) stated that if the erosion rate is 100 ppm, an increase of 50% is a significant warning sign to increase erosion of the devices. Qingfei He (2009) reported that the condition monitoring of machines helps prevent the destruction of machines via analyzing oils, corrosive particles, and oil contaminants. Li Jie (2010) considered the use of oil analysis programs for compressors to predict and prevent early failure of the compressors, as well as the optimal use of oil in compressors. Unfortunately, although the use of suitable oils in machinery is very necessary, there is no definite research in this regard and only parts have been mentioned in different books. One of the most important sources of sugar production is sugarcane. Sugar is one of the eight human food sources (wheat, rice, corn, sugar, cattle, sorghum, millet and cassava). Also, sugarcane is mainly used for livestock feed, electricity generation, fiber and fertilizer and in many countries sugarcane is accounted as a renewable source for biofuel (Haroni *et al.,* 2018). Therefore, the present research was conducted with the aim of optimizing the offline refinement operations of hydraulic oil of sugar cane harvester by examining the effects of independent variables of the operating hours (250, 500 and 750 hours), twin spin filter mesh (7, 9 and 11 microns), and the hydraulic oil refining times (0, 1 and 2) on dependent variables of water contamination, uncleanness level, Si, Vis and TAN (Masoudi, 2011).

Materials and Methods

Materials

The main raw materials used in the present study were hydraulic oil samples taken from cane harvesters (Austoft, 7000). The reason for choosing this model was due to its common use in cultivating the sugarcane industry in Khuzestan province).

Equipment and Appliances

For every oil-tested experiment, an example representative of the entire system was needed. Sampling is the easiest stage to run an oil analysis program, but it is very important and if the sampling is not correct, the results of the oil tests will not be valid. The main items in the oil sampling are the selection of tools, determination of sampling frequencies for different components, determination of oil sampling points in different components and oil sampling method. Some equipment was used for sampling such as 1- Sampling pump (Manual suction pump), 2- Polyethylene tube (hoses with an external diameter of one quarter or five sixteen inches), 3- Sample carrying case (Masoudi, 2003). All of the oil samples, after encoding and labeling, with a fresh and unused oil sample, were sent to the Alborz Tadbir Khuzestan Technical & Engineering Co. Laboratory (Address: 127 Azadi, km 5, Asia Road, Mashhad, IRAN) from the sample of the hydraulic oils tested.

Determination of the Exact Amount of Water in the Oil (water contamination)

The amount of water in the oil was measured by the Karl Fischer test. The result of the test reports the exact amount of water in ppm. This test, known as Crackle Test, used to identify the approximate level of water contamination in the oil. In this way, a few drops of oil are poured on a hot plate (approximately 150 ˚C). If water is present in the oil, it will be bubbled out and removed from the oil. The amount of water in hydraulic oil should not exceed 500 ppm (ISO 760, 1978).

Determination of the Uncleanness Level of Oil

Uncleanness level of oil is one of the important parameters that is mainly studied in the evaluation of hydraulic equipment and systems. The presence of impurities in the environment indicates how the filters and vents operate. Counting the solid particles in hydraulic oil was accomplished using an automatic laser method. In this method, the number of corn oil particles can be counted by the resulted shadow of laser waves. Typical uncleanness levels are usually considered for a hydraulic oil sugarcane harvester; the number of particles from 5 to 15 micrometers in oil should not exceed 256000 (ISO 4406, 1999).

Determination of the Si Amount

Silicon (Si), an anti-foaming agent in oil, if exceeds the standard limit, is considered as an

oil contaminant. In order to specify the available amount of Si in hydraulic oil, an elemental analyzer device was used. The amount of Si in hydraulic oil should not exceed 15 ppm (ASTM D6595, 2011).

Viscosity measurement of oil

Viscosity is the most important feature of lubricating oils. The viscosity test shows the internal resistance of the lubricant to the oozing. The viscosity test is normally done at temperature of 40 ˚C and 100 ˚C. Viscosity affected by factors such as the amount of oil function, oil content, contamination, composition, and other abnormalities affecting the service life of the oil. A capillary tube viscometer was used to measure viscosity in the laboratory. In this method, the oil sample is placed into the glassy U-shaped capillary tube and using a suction pump, the sample moves towards the starting point which has been specified on the tube. The suction pump is stopped and then, it is allowed that the sample moves in the opposite direction to the suction due to the gravity. The thin part of the capillary tube controls the velocity of oil flow. The oils with high viscosity take more time than the oils with low viscosity because the flow velocity inside the capillary tube is determined by yielding stress of the oil which is influenced by gravity. In fact, this test measures the kinematic viscosity of the oil. The standard guides for this method are ASTM D445 and ISO 3104. The viscosity of the hydraulic oil should not be changed from ±10% of fresh oil. The viscosity of fresh and used oil is determined in Cst (ASTM D 2270, 2010).

Measurement of the Total Acid Number (TAN)

The total acid number of oil indicates the acidity of the oil. TAN of the oil usually increases gradually with a slight slope. Oils have undergone a qualitative change over time due to various factors such as heat and contamination, where the acid number represents one of the indicators of these changes. The total acid number of hydraulic oil should not be increased by more than 0.2% toward the acid number of the fresh oil. The total acid number of hydraulic oil is measured by the titration method and is determined in (mg KOH g^{-1}) (ISO 6619, 1988).

Experimental Design and Statistical Analysis

The purpose of the present study was to optimize the refinement operations of the hydraulic oil of sugarcane harvester using the RSM method. For this purpose, the effects of independent numerical variables (operating hours, twin suction filter mesh) and categorical (hydraulic oil refinement times) on dependent variables of water contamination, uncleanness level, Vis, Si, and TAN were evaluated. For this purpose, the central composite design used in the Design Expert software included independent variables of work hours (250, 500 and 750 hours), twin suction filter mesh (7, 9 and 11 microns), and the number of hydraulic oil refinements (0, 1 and 2) with 33 treatments and 3 replications at the central point. Table (1) shows the encoded values and different levels of independent variables used for offline hydraulic oil refinement. Table (2) presents the test conditions and the response values obtained for the central composite design used to refine the offline hydraulic oil.

Data analysis was conducted using Design expert 7 software. Experimental data were also tested using the quadratic polynomial equation (Singh *et al.*, 2010).

$$Y = b_0 + b_1A + b_2B + b_3C + b_{11}A^2 + b_{22}B^2 + b_{33}C^2 + b_{12}AB + b_{13}AC + b_{23}BC \quad (1)$$

Where b_n: Regression coefficients for constant factor coefficients (b_o), Linear effect coefficient (b_1, b_2 and b_3), second-degree effect coefficients (b_{11}, b_{22} and b_{33}) and interaction effect coefficient (b_{12}, b_{13} and b_{23}). Y: The dependent variables or the desired responses include water contamination, uncleanness level, Vis, Si, and TAN. In analysis of a process, one qualitative factor is not considered, but multipurpose optimization is sought. The purposes are in contradiction with each other and have an inverse relationship. One of the problems solving methods of multipurpose issues is combining the response surfaces or the mentioned graphical solution.

Table 1- The encoded different levels of independent variables of offline hydraulic oil refinement

Independent variables	Encoded independent variables and their different levels		
Code	-1	0	+1
Operating hours	250	500	750
Filter mesh	7	9	11
Times of oil refinement	0	1	2

Table 2- Experimental design levels and measured values

Independent variable (input)					Dependent variables (responses)			
No.	Operating (hour)	Filter mesh (micron)	Times of oil refinement	Water contamination (ppm)	(NAS*1000)	Si (ppm)	Vis (centistokes)	TAN (mg KOH g^{-1})
1	250	11	2	100	109	4.2	59	0.51
2	500	9	0	100	102	4.4	67	0.52
3	750	11	0	178	282	5.8	61	0.63
4	500	7	1	97	106	3.9	72	0.51
5	500	9	0	103	112	4.5	69	0.53
6	250	9	1	75	77	3.1	63	0.48
7	500	9	2	126	122	5.2	64	0.55
8	750	7	0	153	192	4.3	68	0.54
9	250	7	1	71	70	2.5	67	0.46
10	250	11	0	80	90	3.1	61	0.48
11	250	9	0	69	74	2.3	64	0.47
12	500	11	1	131	141	5.6	62	0.59
13	500	9	0	105	122	4.7	71	0.53
14	500	9	1	108	109	4.8	66	0.54
15	500	9	1	112	122	4.9	68	0.55
16	500	7	0	90	99	3.1	73	0.5
17	250	9	2	86	93	3.5	62	0.5
18	500	9	2	130	141	5.5	66	0.56
19	500	11	0	122	125	4.8	63	0.57
20	250	11	1	88	96	3.7	60	0.49
21	750	9	0	160	218	5.1	63	0.58
22	250	7	0	66	64	2.1	68	0.45
23	250	7	2	80	83	3.2	65	0.48
24	750	7	1	172	205	5.5	67	0.61
25	500	9	1	115	154	5.1	70	0.54
26	750	9	2	210	333	6.4	61	0.72
27	750	9	1	183	230	5.8	62	0.65
28	750	11	1	205	384	6.1	60	0.71
29	750	7	2	200	230	6.2	66	0.68
30	750	11	2	241	512	6.9	59	0.77
31	500	9	2	133	166	5.7	68	0.56
32	500	11	2	148	166	6.5	60	0.6
33	500	7	2	110	115	4.8	70	0.52

Many researchers have introduced a multi-response technique and named it Satisfaction. This technique creates the objective function that equation (2) depicts Satisfaction function (D) and it indicates the range of Satisfaction for each response. The range of Satisfaction varies from zero to one among which, one is the maximum Satisfaction.

$$D=(d_1 d_2 \dots d_n)^{\frac{1}{n}} = (\prod_{i=1}^{n} d_i)^{\frac{1}{n}} \quad (2)$$

"n" represents the number of responses. If any of the responses or independent variations are placed out of the Satisfaction range, the function equals to zero. In optimization based on Satisfaction function, an objective can be defined for each response and variable. For

instance, there are some favorable interventions in which the response of y1 and y2 would be maximum and minimum respectively, provided that X1 would be in the specific range, X2 exactly equal to the specific number and X3 would be maximum (Qasemi *et al.*, 2015).

Results and Discussion

Water contamination modeling

The result of the analysis of variance for water contamination of oil samples is presented after the test of the exact determination of the amount of water in the oil (Table 3). According to the results, the quadratic polynomial equation used to predict oil contamination was statistically significant (P <0.01) and its lack of fit test was not significant (P>0.05), which indicates the suitability of the model used to predict the effect of independent variables on water contamination. In addition, all linear statements of the model used (A, B, C) were significant (P <0.01). Among the second-level expressions, the second-level expressions of operating hours (P <0.01,A^2) and filter mesh (P <0.05,B^2) were significant. Among independent variables, interacting hours of work- filter mesh (P <0.05, AB) and operating hours-number of refinement (P <0.01, AC) were significant. The obtained results for the correlation coefficients of the model (R^2=0.995 and $R^2_{adjusted}$ =0.992) also indicate that the regression model used with the tested points and its high accuracy in predicting the value of the dependent variable of water contamination was very good. Equation (3) indicates a Quadratic polynomial model used to predict the amount of water contamination based on the actual values after eliminating non-significant factors.

$$\text{Water} = +113.82 + 54.83\ time + 14.11\ mesh - 14.21\ filter[1] - 2.30\ filter[2] + 4.00\ time * mesh - 8.83\ time * filter[1] - 0.50\ time * filter[2] + 17.94\ time^2 + 3.77\ mesh^2 \quad (3)$$

Table 3- Analysis of variance of water contamination of oil samples

Source	Sum of squares	df	Mean square	F Value	Prob > F	
Model	67279.44	11	6116.31	351.04	<0.0001	significant
A-time	54120.50	1	54120.5	3106.2	<0.0001	
B-mesh	3584.22	1	3584.22	205.71	<0.0001	
C-filter	5280.42	2	2640.21	151.53	<0.0001	
AB	192.00	1	192.00	11.02	0.0033	
AC	992.33	2	496.17	28.48	<0.0001	
A2	2445.63	1	2445.63	140.36	<0.0001	
B2	108.13	1	108.13	6.21	0.0212	
Residual	365.89	21	17.42			
Lack of Fit	303.89	15	20.26	1.96	0.2084	not significant
Pure Error	62.00	6	10.33			
Cor Total	67645.33	32				

In this case (after eliminating non-significant factors), the possibility of using the new model was also examined and the significance of the model (P <0.01) and non-significance of lack of fit, as well as the significance of the linear effects (A, B, and C), the second degree (A^2 and B^2), and the interactions (AB and AC) was confirmed. In general, the first-degree expressions A, the second-degree expressions A^2, the first-degree C, the first-degree B, as well as the AC interaction effect, had the highest effect on the degree of contamination of water, respectively. The interaction effect AB and the second-degree B^2expression were also important at a later stage.

Fig 1 shows the interaction effects of operating hours and the filter mesh (times of oil

refinement at the central point) on the amount of water contamination. As it can be seen, the graph has an upward edge and in every operating hour, by increasing the filter mesh, the water contamination increases nonlinearly (second degree). In this case, the significance of the effect of the second- degree expression of the filter mesh affirms this observation (Table 3). This increase is higher at higher operating hours, which can be attributed to the effect of the operating hours with a higher filter mesh on the amount of water contamination. In each mesh of filtering, with increasing hours, water contamination also increased nonlinearly, and the highest water contamination was at 750 operating hours and the 11 of the filter mesh. Finally, concerning the changes' reasons, it can be concluded that the more operating time, the more depreciation and the parts rust could happen; accordingly leading to contamination of the oil, and also, passing time causes an increase in water influx into the oil.

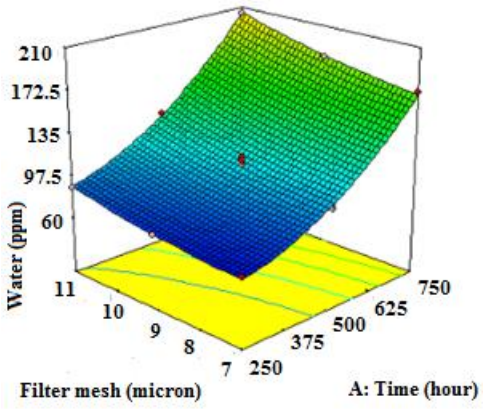

Fig.1. Interaction between the operating hours and filter mesh on the amount of water contamination

Modeling the Level of Oil Uncleanness

The results of the analysis of variance for the level of the uncleanness of oil samples are presented in Table 4. According to the results, the quadratic polynomial equation used to predict the level of oil uncleanness was statistically significant (P<0.01) and lack of fit test was not significant (P>0.05), which indicates the suitability of the model used to predict the effect of independent variables on determining the level of oil uncleanness. In addition, all linear statements of the model used (A and B at P <0.01 and C at P<0.05) were significant.

Table 4- Results of the variance analysis of the uncleanness of oil samples

Source	Sum of squares	df	Mean square	F Value	Prob > F	
Model	2.937E+005	11	26699.93	30.64	<0.0001	significant
A-time	1.860E+005	1	1.860E+005	213.48	<0.0001	
B-mesh	30504.50	1	30504.50	35.00	<0.0001	
C-filter	16220.36	2	8110.18	9.31	0.0013	
AB	18644.08	1	18644.08	21.39	0.0001	
AC	9145.33	2	4572.67	5.25	0.0142	
A2	23878.42	1	23878.42	27.40	<0.0001	
Residual	18301.47	21	871.50			
Lack of Fit	16054.80	15	1070.32	2.86	0.1009	not significant
Pure Error	2246.67	6	374.44			
Cor Total	3.120E+005	32				

Among the second-degree expressions, the only second-degree expression operating hours (A^2 at P <0.01) was significant. Among the independent variables, the interaction of operating hours-filter mesh (AB at P <0.01) and operating hours-frequency of refinement (AC at P <0.05) were significant. The obtained results for the correlation coefficients of the model (R^2=0.941, $R^2_{adjusted}$= 0.911) also indicate a very good correlation between the regression model used with the tested points and its high accuracy in predicting the value of the dependent variable on the level of oil uncleanness. Equation (4) shows a quadratic polynomial model used to predict the level of the uncleanness of oil based on the actual values after eliminating non-significant factors.

$$NAS = +122.58 + 101.67\ \text{time} + 41.17\ \text{mesh} - 24.36\ filter[1] - 4.91\ \text{filter}[2] + 39.42\ time * mesh - 24.33\ time * filter[1] - 5.67\ time * filter[2] + 56.05 time^2 \quad (4)$$

In this case (after eliminating non-significant factors), it was also possible to use the new model and the significance of the model (P<0.01) and non-significance of the lack of fit and also the significance of linear effects (A, B, And C), second degree (A^2) and interactions (AB and AC) was confirmed. Generally, the first-degree expressions A, the second-degree A^2, as well as the AB interaction effect, had the most effect on the level of oil uncleanness. The interaction of AC and the linear effect of C were also important in the next step. Figure 2 indicates the interactions between operating hours and filter meshes (times of oil refinement at the central point) on the level of oil purification.

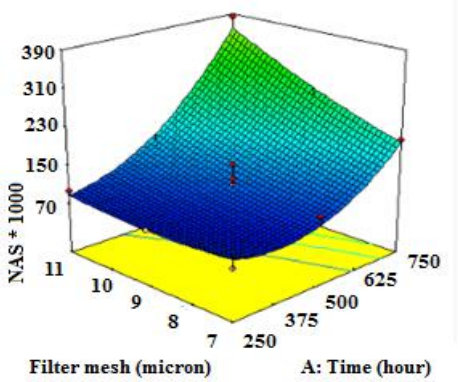

Fig.2. Interaction of the operating hours and filter mesh on the level of oil uncleanness

As can be seen, in any mesh of the filter, with increasing operating time (hours), the level of oil uncleanness increases linearly. The significance of the second-degree operating hour's expression in Table 4 confirms this conclusion. In every operating hour with increasing filter mesh, the level of oil uncleanness increased almost linearly and the highest level of oil uncleanness was 384000 particles (number of particles 5 to 15 micrometers) in 11 filter mesh and 750 hours of the operating hours. The positive coefficients of Equation (4) and the significance of quadratic and linear expressions of Table (4) confirm these trends.

Modeling the Si Rate

The results of the analysis of variance of Si of oil samples are presented in Table (5). According to the results, the second-degree polynomial equation used to predict the amount of Si of oil which was statistically significant (P<0.01) and its lack of fit test was not significant (P>0.05), which indicates the suitability of the model used to predict the effect of independent variables on determining the amount of Si oil. In addition, all linear

statements of the model used (A, B, and C) were significant (P<0.01).

Among the second-degree expressions, the only second-degree expression the operating hours (A^2 at P <0.01) was significant. The obtained results for the correlation coefficients of the model (R^2= 0.971, $R^2_{adjusted}$= 0.956) also indicate a very good correlation of the regression model used with the tested points and its high precision in predicting the value of the dependent variable of the amount of Si of oil.

Table 5- Analysis of variance of Si in samples of oil

Source	Sub of squares	df	Mean square	FValue	Prob > F	
Model	50.64	11	4.60	64.47	<0.0001	significant
A-time	33.08	1	33.08	463.21	<0.0001	
B-mesh	6.84	1	6.84	95.86	<0.0001	
C-filter	8.78	2	4.39	61.51	<0.0001	
A2	1.58	1	1.58	22.15	0.0001	
Residual	1.50	21	0.071			
Lack of Fit	1.28	15	0.085	2.33	0.1523	not significant
Pure Error	0.22	6	0.037			
Cor Total	52.14	32				

Equation (5) shows a second-degree polynomial model used to predict the amount of Si of oil based on the actual values after eliminating non-significant factors.

$$Si = +4.92 + 1.36\ time + 0.62\ mesh - 0.63\ filter[1] - 003\ filter[2] - 0.46\ time^2 \quad (5)$$

In this case (after eliminating non-significant factors), the possibility of using the new model was also examined and the significance of the model (P<0.01) and non-significance of the lack of fit and also the significance of linear effects (A, B, and C) and the second degree (A^2) were confirmed. In general, the first-degree expression of the model (A, B and C) and the second-degree A^2expression had the most effect on the amount of Si of oil.

Modeling the Viscosity Rate of Oil

The results of the variance analysis of Vis of oil samples are presented in Table 6. According to the results, the second-degree polynomial equation used to predict the viscosity of oil was statistically significant (P<0.01) and its lack of fit test was not significant (P>0.05), which indicates the suitability of the model used to predict the effect of independent variables on Vis of oil; in addition, linear statements of the model used, B (P<0.01) and C (P<0.05) were significant. Among the second-degree expressions, the only second-degree expression of the operating hours (A^2 at P<0.01) was significant. The results obtained for the correlation coefficients of the model (R^2= 0.913, $R^2_{adjusted}$=0.867) also indicate a very good fit of the regression model used with the tested points and its high accuracy in predicting the value of the dependent variable of the viscosity of the oil. Equation (6), the second-degree polynomial model used to predict the viscosity of oil based on the actual values after eliminating non-significant factors.

$$Vis = +67.26 - 3.94\ mesh + 1.18\ filter[1] + 0.18\ filter[2] - 4.16\ time^2 \quad (6)$$

In this case (after eliminating non-significant factors), the possibility of using the new model was also examined and the significance of the model (P<0.01) and the non- significance of lack of fit, as well as the significance of the linear effects (B, C) and the second degree (A^2), was confirmed. In general, the second-degree expressions A^2 and first-degree B had the greatest effect on Vis. The first-degree expression C was also important in the next step.

Modeling of the Acid Number (TAN) of Oil

The results of the analysis of variance for the TAN of the oil samples are presented in Table 7. According to the results, the second-degree polynomial equation used to predict oil TAN was statistically significant (p<0.01) and the lack of fit test was not significant (P>0.05), which indicates that the model was used to

predict the effect of independent variables on the acid number of oil. In addition, all linear statements of the model used (A, B, and C) were significant (P<0.01).

Table 6- The results of the variance analysis of Vis in oil samples

Source	Sum of squares	df	Mean square	F Value	Prob > F	
Model	458.05	11	41.64	19.90	<0.0001	significant
B-mesh	280.06	1	280.06	133.83	<0.0001	
C-filter	36.18	2	18.09	8.65	0.0018	
A2	131.39	1	131.39	62.79	<0.0001	
Residual	43.95	21	2.09			
Lack of Fit	19.95	15	1.33	0.33	0.9610	not significant
Pure Error	24.00	6	4.00			
Cor Total	502.00	32				

Among the second-degree expressions, only the second-degree of operating hours (A^2 at P<0.05) was significant. Among the independent variables, interacting with operating hours- filter mesh (AB at P<0.05) and operating hours-times of refinement (AC at P<0.01) were significant. The results for the correlation coefficients of the model (R^2= 0.974, $R^2_{adjusted}$= 0.961) also indicate that the regression model used with the tested points is very appropriate and its high accuracy in predicting the value of the dependent variable of the acid number of the oil. Equation (7) shows a second-degree polynomial model used to predict the acid number of oil based on the actual values after eliminating non-significant factors.

$$TAN = +0.54 + 0.087\ time + 0.033\ mesh - 0.030\ filter[1] - 004\ filter[2] + 0.016\ time * mesh - 0.029\ time * filter[1] - 003\ time * filter[2] + 0.022\ time^2 \quad (7)$$

In this case (after eliminating non-significant factors), the use of the new model was also examined and the significance of the model (P<0.01) and the non- significance of lack of fit and also the significance of linear effects (A, B and C), second degree (A^2) and interactions (AB and AC) were confirmed. In general, the first-degree expressions of the model and the interaction effect (AC), respectively, had the most effect on the acid number of the oil. The second-degree expression $A^2$and the interaction effect of AB were also important in the next step.

Table 7- results of variance Analysis for determining the TAN of oil samples

Source	Sum of squares	df	Mean square	F Value	Prob > F	
Model	0.19	11	0.018	71.82	<0.0001	significant
A-time	0.14	1	0.14	561.78	<0.0001	
B-mesh	0.020	1	0.020	82.05	<0.0001	
C-filter	0.019	2	9.603E-003	39.40	<0.0001	
AB	3.008E-003	1	3.008E-003	12.34	0.0021	
AC	9.144E-003	2	4.572E-003	18.76	<0.0001	
A2	3.568E-003	1	3.568E-003	14.64	0.0010	
Residual	5.119E-003	21	2.438E-004			
Lack of Fit	4.919E-003	15	3.279E-004	9.84	0.50	not significant
Pure Error	2.000E-004	6	3.333E-005			
Cor Total	0.20	32				

Figure 3 indicates the interaction effects of the operating hours and the filter mesh (times of oil refinement at the central point) on the acid number of the oil (TAN). As can be seen, the graph has an upward edge, and each hour of the function, with increasing filter mesh, the acid number of the oil increases almost linearly. In each mesh of the oil filter, increasing the operating time of the harvester, the acid number of the hydraulic oil increases non-linearly (second degree). The highest acid number of oil was 0.71 (mg KOH g^{-1}) after 750 hours of operation and the filter was used with a mesh of 11. The positive coefficients of

equation (7) and the significance of second-degree and linear expressions of Table (7) confirm these trends. Finally, with regard to the changes' reasons, it can be concluded that influx of suspended particles in the oil is increased as the filter mesh (diameter of filter grids) rises, and also it brings about some increases in the depreciation, rust, and contamination which can change the chemical properties of the oil and the times of filtration of the remaining suspended particles in the oil are increased due to overuse of the oil before the oil change which could bring about more depreciation and the parts rust and consequently, causing an increase in the oil contamination and the chemical changes of the oil. In order to confirm the achieved results, it can be stated that Blouki (2009) in research titled "determination of the best time to change engine oil of transtainer crane (RTG) using oil condition monitoring techniques" analyzed the oil condition monitoring techniques to decrease the cost and environmental damages. Therefore, it was concluded that a precise viewpoint concerning the future status of the machine can be achieved. Reducing the engine oil consumption as a result of rising its operating time can help the national economy by reducing the currency exchange costs arising from the importing inputs of petrochemical industries. This research was focused on the mentioned machines and equipment which are being worked in Imam Khomeini port. In order to test the oil degradation, the specified amount of the oil samples was prepared at regular intervals (110, 130, 150 and 170 hours) during the operating time of the crane. In this research, two operational and predictive criteria were utilized to analyze the oil condition in which the two criteria evaluate the existing rust in the oil so that the normal amount of various rusting elements is up to 100 ppm. A 50% increase in these elements could be a proper warning. It should be noted that for further rusting, this percentage should be declined while this value should be considered more for the slow rusting condition. Therefore, it was observed in the study that engine oil of the studied cranes can work for 170 hours without any problem and the oil change is not economical in 125 hours. The percentage of changes in rusting elements of the oil was less than 50 % for all elements, however, several elements such as Iron and Chromium are in warning threshold. Finally, evaluating five categories of oil index achieved by oil analysis concluded that the engine oil can work for 170 hours and the oil change in 125 hours has brought a decline in efficiency. Furthermore, Masoudi (2001) stated that the maintenance group of the locomotive condition of Iran railways has reported 123 cases of oil change in the first ten months of 2000 which were due to diagnosing unfavorable condition like water contamination, excessive increase or decrease of viscosity and unusual increase of rusting elements. Hence, the damages to 67 cylinders, 58 pistons, 281 rings and 40 sets of bearings have been prevented which can result in saving more than 309,000 dollars. Moreover, by increasing the oil function from 65000 Km to 96000 Km and preventing the unnecessary oil change, this unit has been able to save 734,000,000 rials in oil consumption. Masoudi (2001) stated that during the implementation of a Base-Line aiming to determine the rusting effect of erosive particles for a steam turbine of Arak petrochemical complex with a volume of 18000 liters, the unusual amount (17 ppm) of Silica element was identified. The amount of Tin and Aluminum rose simultaneously which implies an uncommon erosion of the device. The following graph returns to a normal situation after eliminating the contamination, and the device continues to function normally. Thus, identifying and controlling the amplifier erosion elements of expensive petrochemical and power plant equipment, using the maintenance condition of the machines lead to enormous economic savings. It should be mentioned that the financial loss due to the unplanned stoppage of the mentioned turbine was 200 million rials per hour and its major maintenance is estimated hundreds of thousands of dollars.

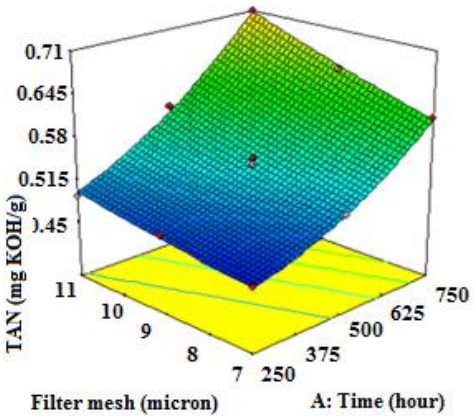

Fig.3. Interaction of the operating hours and filter mesh on the acid number of the oil

Optimization

In order to achieve optimum conditions for the offline hydraulic oil refinement operation, the numerical optimization technique was used. In general, the final decision on the choice of optimal conditions depends on taking into account some economic factors (costs), industrial, etc. However, it should be noted that since regression models are valid only in the area and conditions under consideration, limited economic and qualitative constraints are considered for determining operating conditions. In the present study, operating hours (250, 500 and 750 hours), twin suction filter mesh (7, 9 and 11 microns), and the number of hydraulic oil refinements (0, 1 and 2) were selected in the range. In this study, the aim was to optimize the operation, maximize the operating hours and the frequency of filtering of the oil according to the permitted range of dependent factors. According to the stated contents and results, the permissible range for water contamination was less than 500 ppm; the level of uncleanness or NAS (the number of particles 5 to 15 microns was less than 256 thousand), Si was less than 15 ppm; Vis was between 62.8 and 76.8 Centistokes and TNA was less than 0.65 mg KOH g^{-1}. This goal was chosen to increase the efficiency of offline hydraulic oil refinement operations. Finally, using the desirability function method, the optimal conditions for the offline refinement of hydraulic oil included 728.61 hours, 7-micron filter mesh and oil refinement frequency was two. Under these conditions, the amount of water contamination parameters, the level of uncleanness (NAS), Vis, Si and TAN of hydraulic oil was 187.63 ppm, 234000, 5.91 ppm, 66.34 centistokes and 0.65 mg KOH g^{-1}, respectively. The desirability obtained in optimal conditions for the variables and responses analyzed was 0.957. In sum, the results of this study showed that the offline oil refinement operation of the hydraulic oil could do the trick at high operating hours (728.61) with good performance (water contamination, level of uncleanness, Vis, Si and TAN within the permitted range). In order to confirm the model's prediction, the dependent variables were evaluated in optimal conditions and were determined with a difference of less than 5%, which confirmed the accuracy of the model.

Conclusions

In order to increase the operating hours of sugarcane harvester hydraulic oil, determination of the optimum conditions for performing offline refinement of hydraulic oil can be beneficial and economically feasible. In this research, the effect of independent variables of operating hours, filter mesh and the frequency of hydraulic oil purification were evaluated on the responses studied and optimal operating conditions were also

determined. The results of the optimization of the offline hydraulic oil refinement operation indicated that under operating conditions 728.61 hours, 7-micron filter mesh and oil filtration rate of two, water contamination level, uncleanness level (5 to 15 micrometers), Vis, Si and TAN of hydraulic oil was 187.63 ppm, 234000, 5.91 ppm, 66.34 centistokes and 0.65 mg KOH g^{-1}, respectively. The desirability obtained in optimal conditions for the variables and responses analyzed was 0.957. In sum, a second-degree polynomial model was used to predict the extent of the dependent variables concerning the effect of independent variables used. Therefore, the data obtained from the above model can be used to obtain offline refinement hydraulic oil with a degree of water contamination, level of uncleanness, Vis, Si and TAN in the permitted range.

References

1. Ahmadi, H., and M. S. Blouki. 2009. Comparison and selection of the best time of oil change of transtainer crane (RTG) using oil condition monitoring method. Third technical conference of condition monitoring and diagnosis, Tehran, Sharif University of technology, committee of repair and maintenance. (In Farsi).
2. ASTM D 2270: 2010. Standard Practice for Calculating Viscosity Index from Kinematic Viscosity at 40 and 100°C.
3. ASTM D6595: 2011. Standard Test Method for Determination of Wear Metals and Contaminants in Used Lubricating Oils or Used Hydraulic Fluids by Rotating Disc Electrode Atomic Emission Spectrometry.
4. Cargol, T. 2005. An overview of online oil monitoring technologies. In Fourth Annual Weidmann-ACTI Technical Conference pp. 1-6.
5. Haroni, S., M. J. Sheykhdavodi, and M. Kiani Deh Kiani. 2018. Application of Artificial Neural Networks for Predicting the Yield and GHG Emissions of Sugarcane Production. Journal of Agricultural Machinery 8: 389-401. (In Farsi).
6. He, Q., G. Chen, X. Chen, and C. Yao. 2009. Application of oil analysis to the condition monitoring of large engineering machinery. In Reliability, Maintainability and Safety, 2009. ICRMS 2009. 8th International Conference on (pp. 1100-1103). IEEE.
7. ISO 760: 1978, Determination of water - Karl Fischer method (General method).
8. ISO 6619: 1988, Petroleum products and lubricants - Neutralization number - Potentiometric titration method.
9. ISO 4406: 1999. Hydraulic fluid Power- Fluids- Method for coding the level of Contamination by solid Particles.
10. Li, J. 2010. Oil Analysis Cost-Effective Compressor Condition Monitoring Technique. In Computational Intelligence and Software Engineering (CiSE), 2010 International Conference on (pp. 1-3). IEEE.
11. Macian, V., B. Tormos, P. Olmeda, and L. Montoro. 2003. Analytical approach to wear rate determination for internal combustion engine condition monitoring based on oil analysis. Tribology International 36 (10): 771-776.
12. Macian, V., B. Tormos, A. Sala, and J. Ramirez. 2006. Fuzzy logic-based expert system for diesel engine oil analysis diagnosis. Insight-Non-Destructive Testing and Condition Monitoring 48 (8): 462-469.
13. Masoudi, A. R. 2001. Silica particles in engine oils, Proceedings of technology. The paper No. 10. (In Farsi).
14. Masoudi, A. R. 2001. Study of economic aspects of CM program using oil analysis, Proceedings of technology. Research group of Alborz Tadbir laboratory of Khouzestan Co. the paper No. 15. (In Farsi).
15. Masoudi, A. R. 2003. Care of mechanical systems, sampling techniques, technology series. Laboratory Research Group of AlborzTadbir Khuzestan Co. Article number 12. (In Farsi).

16. Masoudi, A. R. 2011. Introduction to Oil Analysis (translation), Technical and Engineering Company of Alborz Tadbirkaran, Tehran. (In Farsi).
17. Qasemi, Y., M. H. Kianmehr, and B. Azadegan. 2015. Investigation of the effect of granulate compost parameters using response surface method. Journal of Agricultural Machinery 5 (1): 191-198. (In Farsi).
18. Ranjbar, A., H. R. Ghasemzadeh, and Sh. Davoudi. 2003. Engine power and tractor (translation), Printing and Publishing of Tabriz University, pages 601 to 612. (In Farsi).
19. Saghafi, M. 2008. Tractor and its mechanism (translation), Center for Academic Publishing, Ministry of Culture and Islamic Guidance, Tehran. Pages 186 to 199. (In Farsi).
20. Singh, B., P. S. Panesar, V. Nanda, and J. F. Kennedy. 2010. Optimisation of osmotic dehydration process of carrot cubes in mixtures of sucrose and sodium chloride solutions. Food Chemistry 123 (3): 590-600.

نشریه ماشین‌های کشاورزی
جلد ۱۰، شماره ۱، نیمسال اول ۱۳۹۹، ص ۷۲-۵۹

Journal of Agricultural Machinery
Vol. 10, No. 1, Spring- Summer 2020, p. 59-72

بهینه‌سازی عملیات پالایش آفلاین روغن هیدرولیک دروگر نیشکر

حدیث نعمت‌پور ملک‌آباد[۱]، محمد جواد شیخ‌داودی[۲*]، عیسی حزباوی[۳]، افشین مرزبان[۴]

تاریخ دریافت: ۱۳۹۷/۰۷/۱۹
تاریخ پذیرش: ۱۳۹۷/۱۰/۱۲

چکیده

روش سطح پاسخ (RSM)، مجموعه‌ای از تکنیک‌های آماری و ریاضی برای طراحی آزمایش‌ها، مدل‌سازی، بهبود دادن و بهینه‌سازی فرآیندها می‌باشد. هدف از مطالعه حاضر مدل‌سازی و بهینه‌سازی عملیات پالایش آفلاین روغن هیدرولیک دروگر نیشکر به روش RSM بود. بدین‌منظور، اثرات متغیرهای مستقل ساعات کارکرد (۲۵۰، ۵۰۰ و ۷۵۰ ساعت)، مش فیلتر مکشی دوقلو (۷، ۹ و ۱۱ میکرون) و دفعات تصفیه روغن هیدرولیک (۰، ۱ و ۲) روی متغیرهای وابسته آلودگی آب، سطح عدم تمیزی (NAS)، سیلیسیوم (Si)، ویسکوزیته (Vis) و عدد اسیدی روغن (TAN) ارزیابی شد. نتایج نشان داد که همه‌ی مدل‌های به‌دست آمده برای آلودگی آب، سطح عدم تمیزی (NAS)، سیلیسیوم (Si)، ویسکوزیته (Vis) و عدد اسیدی روغن (TAN) برای توصیف داده‌های آزمایشی مناسب بودند. علاوه‌بر این تابع مطلوبیت نشان داد که شرایط بهینه عملیات پالایش آفلاین روغن هیدرولیک دروگر نیشکر شامل ساعت کارکرد ۷۲۸/۶۱ ساعت، مش فیلتر ۷ میکرون و دفعات تصفیه روغن ۲ بود. تحت این شرایط، مقدار پارامترهای آلودگی آب، سطح عدم تمیزی (تعداد ذرات ۵ تا ۱۵ میکرومتر)، Si، Vis و TAN به‌ترتیب برابر با ۱۸۷/۶۳ ppm، ۲۳۴۰۰۰، ۵/۹۱ ppm، ۶۶/۳۴ سانتی استوک و ۰/۶۵ mg KOH/g به‌دست آمد.

واژه‌های کلیدی: بهینه‌سازی، پالایش آفلاین روغن هیدرولیک، دروگر نیشکر، روش سطح پاسخ

۱- دانش‌آموخته دکتری مکانیزاسیون کشاورزی، گروه مهندسی بیوسیستم، دانشگاه شهید چمران اهواز
۲- استاد گروه مهندسی بیوسیستم، دانشگاه شهید چمران اهواز
۳- استادیار گروه مهندسی بیوسیستم، دانشگاه لرستان
۴- دانشیار گروه ماشین‌های کشاورزی و مکانیزاسیون، دانشگاه علوم کشاورزی و منابع طبیعی خوزستان
(*- نویسنده مسئول: Email: javad1950@gmail.com)

DOI: 10.22067/jam.v10i1.75912

Journal of Agricultural Machinery
Vol. 10, No. 1, Spring- Summer 2020, p. 73-82

نشریه ماشین‌های کشاورزی
جلد ۱۰، شماره ۱، نیمسال اول ۱۳۹۹، ص ۸۲-۷۳

ANN-based Modeling of Sunflower Threshing Process and Defining the Optimal Operation Point for Separation Efficiency

P. Ghiasi[1*], A. Masoumi[2], A. Hemmat[2], G. Najafi[3]

Received: 28-10-2018
Accepted: 27-01-2019

Abstract

Harvesting is one of the most important field operations in sunflower production. Seed damage and low separation efficiency are the top concerns of harvesting sunflower. In this study, a threshing cylinder with rubber teeth and a concave for harvesting sunflower were designed and evaluated. The variable parameters were threshing cylinder speed (TCS), threshing space (TS) and moisture content (MC) of sunflower head. Azargol variety was used to evaluate the threshing unit. The tests were performed at three cylinder speed levels (280, 380 and 480 rpm), two threshing spaces (8 and 10 cm) and two moisture content of sunflower head based on the crop condition (20% and 45% wet basis). An ANN model was developed to predict the amount of materials in each part of the concave. Results showed that the sunflower seeds had no damage during the threshing process and the presented model could predict the amount of materials in each part of the concave with a regression coefficient R^2=0.95. Based on the ANN model, with a decrease in MC and TS, and an increase in TCS, the separation efficiency was increased. Furthermore, optimal parameters for the threshing unit which were suggested by Design Expert software to maximize the separation efficiency were 18% w.b, 450 rpm and 10.5 cm for MC, TSC, and TS, respectively and in this condition separation efficiency was determined to be 94.92%.

Keyword: Sunflower harvesting, Threshing model, Threshing unit

Introduction

Oilseeds are one of the most important agricultural crops that are used as raw materials for providing oil and supplying the needs of fat, protein, and vitamins for human and living organisms. Oil production has been increased recently and most of this increase has been related to the sunflower seed oil (Inna, 2010). Sunflower planting is mostly for two main purposes; oil production and direct consumption (Schneiter and Miller, 1981). Harvesting is often done manually in Iran because mechanized harvesting is very expensive and is not still economical. Mechanized harvesting methods are conducted with rasp bar drum and concave and can make a seed loss of 46% during the threshing operation in the threshing unit (Farokhi *et al.*, 2013). Although the seed damage is not very important in oilseeds, mechanical damage leads to weakening germination and reduces the storage and grain growth potential (KhajePor, 2012). The damage to sunflower seeds in fresh market results in reducing the crop price significantly. Harvesting operation when the moisture content is not reduced enough, would reduce the sunflower seeds quality and increases the possibility of disease outbreaks (Giner and Gely, 2005). The mechanized harvesting of sunflower has been studied by several researchers (El-khateeb and Saad, 2008; Ghiasi *et al.*, 2016; Sudajan *et al.*, 2002). In all of these studies, separation efficiency and sunflower seed damage have considered as two important parameters for evaluation of the threshing unit which express how materials were spread through the threshing unit and to what extent threshing unit was able to chop the crop into appropriate pieces.

1- PhD candidate, Department of Biosystems Engineering, Tarbiat Modares University,Tehran, Iran
2- Faculty Member, Department of Biosystems Engineering, Isfahan University of Technology, Isfahan, Iran
3- Faculty Member, Department of Biosystems Engineering, Tarbiat Modares University,Tehran, Iran
(*- Corresponding Author Email: p.ghiasi@modares.ac.ir)
DOI: 10.22067/jam.v10i1.76264

The effects of the threshing parameters have been studied for several crops to optimize the threshing condition. The proposed models can be offered for simulating the behavior of the threshing unit (Miu and Kutzbach, 2007). In this case, they modeled the kinematic behavior of the material into the threshing unit with a regression coefficient of R^2= 0.9. The dynamical model of materials in the threshing unit was presented by (Ning *et al.*, 2015) then through fuzzy control, the forward speed of the combine harvester was controlled. Among the statistical and mathematical models, intelligent systems were better to predict nonlinear behavior because of the use of complex algorithms. The effect of concave clearance, cylinder speed, feed rate, and moisture content was studied on the percentage of grain damage, separation efficiency, and percentage of germination for chickpea threshing (Salari *et al.*, 2013). Results showed that with an increase in the cylinder speed and decrease in the moisture content, the feed rate, and the concave clearance as well as the threshing efficiency were increased. The number of lost seeds in paddy harvester were simulated by Hiregoudar *et al.* (2011) using artificial neural networks and the minimum amount of lost seeds for the harvester. Mirzazadeh *et al.* (2012) used an artificial neural network (ANN) to model wheat behavior in a threshing unit. The results showed that the neural network with 7 neurons can simulate the behavior of wheat in the threshing unit with a regression coefficient of R^2 = 0.81.

Providing a proper model for threshing can be a powerful tool for optimizing and managing the threshing process. The study of some researches about the modeling of materials behavior in the threshing unit showed that the behavior of the materials in the threshing unit not only depended on the type, physical and rheological properties of crops but also can be completely different in each crop. Generally, to mechanistically harvest new crops and design other sections of the combine harvester, it is necessary to analyze the behavior model of materials. In this study, the behavior of the sunflower head in the threshing unit with robber teeth was modeled by using ANN. The present study aimed to predict the behavior of the sunflower head in the threshing unit with an ANN model and to define the optimal point of the threshing unit to maximize the separation efficiency.

Material and Methods

Threshing cylinder and concave

A threshing unit was designed and developed on a chassis to join a conveyor. The schematic design of the machine units is shown in Fig.1, which includes threshing cylinder, concave, flanges, rubber grips, and shaft. The diameter and width of the threshing cylinder were both 50 cm. As shown in Fig.1, the threshing unit has four rows of rubbers, two rows had four and the other two rows had five rubbers, and all of them were fixed on a shaft with a diameter of 30 mm. The concave's arc was 135 degrees and was divided into five sections to collect the seeds and MOG[1] of each part and also to record the amount of them. After the threshing process, the remaining materials of each part were checked carefully by three adult persons to check the surface damages on sunflower seeds. Then, broken and cracked seeds were separated and weighted to calculate the surface damages.

The machine was evaluated with Azargol sunflower variety. Variable parameters including TCS[2] in three levels (280,380 and 480 rpm), MC[3] in two levels (45 and 20 w.b), TS[4] in two levels (8 and 10 cm which were the distance between threshing cylinder and concave in front of the threshing unit and distance between threshing cylinder and concave in the back of the threshing unit was 5 cm) and constant feed rate (670 $kg.h^{-1}$) were selected. The study was conducted based on a 2×3×2 factorial design with three replications, and the experiment was a completely randomized design with three factors including MC, TSC, and TS. For each test, the input

1- Material Other than Grain
2- Threshing Cylinder Speed
3- Moisture Content
4- Threshing Space

weight of the threshing unit and the weight of the threshed sunflower head under the concave and behind it were measured. Note that, in numbering the different sections of the concave, the behind section was named "part 6".

Artificial neural network

The artificial neural network is one of the computational methods that strives to recognize the relationships between the input and output data using the process of learning and neuron. Artificial neural networks were implemented with 4 inputs including the number of parts, moisture content, threshing cylinder speed, and threshing space and one output includes the separation efficiency (Fig.2). The tan-sigmoid transfer function was used for the nodes in the hidden layer as it was a powerful configuration for complex non-linear function approximation (Zurada, 1992).

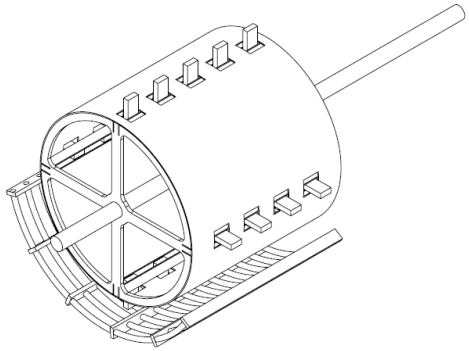

Fig.1. Schematic of the threshing unit

A network model is characterized by an error space representing the error of the system for every possible combination of the weights and biases (Uno *et al.*, 2005). Mean Sum-squared Error (MSE) was used as the performance function, and the batch training was used in which the weights and biases were updated in the direction of the negative gradient of the performance function only after the entire training samples (epoch) had been applied to the network. The gradients calculated at each training sample were added together to determine the change in the weights and biases. The performance of the neural network was evaluated with MSE and the correlation coefficient of R^2, which are presented in equations 1 and 2, respectively.

$$MSE = \frac{\sum_{i=1}^{n}(y_{O,i} - y_{M,i})^2}{n} \quad (1)$$

$$R = \frac{\sum_{i=1}^{n}(y_{O,i} - y_{O,mean})(y_{M,i} - y_{M,mean})}{\sqrt{\sum_{i=1}^{n}(y_{O,i} - y_{O,mean})^2(y_{M,i} - y_{M,mean})^2}} \quad (2)$$

Where n is the number of data, $y_{O,i}$ and $y_{M,i}$ are the output value predicted by the model and the measured output value, respectively, $y_{O,mean}$ and $y_{M,mean}$ are the measured average output value and the predicted average value by the model.

In this study, the Neural Network Toolbox of MATLAB R2016a software was used to predict the percentage of materials in different concave parts. For this research, 70% of the data were used for training, 15% for testing and 15% for validation of network (Shahgoli *et al.*, 2018). The number of neurons obtained during the test and error was 15 neurons for the network. The number of neurons in the output layer depends on the number of output parameters. In this research, the output of the model was the percentage of material deposited in different parts of the concave, so the number of neurons in the outer layer was one.

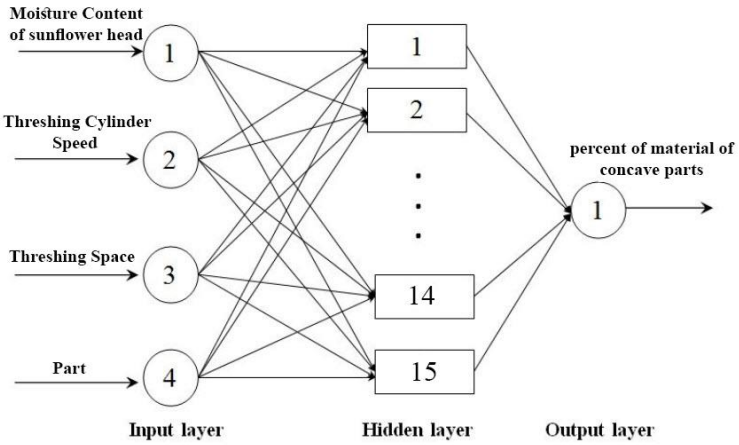

Fig.2. The artificial neural network structure

Optimal point of the threshing unit

The model was presented and the suitability of the model was ensured for predicting the amount of material. In each part before obtaining the amount of material in different parts of the concave, the range of each independent parameter for the moisture content of sunflower head was expanded. The minimum and maximum moisture content of sunflower head were determined based on seed handling, then 5 levels of MC were selected. The maximum level of the threshing cylinder speed was limited by input power in the threshing unit and due to mechanical constraints in the threshing unit, the range of distance between the threshing cylinder and the concave was defined. The moisture content of sunflower head in 5 levels (18, 28, 38, 48 and 58 w.b.), the threshing cylinder speed in 4 levels (250, 450, 650 and 850 rpm) and the threshing space in 4 levels (7.5, 8.5, 9.5 and 10.5 cm) as the new inputs were entered to the model. The data for the parts of 1 to 5 were related to the materials which had passed through the concave and the data for the part of 6 was related particularly to the materials that had not passed through the concave. Based on the separation efficiency equation for the concave, (Equation 3) (El-khateeb and Saad, 2008), the more material passed into the concave, the more separation efficiency of the concave was increased. Accordingly, the optimum operating conditions were obtained when the percentage of the material accumulated in section 6 was minimized (Griffin *et al.*, 1981). For this purpose, design expert 7.0.0 software and the general factorial choice were used.

$$\eta_{SE} = \frac{mass\ of\ material\ passed\ into\ the\ concave}{total\ material\ input} \times 100 \quad (3)$$

ANN model validation

After developing the model, training process was done by using 70% of experimental data and tested by using 15% of experimental data. The variable parameters of the experimental test, were entered to the model as new inputs and compared with the actual results. The correlation coefficient between actual results and output of the ANN model for separation efficiency was calculated by using Microsoft Excel 2016 software.

Result and Discussion

Threshing efficiency

The threshing unit with different levels of MC, TCS, and TS was tested and then the analysis of variance was done. The analysis of variance was performed in the completely randomized design on three factorials. Obtained results are tabulated in Table 1. Results indicated that the effects of MC, TCS, and TS on the percentage of material in part 6 were significant at 1% level of confidence. The interaction between the first degree of MC*TCS was not significant at 5% level and the interaction effect of the first degree of MC*TS and TCS*TS was significant at 5%

level. The interaction between the second degree of MC*TCS*TS was not significant at 5% level.

Fig. 3a shows the percentage of material for the concave parts in MC levels of 20% and 45% w.b in the primary parts of the concave. In the MC level of 45% w.b , the amount of separated material was low; because of a smaller space and high sunflower head density, the amount of material passed through the concave parts was increased. In the MC level of 20 w.b %, because of the fragility of sunflowers head and rheological properties, the material passed through the concave was increased in the primary parts. Sudajan *et al.* (2002) reported that the attaching force between seed and flower head reduced and hence seeds might be separated easily. This might result in a higher separation efficiency in the lower MC. The effect of TCS on the percentage of material in each part is shown in Fig. 3b. An increase in TCS caused the threshing unit to break the sunflowers head at the primary parts so less material went to the last parts. Then, either the part 6 or back of the concave received less amount of material. These findings are in line with Vejasit and Salokhe (2006) study that increasing TCS led to increasing separation efficiency. The distance between the threshing cylinder and the concave affected the material density. Furthermore, the density of the material between the threshing cylinder and the concave was increased and the amount of material in the primary parts was increased in the low TS as well (Fig. 3c). Seidirad and Javadi (2011) reported a similar result for decreasing the TS.

Table 1- Analysis of variance to evaluate the effects of MC, TCS and TS and the interaction between them on the amount of material in part 6

S.V	DF	Sum of squares	F Percent of material
MC	1	1184.74	86.93^{**}
TCS	2	1101.68	40.42^{**}
TS	1	387.96	28.46^{**}
MC*TCS	2	69.21	2.54^{ns}
MC*TS	1	114.13	8.37^{*}
TCS*TS	2	114.38	4.2^{*}
MC*TCS*TS	2	4.28	0.16^{ns}
Error	24	327.10	

* * Highly significant at 1% level; * significant at 5% level; ns, not significant; df, degrees of freedom

Seed damage

In the threshing process of the sunflower head, the force which was applied by the threshing teeth on sunflower seeds, did not catch the fracture force. Therefore, seeds crossed the concave without any damage or spot and seed damage amount was zero. Because of the lack of data for seed damage, it was not considered in the output of the ANN model and there were maybe a small amount of seed damage in expended input data.

The most important factors that kept seeds intact were: 1- the open space of the concave, 2- bars diameters 3- flexible teeth of the threshing cylinder 4- closed threshing cylinder which prevented seeds from striking to the metal parts.

Modeling

After the formation of the input and output matrix, the most suitable artificial neural network was chosen to simulate the amount of material accumulated in the concave parts. Fig.4 shows the correlation coefficient of the proposed artificial neural network model to simulate the amount of material accumulated in concave parts in the validation sections. The correlation coefficient for prediction of separation efficiency was 0.95 and the mean squared error for the network was 0.56, with the minimum value obtained during the trial and error. By rotating the threshing cylinder, sunflower heads were under the influence of impact and abrasion in the space between the threshing cylinder and the concave. Then the seeds were separated from sunflower head.

Since the distance between the threshing cylinder and the concave in the front part was long enough, seeds in this area were separated and passed through the concave, then the impact force would be more effective than abrasion on the threshing process. In the back parts of the concave, because of a higher material density, seeds were separated by abrasion of other sunflower heads and bars and cans of the concave (Lizhang *et al.*, 2013). Understanding what action is more effective during the threshing process, can be useful.

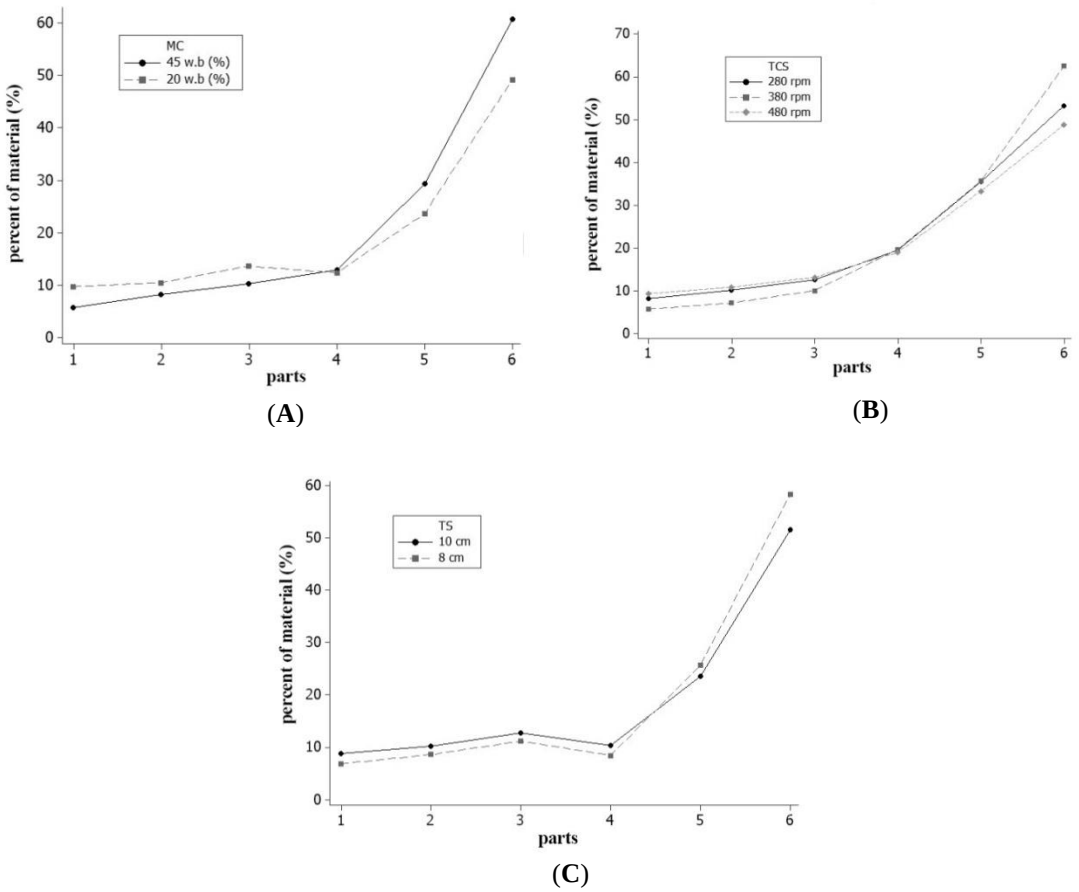

Fig. 3. (**A**) Effect of MC on MOG (**B**) Effect of TCS on MOG (**C**) Effect of TS on MOG

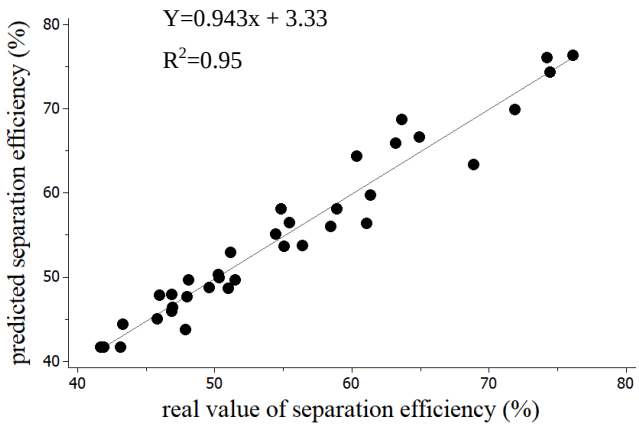

Fig. 4. Artificial neural network performance

Results of the artificial neural network model related to the effect of MC on the percentage of the material existent in the concave parts are shown in Fig. 5a. The decrease in MC changed rheological properties of sunflower head to fragility, increased the amount of material in the primary parts of the concave and reduced the volume of the remaining materials in the last part. In a higher moisture content, due to the impact of the rubber component on sunflower head, the head was torn and cut into smaller pieces at the last parts by abrading other sunflower heads, bars, and cans of the concave, and passing through the concave. Under this circumstance, the concave separation efficiency was increased in lower moisture content. El-khateeb and Saad, (2008) achieved similar results for two sunflower thresher machines that decreasing in MC of sunflower head led to increasing the separation efficiency but seed damage increased in both thresher machines by decreasing in MC.

Fig. 5b shows the results of the ANN model for the effect of the threshing cylinder speed on the percentage of material in the concave parts. With increase in TCS, the effect of impact force on the threshing process was increased, so it caused more materials to drop into the primary part of the concave. With increase the threshing cylinder speed, not only the intensity of the threshing process was increased which was because of the increase in the impact effect, but also the passage of material was increased in the primary part. As a result, the separation efficiency of concave was increased. These findings are in consistent with Sudajan *et al.*, (2002), El-khateeb and Saad, (2008) and Seidirad and Javadi (2011) for threshing sunflower seeds and cumin.

The effect of the threshing space on the percentage of material in the concave parts based on the artificial neural network modeling is presented in Fig. 5c. Accordingly, the more open space of threshing unit, the more chance for unthreshed sunflower head to drop into the back parts of the concave. The reduction in the threshing space led to an increase in the density of the material which consequently increased the effect of abrasion on the threshing process. Based on the results reported by Seidirad and Javadi (2011), decreasing in the TS in lower MC was more effective on the threshing efficiency than higher MC. According to Fig. 5c, with a decrease in the TS, the percentage of the material was decreased in section 6 and as a result, the separation efficiency was improved.

Optimal working point

The experiment data was exported from the ANN model. Because of significant interaction between MC*TS and TCS*TS, Design Expert software was used for defining the optimal point. Then the optimum point was determined to maximize the concave separation efficiency. The concave parts included 6 sections: parts 1 to 5 were specifically for those materials that passed into the concave open area and section 6 was a place for the accumulation of materials that did not pass into the concave open area. Therefore, according to equation 3, the percentage of the material had to be minimized in Section 6 to achieve the maximum concave separation efficiency. The optimum points with utility index are given in Table 2. The optimal point of the threshing unit was obtained in 18% w.b of MC, 450 rpm of TCS and 10.5 cm of TS.

Conclusions

The results of the ANN model showed that the trends of separation efficiency with MC of sunflower head, TCS and TS, had a good agreement with those which were obtained from the real tests. Because of the design property, the sunflower seeds were not damaged. With a decrease in MC from 58% to 18% w.b, the separation efficiency was increased from 71.67% to 74.2% and also an increase in TCS from 250 rpm to 850 rpm improved the concave separation efficiency from 67.5% to 72.25%. With the reduction in TS from 10.5 cm to 7.5 cm, the concave separation efficiency was increased from 70.6% to 77.26%. Finally, to maximize the separation efficiency of the threshing unit, three optimal conditions were proposed with a utility index of 1, 0.977 and 0.873.

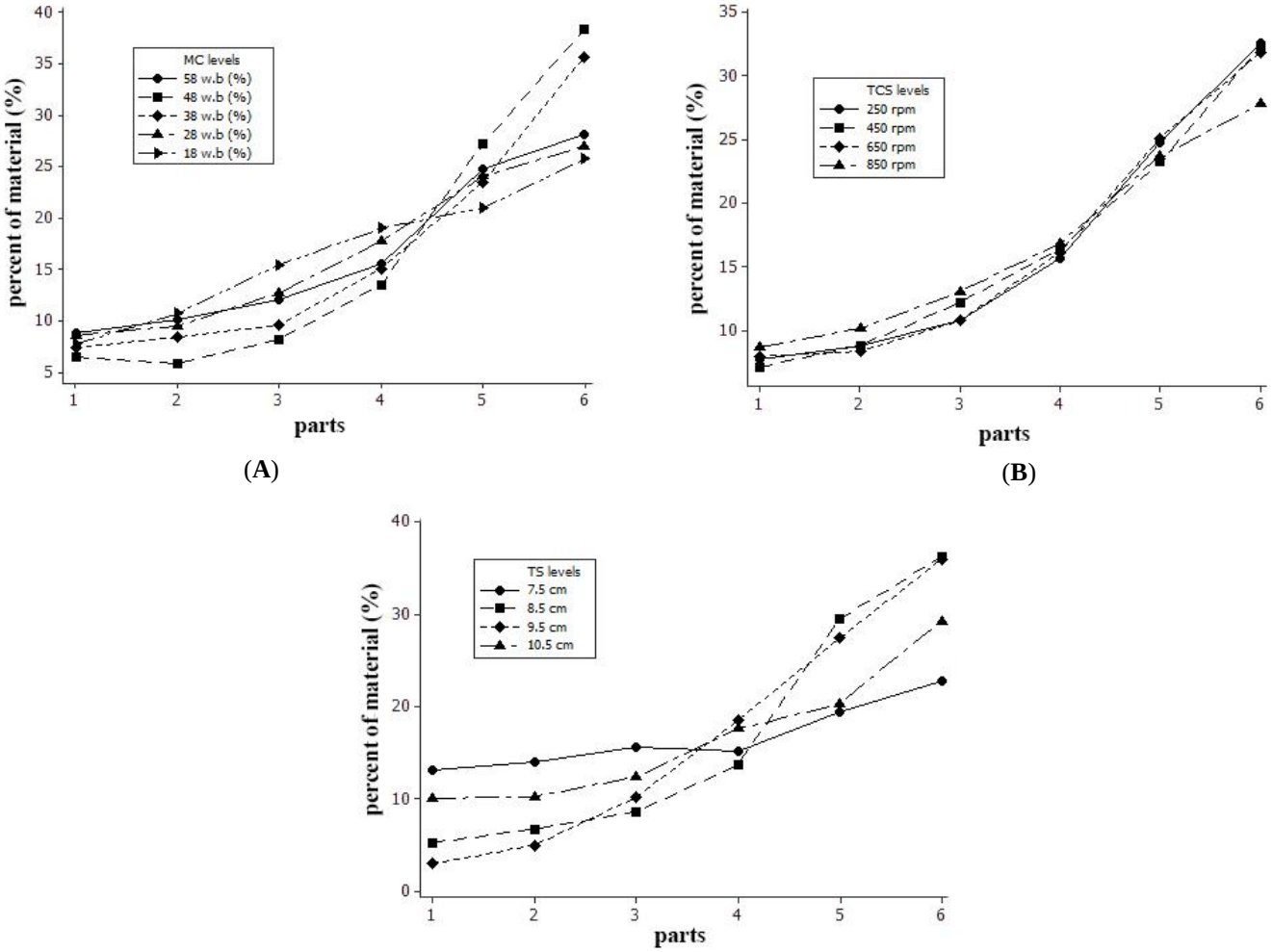

Fig.5. (**A**) Effect of sunflower head MC on the percentage of material in the concave parts (**B**) Effect of TCS on percentage of material in the concave parts (**C**) Effect of TS on the percentage of material in the concave parts

Table 2. Optimal conditions of threshing unit

	MC(% w.b)	TCS (rpm)	TS (cm)	Separation efficiency (%)	Desirability
1	18	450	10.5	94.92	1
2	58	250	7.5	93.75	0.977
3	48	850	7.5	88.35	0.873

References

1. El-khateeb, H., and M. I. Saad. 2008. Operating factors affecting using two different threshing machines for threshing sunflower heads. Agricultural Mechanization and Engineering 251-270.
2. Farokhi, E., A. Nabipor, and J. Daneshian. 2013. Guidelines sunflower production in different regions of the country. Agricultural and Natural Resource Research and Education Center. Tehran. Iran. (In Farsi).

3. Ghiasi, P., A. Masoumi, and A. Hemmat. 2016. Design, development, and evaluation of a threshing cylinder and concave for harvesting sunflower. The 10th national congresss on biosystems Eng. (Agr. Machinery). Mashhad, Iran. (In Farsi).
4. Giner, S. A., and M. C. Gely. 2005. Sorptional parameters of sunflower seeds of use in drying and storage stability studies. Biosystems Engineering 92: 217-227.
5. Griffin, G. A., and Deere and Company. 1981. Combine harvesting. Deere & Co.
6. Hiregoudar, S., R. Udhaykumar, K. T. Ramappa, B. Shreshta, V. Meda, and M. Anantachar. 2011. Artificial Neural Network for Assessment of Grain Losses for Paddy Combine Harvester a Novel Approach. Control, Computation and Information Systems 140: 221-231 Springer, Berlin, Heidelberg.
7. Inna, P. 2010. Agribusiness handbook: Sunflower refined and crude oils. FAO Investment Centre Division: 40-40.
8. KhajePor, M. 2012. Industrial plants. first edition. Isfahan University of Technology Publication Center. Isfahan. Iran. (In Farsi).
9. Lizhang, X., L. Yaoming, M. Zheng, Z. Zhan, and W. Chenghong. 2013. Theoretical analysis and finite element simulation of a rice kernel obliquely impacted by a threshing tooth. Biosystems Engineering 114: 146-156.
10. Mirzazadeh, A., Sh. Abdollahpour, A. Mahmoudi, and A. Ramazani. 2012. Intelligent modeling of material separation in combine harvester ' s thresher by ANN. International Journal of Agriculture and Crop Sciences 23: 1767-1777. (In Farsi).
11. Miu, P. I., and H. D. Kutzbach. 2007. Mathematical model of material kinematics in an axial threshing unit. Computers and Electronics in Agriculture 58: 93-99.
12. Ning, X., J. Chen, Y. Li, K. Wang, Y. Wang, and X. Wang. 2015. Kinetic model of combine harvester threshing system and simulation and experiment of speed control. Nongye Gongcheng Xuebao/Transactions of the Chinese Society of Agricultural Engineering 31: 25-34.
13. Saeidirad, M., and A. Javadi. 2011. Study on machine-crop parameters of cylinder threshers for cumin threshing. Agricultural Engineering International: CIGR Journal 13.
14. Salari, K., R. Amiri Chayjan, J. Khazaei, and J. Amiri Parian. 2013. Optimization of Independent Parameters for Chickpea Threshing Using Response Surface Method (RSM). Journal of Agricultural Science and Technology 15: 467-477.
15. Schneiter, A. A., and J. F. Miller. 1981. Description of sunflower growth stages. Crop Science.
16. Shahgoli, G., H. GhafouriChyane, and M. Tarahom. 2018. Modeling of Soil Compaction Beneath the Tractor Tire using Multilayer Perceptron Neural Networks. Journal of Agricultural Machinery 8: 105-118. (In Farsi).
17. Sudajan, S., V. M. Salokhe, and K. Triratanasirichai. 2002. PM-Power and Machinery: effect of type of drum, drum speed and feed rate on sunflower threshing. Biosystems Engineering 83: 413-421.
18. Uno, Y., S. O. Prasher, R. Lacroix, P. K. Goel, Y. Karimi, A. Viau, and R. M. Patel. 2005. Artificial neural networks to predict corn yield from Compact Airborne Spectrographic Imager data. Computers and Electronics in Agriculture 47: 149-161.
19. Vejasit, A., and V. Salokhe. 2004. Machine-Crop Parameters Affecting Performance of an Axial-Flow Soya Bean Thresher. Agricultural Engineering International: The CIGR Journal of Scientific Research and Development, Manuscript PM 04, 004.
20. Zurada, J. M. 1992. Introduction to artificial neural systems. West.

نشریه ماشین‌های کشاورزی
جلد ۱۰، شماره ۱، نیمسال اول ۱۳۹۹، ص ۸۲-۷۳

Journal of Agricultural Machinery
Vol. 10, No. 1, Spring- Summer 2020, p. 73-82

تعیین نقطه بهینه کاری برای بیشینه کردن بازده جداسازی کوبش آفتابگردان بر اساس مدل عصبی

پدرام قیاسی[1*]، امین اله معصومی[2]، عباس همت[2]، غلامحسن نجفی[3]

تاریخ دریافت: ۱۳۹۷/۰۸/۰۶
تاریخ پذیرش: ۱۳۹۷/۱۱/۰۷

چکیده

برداشت آفتابگردان یکی از فرآیندهای مهم در زراعت آفتابگردان می‌باشد. آسیب دانه‌ای و بازده جداسازی کم از مشکلات برداشت آفتابگردان می‌باشند. در این مطالعه، سیلندر کوبنده با دندانه‌های لاستیکی و ضد کوبنده برای برداشت آفتابگردان طراحی و ساخته شد. سرعت سیلندر کوبنده، فضای کوبنده و رطوبت طبق آفتابگردان، پارامترهای مستقل در ارزیابی واحد کوبش تعیین شد. از رقم آفتابگردان آذر گل برای ارزیابی استفاده شد. آزمون‌ها در سه سطح سرعت سیلندر کوبند (۲۸۰، ۳۸۰ و ۴۸۰ دور در دقیقه)، دو سطح فضای کوبنده (۸ و ۱۰ سانتی‌متر) و دو سطح رطوبت طبق آفتابگردان (۲۰ و ۴۵ بر اساس ماده تر) انتخاب شد. برای پیش‌بینی مقدار مواد جمع‌شده در هر بخش ضد کوبنده، شبکه عصبی مصنوعی ارائه شد. نتایج حاکی از آن است که دانه‌های آفتابگردان بدون آسیب توسط واحد کوبش، کوبیده می‌شود و مدل ارائه شده برای کوبش با ضریب همبستگی ۰/۹۹ می‌تواند مقدار مواد ریخته شده در هر بخش ضد کوبنده را پیش‌بینی کند. بر اساس مدل عصبی ارائه شده با کاهش رطوبت طبق آفتابگردان و فضای کوبنده و افزایش سرعت سیلندر کوبنده، بازده جداسازی واحد کوبش افزایش می‌یابد. نقطه بهینه کاری بر اساس مدل شبکه عصبی مصنوعی برای بیشینه کردن بازده جداسازی، رطوبت طبق آفتابگردان ۱۸٪ بر اساس ماده تر، سرعت سیلندر کوبنده ۴۵۰ دور بر دقیقه و فضای کوبنده ۱۰/۵ سانتی‌متر تعیین شد.

واژه‌های کلیدی: برداشت آفتابگردان، مدل‌سازی کوبش، واحد کوبش

۱- دانشجوی دکتری، گروه مهندسی مکانیک بیوسیستم، دانشگاه تربیت مدرس، تهران، ایران
۲- عضو هیئت علمی، گروه مهندسی مکانیک بیوسیستم، دانشگاه صنعتی اصفهان، اصفهان، ایران
۳- عضو هیئت علمی، گروه مهندسی مکانیک بیوسیستم، دانشگاه تربیت مدرس، تهران، ایران
(*- نویسنده مسئول: Email: p.ghiasi@modares.ac.ir)

DOI: 10.22067/jam.v10i1.76264

Journal of Agricultural Machinery
Vol. 10, No. 1, Spring- Summer 2020, p. 83-92

نشریه ماشین‌های کشاورزی
جلد ۱۰، شماره ۱، نیمسال اول ۱۳۹۹، ص ۹۲-۸۳

The Numerical Simulation of Rebound Velocity Pendulum Method for Ripening Detection of Melon

F. Khoshnam[1], M. Namjoo[2*]

Received: 08-04-2018
Accepted: 29-10-2018

Abstract

A robust numerical analysis was proposed for simulating the rebound velocity pendulum method for melon. For considered varieties (*Zard-Eyvanekey* and *Sousky-Sabz* varieties), the change in impact parameters (extracted from excitation by pendulum) was studied for five stages of ripening. With the melon ripeness, the rebound velocity, rebound height, relative rebound height, rebound angle, rebound energy and coefficient of restitution (velocity ratio) increased, while the absorbed energy decreased (from 37.6 to 27.9 MJ for Zard-Eyvanekey and from 38.5 to 27.9 MJ for Sousky-Sabz). The regression analysis showed a highly significant linear relationship (coefficient of determination, R^2 more than 0.8059) between impact parameters and five stages of ripening. So the results of the analysis are feasible in ripening detection and hence in the classification of the melon maturity.

Keywords: Firmness, Impact analysis, Melon, Non-destructive method

Introduction

There are several non-destructive, fast and objective quality measures that have been proposed and some of them are commercially available (De Ketelaere *et al.*, 2006). Some promising dynamic methods for fruit quality evaluation are based on measurement of fruit response to force vibration or impact (Lien *et al.*, 2009). The use of mass impact either by a light rigid mass or fruit falling has been widely applied in the detection of fruit maturity (Delwiche *et al.*, 1987). The material is either dropped freely onto a force transducer or hammered with an accelerating rigid mass. The impact responses are interpreted in either the frequency or the time domain. The impact indices show a strong correlation with the firmness of vegetables and fruits (Garcıa-Ramos *et al.*, 2003). There is a vertical impact sensor to measure the response of fruit to impacts. The sensor consisted of a small, semi-spherical mass with an accelerometer, which was dropped from different heights onto the fruit. Manual impact sensors, lateral impact sensors are some other sensors used as mechanical measures (Khalifa *et al.*, 2011; Nourain, 2012). Researchers have shown interest in using impact techniques for predicting firmness of fruits. Previous studies have shown that impact techniques such as impacting of fruits on a load-cell (Lien *et al.*, 2009; Ragni *et al.*, 2010) and impacting the fruit with a small spherical impactor (Homer *et al.*, 2010; Yurtlu, 2012) can be used to evaluate the firmness of fruits successfully. García-Ramos *et al*. (2005) describe many ways of using impact sensors, such as hitting the fruit with some element that includes the sensor, putting the fruit over a load cell and letting a weight fall on it, or placing the fruit on a flat plate with a load cell located beneath it. Moreover, some of them reached a commercial use, as is the case of iFD (Intelligent Firmness Detector, Greffa, Netherlands), Aweta (Netherlands), and Sinclair iQ Firmness Tester (García-Ramos *et al.*, 2005).

Lien *et al*. (2009) used nondestructive impact technique to determine tomato ripeness. They reported that maximum impact force, impact time and fruit mass was highly related with Magness-Taylor force of the tomatoes dropped on a force sensor with a classification precision of 82.30% (Lien *et al.*, 2009). Mao *et al*. (2016) developed an

1- Assistant Professor, Department of Mechanical Engineering of Biosystems, Faculty of Agricultural, University of Jiroft, Jiroft
2- Ph.D. Student, Biosystems Engineering Department, College of Agriculture, Shiraz University, Shiraz
(*- Corresponding Author Email: m.namjoo@shirazu.ac.ir)
DOI: 10.22067/jam.v10i1.71925

acoustic device after investigating the influence of hitting ball and fruit tray on spectrum. They proposed three firmness indices to correlate with the firmness of watermelon. They found that significant correlation was between firmness and these indices using linear regressive model and nonlinear model of artificial neural network (ANN) (Mao *et al.*, 2016). In a study, the ripening of watermelon was examined using sound analysis by an impactor. The results showed that the intensity and location of impact effect had a significant effect on the sound signals. There was no significant difference between the biomechanical properties of the peel of the unripe, ripe, and over ripe fruits, and it is therefore expected that the observed difference in the sound properties of the watermelons is more due to the difference in the properties of the flesh than the peel (Saadatinia *et al.*, 2014). Khoshnam *et al*. (2017) examined the effect of acoustic system variables on sound signals of melon varieties. They concluded that the impactor ball, pendulum angle, sound level meter position and variety type factors did not show significant effect on resonance frequency but they had a significant effect on FFT magnitude and sound pressure meter (Khoshnam *et al.*, 2017).

Rebound technique has been used with some success to qualify firmness of fresh product after an impact with surface (Gan-MorGalili, 2000). Ragni *et al*. (2010) developed an impact measuring device for prediction of firmness online in kiwifruit pack house (Ragni *et al.*, 2010). Lien and Ting (2014) in guaya predicted maturity by using an automated sorting machine by analyzing the impact response of dropped fruit (LienTing, 2014).

The objective of the present study is to study the impact of parameters change such as rebound velocity, rebound height, relative rebound height, rebound angle, absorbed energy, rebound energy and coefficient of restitution (velocity ratio) after impact in during of melon ripening (*Zard-Eyvanekey* and *Sousky-Sabz* varieties) and investigation some best linear and single regressions between the impact variables and stage period of ripening. The ultimate goal of this study was to investigate the feasibility of non-destructive maturity sorting of melon by impact rebound response technique without affecting the fruit quality.

Materials and Methods

Sampling of melon

This research was conducted on *Zard-Eyvanekey* and *Sousky-Sabz* variety (export varieties) obtained from a plantation in Garmsar township (35° 13' 20" N, 52° 20' 26" E). They were carefully picked by hand during the summer and autumn in the early morning from the area of Davarabad, Garmsar, Iran. Fruits were selected according to color, size and lack of blemishes in order to obtain homogeneous samples. They were selected at five different stages of ripening. Before each test series, the melon was transferred to department laboratory at 18 to 22 $^{\circ}$C temperature for 24 hours. They were selected at five different stages of ripening (Table 1).

Table 1- Date of harvesting and tests series

Stage	Operation	Date	Description
1	First series of test	Mid-August	Immature
2	Second series of test	Late-August	Early ripening
3	Third series of test	Mid-September	Moderately ripe
4	Forth series of test	Late-September	Ripe
5	Fifth series of test	Mid-October	Over ripe

Excitation method

A pendulum is defined as a mass, or ball, connected to a rod or rope. The equilibrium position of the pendulum is the position when the mass is hanging directly downward. At any given moment, the velocity of the pendulum bob will be perpendicular to the rope. The pendulum's trajectory describes an arc of a

circle, where the rope is a radius of the circle and the bob's velocity is a line tangent to the circle. The mechanical energy of the pendulum is a conserved quantity. The potential energy of the pendulum, mgh, increases with the height of the ball; therefore, the potential energy is minimized at the equilibrium point and is maximized at $\theta = \pm \theta_{max}$. Conversely, the kinetic energy and velocity of the pendulum are maximized at the equilibrium point and minimized when $\theta = \pm \theta_{max}$. In the following discussion, v signifies velocity, U signifies potential energy, and KE signifies kinetic energy.

The total mechanical energy is equal to the kinetic energy at the equilibrium point where U= 0 (point 1). The total mechanical energy is also equal to the total potential energy at $\pm \theta_{max}$ where KE=0 (point 2). Putting these equalities together, we get From the figure 1, we see that, $h = l - l\cos(\theta_{max})$.

$$(mgh + \frac{1}{2}mv^2)_1 = (mgh + \frac{1}{2}mv^2)_2 \Rightarrow 0 + \frac{1}{2}mv^2 = mgh + 0 \Rightarrow v = \sqrt{2gh} \quad (1)$$

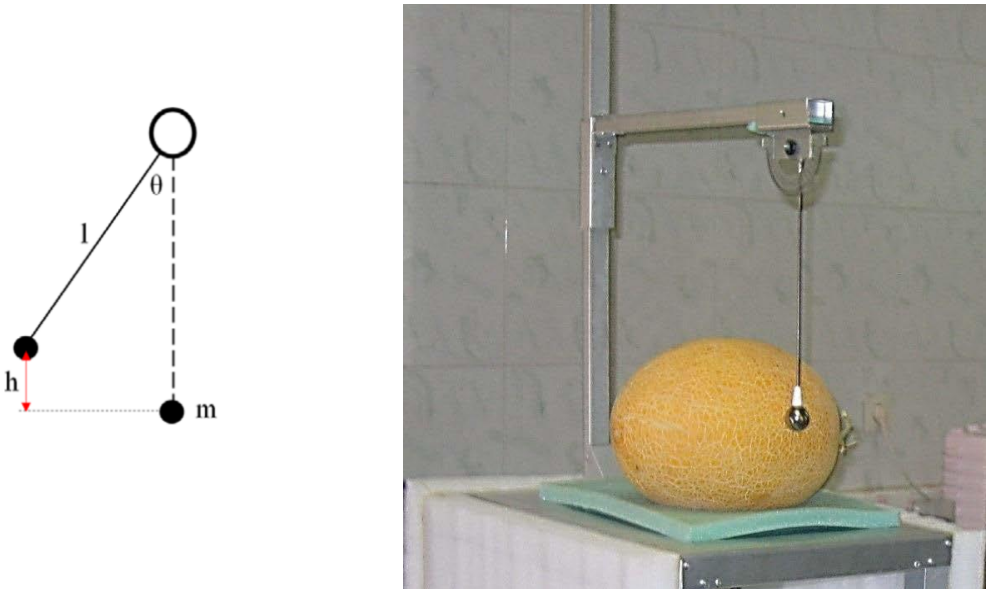

Fig.1. (Right) General view of experimental setup (Left) schematic representation of the pendulum model, assumes massless rod

If we plug that value into the equation (1), we can solve for *v*:

$$\upsilon = \sqrt{2gl(1-\cos\theta)} \quad (2)$$

This relationship shows the velocity at impact pendulum. Where v= impact velocity, g= gravitational acceleration, l= length of pendulum rod and θ=impact angle. It is clear that the longer the rod and the greater the angle, the faster the pendulum ball will move.

Knowing the rebound velocity (υ') from the energy conservation law we determine the rebound height (h'):

$$h' = \frac{v'^2}{2g} = l(1-cos\theta') \quad (3)$$

The relative rebound height (h_{rel}) is the rebound height (h') divided by the impact height (h) and is defined as:

$$h_{rel} = \frac{h'}{h} \quad (4)$$

Knowing the rebound velocity (υ') by the equation (1) we determine the rebound angle (θ'):

$$\theta' = Arccos(1 - \frac{v'^2}{2gl}) \quad (5)$$

The kinetic energy of the pendulum is calculated as following equation:

$$E = \frac{1}{2}mv^2 = \frac{1}{2}m(\sqrt{2gl(1-cos\theta)})^2 = mgl(1-cos\theta) = mgh \quad (6)$$

Where E= total energy or energy of impact (J)
Absorbed energy is calculated by subtracting rebound energy of the impact energy. The value of the absorbed energy during the impact can be determined by the formula:

$$E_{abs} = E - E' = mg\left(h - h'\right) \quad (7)$$

Where E_{abs}= energy absorbed by the sample (J)

The value of the rebound energy of the pendulum arm can be determined by the formula:

$$E' = E(\frac{h'}{h}) \quad (8)$$

The coefficient of restitution (e) determines the amount of kinetic energy retained by the body during the impact and it describes the rebound characteristics were calculated from:

$$e = \frac{v'}{v} = (\frac{h'}{h})^{1/2} \quad (9)$$

The coefficient is usually defined as the ratio of final to initial relative velocity components of the striking bodies in the direction normal to the contact surfaces (Amer Eissa, 2004).

The setup is comprised of a melon sample, melon-bed and an impactor (pendulum). During the test, the fruit (melon) was placed on soft foam support in order to create free support conditions and not to disturb the vibration pattern. The rebound velocity of all individual fruit was measured on the three positions along the equator approximately 120º between them. The impact needs a sufficient stroke, mass, velocity, and right angle. The combination of this causes problems to miniaturize the little impactor. The impactor consists of a steel ball of diameter, 26 mm and a 256 mm long copper rod. The weight of the impactor was 72.13 g.

Preliminary tests were performed in order to identify a proper peripheral velocity of the pendulum. Several different velocities of the ball pendulum, from 15 to 75 degrees, were attempted. It was concluded that impact parameters were affected by the impacted velocity of the pendulum in this range of angles. In addition, within the tested range of angles, repeated hits of the pendulum did not cause any damage to the melon peel and flesh. Because the impactor was designed also considering the fruit elasticity threshold, low impact forces were composed during the impact on the fruit surface, therefore, mechanical damage did not occur on the fruit surface. For this reason, measurements by means of the impactor were named as "nondestructive measurement". As a result of the preliminary tests, an angle of 45 degrees was selected for the impact device for all further tests.

Finite element modeling

Finite element models of fruit were first created using Abaqus version 6.14-5. For the FE model, the melon was considered as an elastic body with a seed cavity. The nonlinear visco-elastic texture of the melon was therefore simplified as linear elastic texture. For the melon model the structural element C3D8I was used for rind and flesh. The element is defined by 20 nodes having three degrees of freedom at each node: translations in the nodal x, y, and z directions. C3D8I is well suited to modeling of irregular meshes. The melon fruit can be considered a multibody system, which consists of epicarp, mesocarp and endocarp tissues, during modeling. The material properties of different types of tissues in the melon were taken from a previous study that used finite element analysis (Namjoo *et al.*, 2016). The melon is considered to be homogeneous and no boundary constraints have been applied. The first step in the finite element analysis is the construction of the geometrical model of the melon. This construction is a highly complicated task not only for melons, but also for most of the agricultural objects. Fig. 2 shows finite element model before and after impact on melon skin by pendulum. The colorful area indicates the contact between ball pendulum with the model melon. Analysis of variance

(ANOVA) was applied to the data. Means corresponding to the different stages of evolution were compared using Duncan's multiple range tests ($p<0.05$).

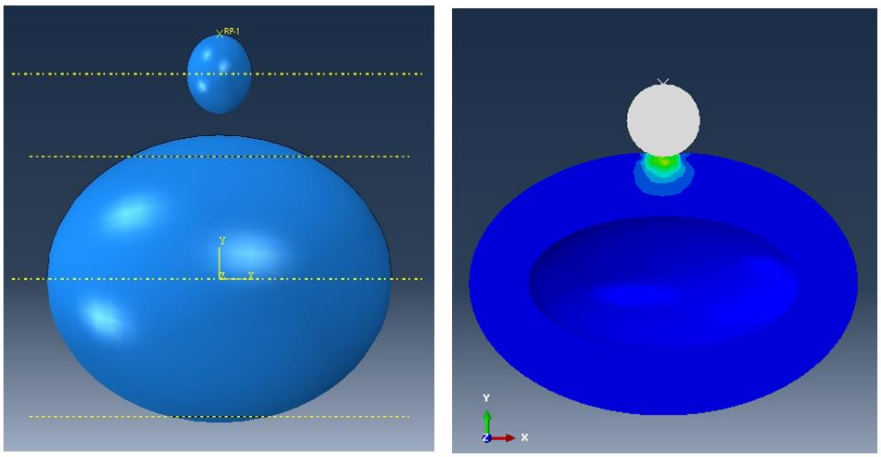

Fig.2. Simulation of ball pendulum and melon before (a) and after (b) impact in Abaqus

Results and Discussion

Figure 3 and 4 show the impact velocity variations on *Sousky-Sabz* and *Zard-Eyvanekey* variety, respectively. These Figures were prepared by using the analysis of Abaqus version 6.14-5 software. It is obviously that the rebound velocity values differ relating to harvesting stage for both varieties. The rebound velocity was high in over ripe stage and decreased by ripening reduction (over ripe to immature) for both varieties. This values extracted and used for others impact parameters.

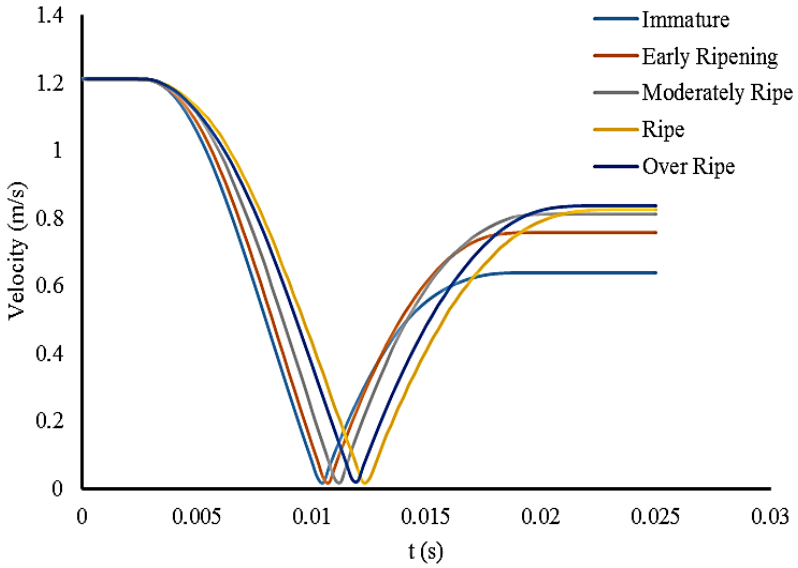

Fig.3. Impact velocity variations on *Sousky-Sabz* variety

Several variables of the impactor on fruit such as rebound velocity, rebound height, rebound angle, absorbed energy, rebound energy and coefficient of restitution (velocity ratio) versus stage of ripening can be obtained. The impactor was held by hand and adjusted on 45 degrees. It saved potential energy and after releasing, its saved potential energy was modified to kinetic energy during the release and impacted the fruit at a velocity of 1.21

m s^{-1}. By substituting values g=9.8 m s^{-2}, l=256 mm, θ=45^{o} and m=72.13 g into Eq. 1 and 5, values were obtained as v=1.21 m s^{-1} and E=52.8 MJ. Indeed, other impact parameters by substituting rebound velocity (from Fig, 2 and 3) on the Eq. 2, 3, 4, 6, 7 and 8 were obtained.

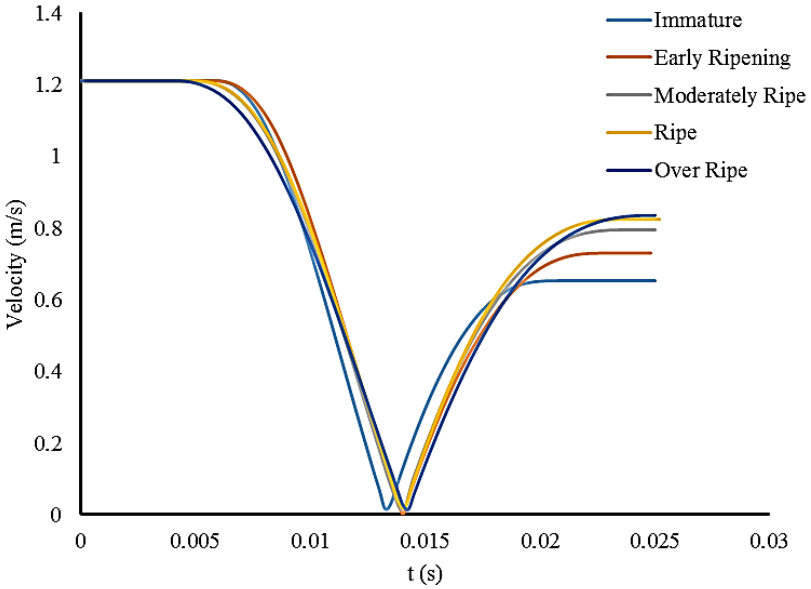

Fig.4. Impact velocity variations on *Zard-Eyvanekey* variety

Melon fruits are made of viscoelastic materials and, for this reason; the impact caused to them is a complicated phenomenon. The mean values are shown in Table 2 on the impact characteristic parameters for each variety and degrees of ripeness. The rebound velocity of impactor (v′) on samples increased during the growing season slowly as the rebound velocity values of Zard-Eyvanekey from 0.653 to 0.835 m s^{-1} (about 27.9%) and the rebound velocity values of Sousky-Sabz from 0.636 to 0.835 m s^{-1} (about 31.3%) increase (Fig. 3). However, the increasing rates were different during the harvesting stages in both varieties: faster rate in the initial stages and lower in the final stages. The average of the rebound velocity in the fourth harvest (ripened) impactor on both varieties estimated 0.824 m s^{-1} (Fig. 4). This phenomenon could be due to the texture of the peel and flesh fruit which had more elasticity and springiness than another maturity stages.

Table 2- Changes of impact parameters of melon during harvesting (l= 256 mm, m= 72.13 g, θ= 45^{o}, h=75 mm, E= 52.8 mJ and v= 1.21 m s^{-1})

Variety	Maturity stage	v′ (m s^{-1})	h′ (mm)	h_{rel}	θ′(^{o})	E_{abs} (mJ)	E′ (mJ)	e
Zard-Eyvanekey	First	0.653 ^{d}	21.8 ^{d}	0.29 ^{d}	23.8 ^{d}	37.6 ^{a}	15.3 ^{d}	0.54 ^{d}
	Second	0.730 ^{c}	27.2 ^{c}	0.36 ^{c}	26.6 ^{c}	33.8 ^{b}	19.1 ^{c}	0.60 ^{c}
	Third	0.795 ^{b}	32.2 ^{b}	0.43 ^{b}	29.1 ^{b}	30.3 ^{c}	22.7 ^{b}	0.66 ^{b}
	Fourth	0.824 ^{ab}	34.6 ^{ab}	0.46 ^{ab}	30.2 ^{ab}	28.6 ^{cd}	24.4 ^{ab}	0.68 ^{ab}
	Fifth	0.835 ^{a}	35.6 ^{a}	0.47 ^{a}	30.6 ^{a}	27.9 ^{d}	25.1 ^{a}	0.69 ^{a}
Sousky-Sabz	First	0.636 ^{d}	20.6 ^{d}	0.27 ^{d}	23.2 ^{d}	38.5 ^{a}	14.5 ^{d}	0.53 ^{d}
	Second	0.756 ^{c}	29.1 ^{c}	0.39 ^{c}	27.6 ^{c}	32.4 ^{b}	20.5 ^{c}	0.62 ^{c}
	Third	0.811 ^{b}	33.5 ^{b}	0.45 ^{b}	29.7 ^{b}	29.3 ^{c}	23.6 ^{b}	0.67 ^{b}
	Fourth	0.824 ^{ab}	34.6 ^{ab}	0.46 ^{ab}	30.2 ^{ab}	28.6 ^{cd}	24.4 ^{ab}	0.68 ^{ab}
	Fifth	0.835 ^{a}	35.6 ^{a}	0.47 ^{a}	30.6 ^{a}	27.9 ^{d}	25.1 ^{a}	0.69 ^{a}

Means in the same column followed by different letters are significantly different according to Duncan's test (p<0.05).

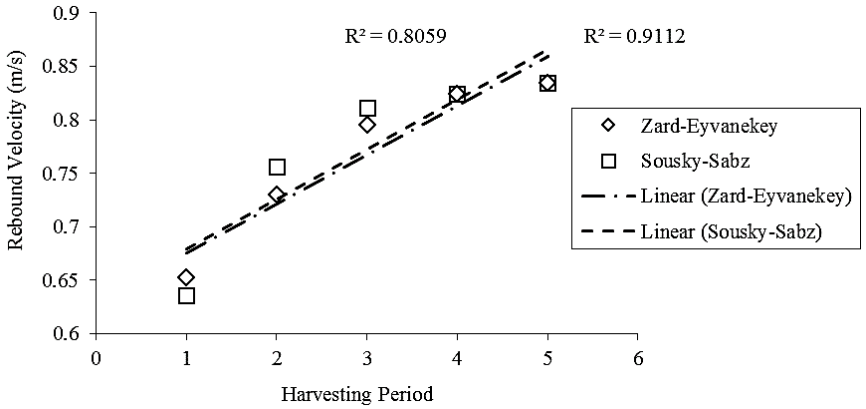

Fig.5. Rebound velocity of melon varieties trend over five test series

The rebound height of impactor on melons increased over the period of ripening (Fig. 5). At initial stages of growth, the change was so noticeable and then was gradually decreased. The rebound height of impactor on Zard-Eyvanekey from 21.8 to 35.6 mm and for Sousky-Sabz from 20.6 to 35.6 mm increase. This value was same (34.6 mm) for both varieties in full ripening.

The rebound angle values of the two cultivars increased over the period of development and ripening. This parameter increased from 23.8 to 30.6^{o} for Zard-Eyvanekey and from 23.2 to 30.6^{o} for Sousky-Sabz cultivar from 1st to 5th stage of ripening. The average of rebound angle values in the ripened stage estimated 30.2^{o} for both varieties.

The absorbed energy values by impactor had shown a decreasing trend. This value, Zard-Eyvanekey, was 37.6 MJ in first stage and 27.9 MJ in fifth stage (reduction 25.8%), whereas these values were 38.5 MJ and 27.9 mJ (reduction 27.5%) for Sousky-Sabz. The absorbed energy value was 28.6 MJ for both varieties in full ripening.

Idah *et al.* (2007) studied the impact damage assessment of fresh tomato fruits to ascertain the effects of drop height, impact surfaces, maturity and size of fruits on bruise area and impact energy. They found that the impact energy on the fruit was greatly influenced by the drop height and the mass of fruits. The bigger and fully ripe fruits generally absorbed more energy than the smaller ones (Idah *et al.*, 2007).

So the ripe and over-ripe melon samples of maturity stages were able to absorb some of impact energy less than another maturity stages, which cause to increase the coefficient of restitution and that reflect on the ripening detection of melon.

Because of the sum of absorbed energy and rebound energy is constant (Eq. 7) the value of the rebound energy of the two varieties increased over the period of development and ripening. The rebound energy value, Zard-Eyvanekey, was 15.3 MJ in first test series and 25.1 MJ in fifth test series, whereas these values were 14.5 mJ and 25.1 MJ for Sousky-Sabz. This value was 24.4 MJ for both varieties at ripe stage.

The coefficient of restitution (e) followed upward trends throughout ripening in both varieties as expected (because it calculated from velocity rebound and velocity impact or rebound height and impact height). This value for Zard-Eyvanekey variety was initially at 0.54 and reached the value of 0.69, these values were o.53 and 0.69 in Sousky-Sabz variety, respectively. The coefficient of restitution in the fourth harvest (ripened), Zard-Eyvanekey and Sousky-Sabz determined 0.68. The coefficient of restitution for the one-dimensional impact between the two bodies, in pure translation movement, is defined as the relative velocity ratio (with changed sign) between the two bodies, at the beginning and end of the collision. This is a measure of

impact energy lost due to internal sources: elastic waves, plastic deformations and frictions in the contact area.

Table 3- Relation between main impact parameters to five stages of ripening for melon varieties (x= harvest period)

Variety	Impact parameters	Equation	R^2
Zard-Eyvanekey	Rebound velocity	$v' = 0.0458x + 0.63$	0.9112
	Rebound height	$h' = 3.5x + 19.78$	0.9277
	Relative rebound height	$h_{rel} = 0.02x + 0.108$	0.9346
	Rebound angle	$\theta' = 1.72x + 22.9$	0.9133
	Absorbed energy	$E_{abs} = -2.46x + 39.02$	0.9280
	Rebound energy	$E' = 2.49x + 13.85$	0.9275
	Coefficient of restitution	$e = 0.038x + 0.52$	0.9070
Sousky-Sabz	Rebound velocity	$v' = 0.0466x + 0.63$	0.8059
	Rebound height	$h' = 3.55x + 20.03$	0.8311
	Relative rebound height	$h_{rel} = 0.021x + 0.107$	0.8167
	Rebound angle	$\theta' = 1.74x + 23.04$	0.8106
	Absorbed energy	$E_{abs} = -2.5x + 38.84$	0.8235
	Rebound energy	$E' = 2.51x + 14.09$	0.8322
	Coefficient of restitution	$e = 0.038x + 0.524$	0.8261

Kafashan *et al.* (2008) found that averages of restitution coefficients for lateral sides, blossom side and stem side on 'Jonagold' apples were calculated 0.524, 0.596 and 0.507, respectively. The results showed that the maximum and minimum restitution coefficients were found on the blossom sides and stem sides of apple fruits, respectively (Kafashan *et al.*, 2008). Table 3 shows correlation coefficients (R^2) nondestructive impact parameters and stage of ripening. The results of this table indicate a highly significant linear relationship between impact parameters and five stages of ripening. There is a better coefficients of correlation for *Zard-Eyvanekey* variety.

Conclusions

Over ripe melons had a maximum rebound velocity, rebound height, relative rebound height, rebound angle, rebound energy and coefficient of restitution (velocity ratio) and minimum absorbed energy, whereas an immature melon shows opposite results. Both varieties had increasingly trends in the impact parameters attributes rebound velocity, rebound height, relative rebound height, rebound angle, rebound energy and coefficient of restitution (velocity ratio) and percentage of absorbed energy of the two varieties decreased over the period of ripening. The regression analysis showed a highly significant linear relationship between impact parameters and five stages of ripening.

References

1. Amer Eissa, A. 2004. A portable pendulum for impact characterization of whole eggshell. Misr Journal of Agricultural Engineering 21: 1-13.
2. De Ketelaere, B., M. S. Howarth, L. Crezee, J. Lammertyn, K. Viaene, I. Bulens, and J. De Baerdemaeker. 2006. Postharvest firmness changes as measured by acoustic and low-mass impact devices: a comparison of techniques. Postharvest Biology and Technology 41: 275-284.
3. Delwiche, M. J., T. McDonald, and S. V. Bowers. 1987. Determination of peach firmness by analysis of impact forces. Transactions of the ASAE 30: 249-0254.
4. Gan-Mor, S., and N. Galili. 2000. Rheological model of fruit collision with an elastic plate. Journal of Agricultural Engineering Research 75: 139-147.

5. Garcıa-Ramos, F., J. Ortiz-Canavate, M. Ruiz-Altisent, J. Dıez, L. Flores, I. Homer, and J. Chávez. 2003. Development and implementation of an on-line impact sensor for firmness sensing of fruits. Journal of Food Engineering 58: 53-57.
6. García-Ramos, F. J., C. Valero, I. Homer, J. Ortiz-Cañavate, and M. Ruiz-Altisent. 2005. Non-destructive fruit firmness sensors: a review. Spanish Journal of Agricultural Research 3: 61-73.
7. Homer, I., F. J. García-Ramos, J. Ortiz-Cañavate, and M. Ruiz-Altisent. 2010. Evaluation of nondestructive impact sensor to determine on-line fruit firmness. Chilean Journal of Agricultural Research 70: 67-74.
8. Idah, P., E. Ajisegiri, and M. Yisa. 2007. An assessment of impact damage to fresh tomato fruits. Au Jt 10: 271-275.
9. Kafashan, J., M. V. Zeebroeck, H. Sadrnia, D. Moshou, J. d. Baerdemaeker, B. Nicolai, H. Ramon, and B. Tijskens. 2008. Effects of impact locations on mechanical and dynamical properties of fruits. Agricultural and biosystems engineering for a sustainable world. International Conference on Agricultural Engineering, Hersonissos, Crete, Greece, 23-25 June, 2008: European Society of Agricultural Engineers (AgEng).
10. Khalifa, S., M. H. Komarizadeh, and B. Tousi. 2011. Usage of fruit response to both force and forced vibration applied to assess fruit firmness-a review. Australian Journal of Crop Science 5: 516.
11. Khoshnam, F., S. R. Hasan-Beigi, M. Namjoo, and M. Doroozi. 2017. The effect of acoustic system variables on sound signals of Melon varieties. Journal of Agricultural Machinery 7: 126-139.
12. Lien, C.-C., and C.-H. Ting. 2014. Assessing guava maturity by statistical analyses of dropped fruit impact responses. Postharvest Biology and Technology 95: 20-27.
13. Lien, C.-C., C. Ay, and C.-H. Ting. 2009. Non-destructive impact test for assessment of tomato maturity. Journal of Food Engineering 91: 402-407.
14. Mao, J., Y. Yu, X. Rao, and J. Wang. 2016. Firmness prediction and modeling by optimizing acoustic device for watermelons. Journal of Food Engineering 168: 1-6.
15. Namjoo, M., F. Khoshnam, H. Golbakhshi, and M. Dowlati. 2016. Kavun Meyve Olgunlaşmasında Fiziksel ve Mekanik Değişiklikler. Yüzüncü Yıl Üniversitesi Tarım Bilimleri Dergisi: 135-144.
16. Nourain, J. 2012. Application of Acoustic Properties in Non–Destructive Quality Evaluation of Agricultural Products. International Journal of Engineering and Technology 2: 668-675.
17. Ragni, L., A. Berardinelli, and A. Guarnieri. 2010. Impact device for measuring the flesh firmness of kiwifruits. Journal of Food Engineering 96: 591-597.
18. Saadatinia, M., B. Emadi, and H. Sadrnia. 2014. Evaluation of Watermelon Ripeness by Analyzing Sounds Generated from Imposed Impact. Journal of Agricultural Machinery 4: 296-304.
19. Yurtlu, Y. B. 2012. Comparison of nondestructive impact and acoustic techniques for measuring firmness in peaches. Journal of Food, Agriculture & Environment 10: 180-185.

نشریه ماشین‌های کشاورزی
جلد ۱۰، شماره ۱، نیمسال اول ۱۳۹۹، ص ۹۲-۸۳

Journal of Agricultural Machinery
Vol. 10, No. 1, Spring- Summer 2020, p. 83-92

شبیه‌سازی عددی روش سرعت بازگشت آونگ جهت تشخیص رسیدگی خربزه

فرهاد خوشنام[۱]، مسلم نامجو[۲*]

تاریخ دریافت: ۱۳۹۷/۰۱/۱۹
تاریخ پذیرش: ۱۳۹۷/۰۸/۰۷

چکیده

در این تحقیق جهت شبیه‌سازی روش سرعت بازگشت آونگ روی خربزه، تجزیه و تحلیل عددی نیرومندی پیشنهاد شد. تغییر پارامترهای ضربه روی دو رقم خربزه (زرد ایوانکی و سوسکی سبز) و در پنج مرحله رسیدگی بررسی شد. نتایج نشان داد که سرعت بازگشت، ارتفاع بازگشت، ارتفاع نسبی بازگشت، زاویه بازگشت، انرژی بازگشت و ضریب پس‌جهش (نسبت سرعت) با رسیدگی خربزه افزایش و انرژی جذب شده کاهش یافت. تجزیه و تحلیل رگرسیون رابطه خطی با معنی‌داری بالایی بین پارامترهای ضربه و پنج مرحله رسیدگی را نشان داد. نتایج تجزیه و تحلیل در تشخیص رسیدگی و از این رو در طبقه‌بندی بلوغ خربزه امکان‌پذیر است.

واژه‌های کلیدی: تجزیه و تحلیل ضربه، خربزه، روش غیر مخرب، سفتی

۱- استادیار گروه مهندسی مکانیک بیوسیستم، دانشکده کشاورزی، دانشگاه جیرفت، جیرفت، ایران
۲- دانشجوی دکترا، بخش مهندسی بیوسیستم، دانشکده کشاورزی، دانشگاه شیراز، شیراز، ایران
(*- نویسنده مسئول: Email: m.namjoo@shirazu.ac.ir)

DOI: 10.22067/jam.v10i1.71925

Journal of Agricultural Machinery
Vol. 10, No. 1, Spring- Summer 2020, p. 93-102

نشریه ماشین‌های کشاورزی
جلد ۱۰، شماره ۱، نیمسال اول ۱۳۹۹، ص ۱۰۲-۹۳

Engineering Properties of Japanese quail Eggs in Different Levels of Dietary Calcium

M. H. Aghkhani[1*], M. Baghani[2]

Received: 26-05-2018
Accepted: 25-08-2018

Abstract

The eggshell of birds, as a natural shield and package, protects the tissues inside it from microbial and mechanical damages. Proper intake of calcium, as an important and effective factor in increasing the strength and quality of the eggshell, could reduce complications. In this paper, the effect of dietary calcium at five different levels on engineering features of Japanese quail eggs in a Parent stock in their first laying period was investigated. The values for an average of mass, volume, specific mass, shell thickness, major diameter, central diameter and rupture force along the longitudinal and transverse axes were measured. Rupture energy or toughness, slope of the rupture curve (hardness), deformation along the longitudinal and transverse axis to the point of rupture as well as longitudinal and transverse deformation of 450 tested quail eggs (3 period of time, 5 treatment of calcium, 5 replication, 6 observation) were measured. The characters of the specific mass, shell thickness, rupture force, and slope of the rupture curve of quail eggs indicate the strength of quail egg. In this study, variations in all parameters indicating shell strength at different levels of dietary calcium were consistent with each other. Five different treatments with 1.5%, 2%, 2.5%, 3%, and 3.5% calcium content were supplied for the study. By increasing the calcium content of the quail diet from 1.5 to 3 wt%, the volume and weight of quail eggs dropped and shell thickness was reinforced. According to the results, the shell strength of quail eggs along the transverse axis was slightly less than the longitudinal axis, but the flexibility and energy required for quail egg rupture were much greater across the longitudinal axis.

Keywords: Calcium, Eggshell, Mechanical properties, Physical properties, Strength

Introduction

The eggshell of birds, as a shield and natural package, protects the embryo and other materials inside it from microbial and mechanical damages. It provides a bacteria and virus-free environment deprived of any contaminants that may damage the embryo. The eggshell also acts as a respiratory organ for the balut and supplies nutrients (mainly calcium) for the growth of the embryo (Ancle *et al.*, 1992). The quail eggshell, given its impact on packaging machinery and equipment, incubation, warehousing and sale market, plays a key role in the profitability of this industry. The economic consequences of neglecting shell defects could be meaningful. Economically, the rupture of eggshells accounts for about 8-10% loss in the industry (Ketta and Tumova, 2016). Therefore, research in this area is necessary and can contribute to boost the industry of egg-laying and breeder quails.

Calcium is one of the most important nutritional factors affecting the quality of eggshell of birds. Both deficiency and excess of calcium in birds' diet decrease the quality of the eggshell (North, 1984). Low levels of calcium in the diet reduces the thickness of the shell and increases the number of thin shells or shell-less eggs. High amounts of calcium also affect phosphorus absorption, reduce the quality of the eggshell and give a bad taste to the bird's diet, which leads to the lower intake of quail feed (Robert and Ball, 1998).

Furthermore, the quality of eggshell of birds is determined by measuring shell thickness and resistance against brittleness. Usually, the resistance of the eggshell increases proportional to the thickness of the

1- Professor, Department of Biosystem Engineering, Faculty of Agriculture, Ferdowsi University of Mashhad, Mashhad, Iran
2- PhD student, Department of Biosystem Engineering, Faculty of Agriculture, Ferdowsi University of Mashhad, Mashhad, Iran
(*- Corresponding Author Email: aghkhani@um.ac.ir)
DOI: 10.22067/jam.v10i1.73027

shell (Ketta and Tumova, 2018), but the thick shell does not always mean a solid shell. The shell strength is chiefly related to the structure of organic and inorganic compounds (Roque and Soares, 1994). The system of growing chickens in a cage produces eggs of higher resistance compared to the method of growing them on the breeding farm (Ketta and Tumova, 2018). The birds' age also affect the quality of the eggshell. It is showed that as birds grow older, the shell thickness is decreased (Ketelaere *et al.*, 2002; Mazzuco and Hester, 2005). Information about the engineering features of animal products is necessary to design equipment for different rearing sectors which affect production costs and the quality of the products (Correa *et al.*, 2010). Experiments have been carried out to study the engineering properties of eggshell. It is reported that the mechanical resistance of quail egg in the longitudinal axis was greater than of the transverse axis (Polat *et al.*, 2007; Altuntas and Sekeroglu, 2008; Buchar *et al.*, 2015; Nedomova *et al.*, 2016). However, deformation and rupture energy along the longitudinal axis of quail eggs were lower than the transverse axis (Altuntas and Sekeroglu, 2008). Some studies also showed that, as the loading rate of quail eggs is increased, the force necessary for egg rupture was amplified (Buchar *et al.*, 2015). Furthermore, some physical properties of quail eggs (e.g., egg weight, specific mass, and shape index) have been assessed in some studies (Yannakopoulos and Tserveni-Goussi, 1986; Gonzalez, 1995). Although these studies have concentrated on the physical and mechanical properties of Japanese quail eggs, no specific study on the effect of different levels of dietary calcium on engineering properties was investigated on a commercial farm. Therefore, the main object of this study was to determine the average mass, volume, specific mass, shell thickness, major diameter, central diameter, rupture force, rupture energy and slope of the rupture curve of quail eggs in five levels of calcium dietary.

Materials and Methods

In this study, 200 female quails and 100 male quails were selected randomly from a quail parent stock commercial farm at the age of 10 weeks. In this way, we had 100 cages, each containing two females (Average Weight of 230 g) and one male bird. The experimental section of this study was carried out in Karaj, Iran. The diet was based on NRC1994 standard nutritional requirements (National Research Council, 1994), and the feeding treatments differed only in terms of calcium content. The light exposure and moisture were maintained equal across the breeding farm throughout the day. During the three-month experiment, lights were switched on from 6:00 AM to 10:00 PM. The temperature of the breeding farm ranged from 18 to 23 °C and humidity was in the range of 40 to 80%.

Five different treatments with 1.5%, 2%, 2.5%, 3%, and 3.5% calcium content were supplied for the study. The quail diet was prepared according to NRC1994, and the recommended calcium in NRC 1394 for quail is 2.5%. Treatments of calcium in this study were recommended diet calcium in NRC1394 ± 1% (National Research Council, 1994). Each treatment included 60 quails (40 females and 20 males) put in 20 cages. Each treatment had 5 repetitions which contained 4 cages per each (5×4). The diet was also provided at 11 weeks of age, after birds' adaptation to the new breeding environment. After one month of breeding under controlled conditions, the sampling of quail eggs was carried out in three stages after 15 weeks, 19 weeks and 23 weeks (Baghani and Aghkhani, 2016). At each sampling stage, 6 samples were taken from each repetition and a total of 450 samples of quail eggs were selected and examined. The sample of quail eggs was always performed at 6:00 PM.

In terms of physical properties, large diameter (L), central diameter (W) and eggshell thickness were measured using a caliper with a precision of 0.01 mm and mass of samples (M) was measured using a digital scale (AND, Japan) with a precision of 0.01 g. The volume (V) of the eggs was determined using fluid displacement or fluid weights

(Mohsenin, 1986). The specific mass, one of the most common parameters for determining the shell strength of eggs (Ketta and Tumova, 2016), was obtained by dividing the mass in egg volume. Eqs. 1 to 5 were used based on (Altuntas and Sekeroglu, 2008; Alahdadi *et al.*, 2012; Rohani *et al.*, 2015) to calculate the geometric mean diameter (Dg), degree of sphericity (Φ), external surface area (S), shape index (SI) and specific deformation (ε).

$$D_g = (LW^2)^{1/3} \quad (1)$$

$$\Phi = (D_g/L) \times 100 \quad (2)$$

$$S = \pi D_g^2 \quad (3)$$

$$SI = (W/L) \times 100 \quad (4)$$

$$\varepsilon = dL/L \quad (5)$$

The strength and other mechanical properties of quail eggs were determined by the rupture resistance method using the quasi-static compression test between two metal plates of universal test apparatus (Instron Universal Testing Machine SMT-5, SANTAM Co., Iran). The loading speed was 6 mm/min and the test was performed along with two directions: longitudinal (large diameter) and transverse (middle diameter) axes of quail eggs (Figures 1 and 2).

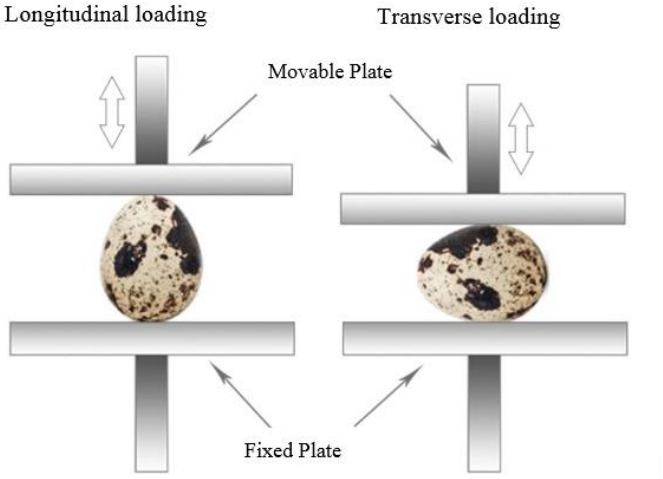

Fig.1. schematic of load applied along the longitudinal and transverse direction on quail eggs in a single axial pressure test. The load applied along the central diameter (right) and the large diameter (left)

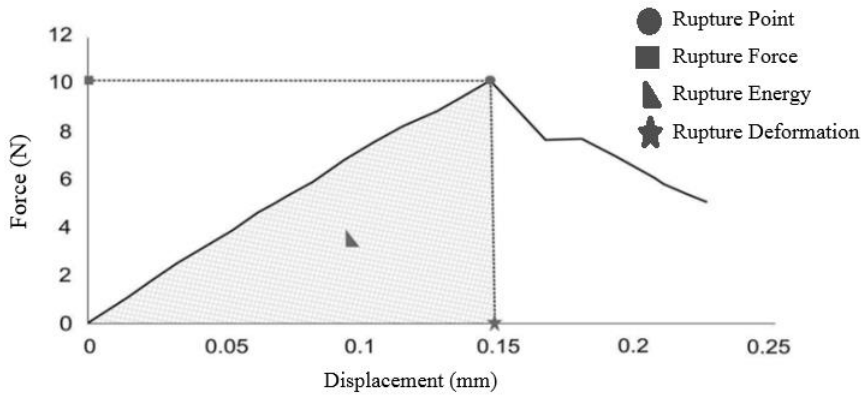

Fig.2. An example of a force- deformation diagram for quail eggs

The gradient of the deformation and rupture energy of quail eggs were calculated using Eqs. 6 and 7 based on Figure 2. (Mohsenin, 1986).

$$Q = F_m / P_m \quad (6)$$

$$W = \int F_{(p)}\, dP \quad (7)$$

Finally, by performing data analysis using SAS® software, all data derived from physical measurements and single-axis pressure tests were compared at different levels of calcium.

Results and Discussion

The values of mass, volume, specific mass and diameter of quail eggs at various levels of calcium are shown in Table 1. By increasing the calcium level of the diet from 1.5% to 3%, the weight and volume of quail eggs dropped. A comparison of mean of measured data for the specific mass is shown in Table 1.

Table 1- Average mass, volume, specific mass, and diameter of quail eggs at different levels of calcium of quail diet

	Sampling age	Calcium levels (%)					CV (%)	SEM
		1.5	2	2.5	3	3.5		
Mass (g)	15 weeks	12.44 a	12.73 a	12.38 a	12.25 a	12.17 a	8.04	0.081
	19 weeks	12.27 a	12.28 a	12.13 a	12.34 a	12.55 a	8.75	0.088
	23 weeks	12.70 a	12.46 a	12.38 ab	12.04 b	12.46 ab	8.90	0.090
Volume CC (cm^3)	15 weeks	11.70 ab	11.95 a	11.53 ab	11.4 b	11.3 b	8.19	0.077
	19 weeks	11.4 a	11.5 a	11.3 a	11.4 a	11.68 a	9.00	0.085
	23 weeks	11.8 a	11.54 ab	11.54 ab	11.1 b	11.51 ab	9.33	0.0088
Specific Mass ($kg.L^{-1}$)	15 weeks	1.064 a	1.068 a	1.073 b	1.076 b	1.074 b	1.01	0.00088
	19 weeks	1.078 b	1.067 a	1.076 b	1.079 c	1.075 bc	0.91	0.00080
	23 weeks	1.070 a	1.079 ab	1.072 a	1.080 b	1.083 b	1.38	0.01225
Middle diameter (mm)	15 weeks	26.14 a	26.51 a	26.13 a	25.9 b	25.8 b	3.05	0.065
	23 weeks	26.4 a	26.16 a	25.97 a	25.8 b	26.02 b	3.29	0.069

Means with different letters are significantly different from each other (P<0.05).

There was a significant difference (level of 0.05) between the average specific mass of quail eggs for different levels of calcium. By increasing the calcium of the quail diet from 1.5 to 3%, the specific mass of the quail egg was increased.

Figure 3 shows the shell thickness of quail eggs at various levels of calcium. The thickness of the quail eggshell was also increased by raising calcium in the diet.

The highest shell thickness, meaningfully was different from other levels of calcium (at the level of 0.05), at 3 and 3.5% of calcium.

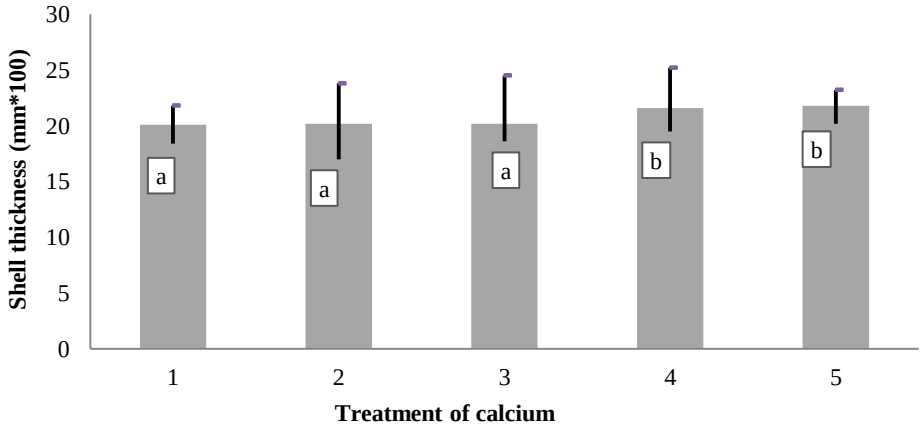

Means with different letters are significantly different from each other (P<0.05).

Fig.3. Average shell thickness of quail eggs (hundredths of a millimeter) at different levels of calcium along with standard deviation

The averages shape index, surface area, degree of sphericity and geometric mean diameter of quail eggs for different levels of calcium at 15th and 23th weeks are shown in Table 3. The statistical analysis of the calculated parameters indicated that the mean values of these physical characters at different levels of calcium did not differ significantly and calcium dietary levels had no effect on the amount of these Characteristics.

Table 3- mean of shape index, surface area, percent of sphericity and geometric mean diameter at different levels of dietary calcium

	Calcium treatments (%)	Number of samples	Shape index	Surface area (mm)	Percent of Sphericity	Geometric mean diameter (mm)
	1.5	30	0.768	2561	83.91	28.54
	2	24	0.781	2604	84.82	28.78
	2.5	29	0.772	2551	84.16	28.48
	3	20	0.760	2536	83.31	28.39
	3.5	16	0.775	2493	84.41	28.16
Average	All	119	0.771	2554	84.12	28.50
CV (%)	All	119	3.729	5.822	2.538	2.917
SEM	All	119	0.0023	12.14	0.0174	0.0679

All the Means of a parameter are not significantly different from each other (P>0.05)

The measured values of the rupture force were analyzed using SAS® software in a completely randomized method. The results of variance analysis are presented in Table 4 and the variations of the rupture force at various levels of calcium are also shown in Figure 4. The difference in mean rupture at different levels of calcium was significant at the level of 0.01. A comparison of the means showed that with an increase in calcium intake of quails from 1.5 to 3 wt% of the diet, the egg rupture rate of quail eggs was raised so that the maximum strength was obtained at 3% calcium diet treatment.

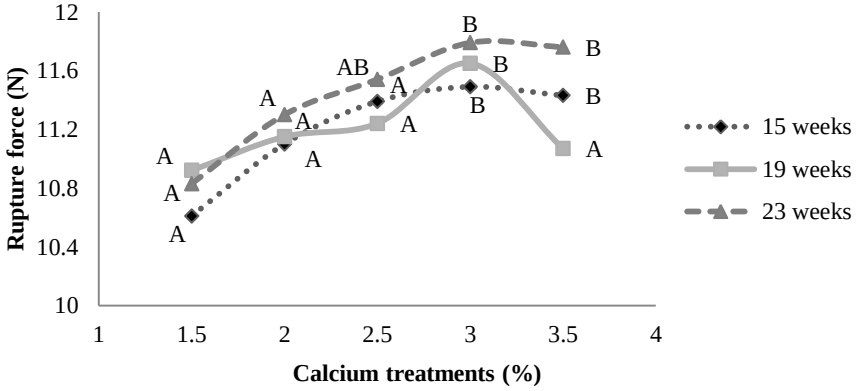

Fig.4. Changes in Rupture Force at various levels of calcium

The slope of the rupture curve (hardness) of quail eggs was raised by increasing the dietary calcium from 1.5 to 3 wt%. The average gradient of the force-deformation curve at various levels of calcium is shown in Table 5. A summary of values obtained from three stages of measuring the gradient of the force-deformation curve were also shown in Figure 5.

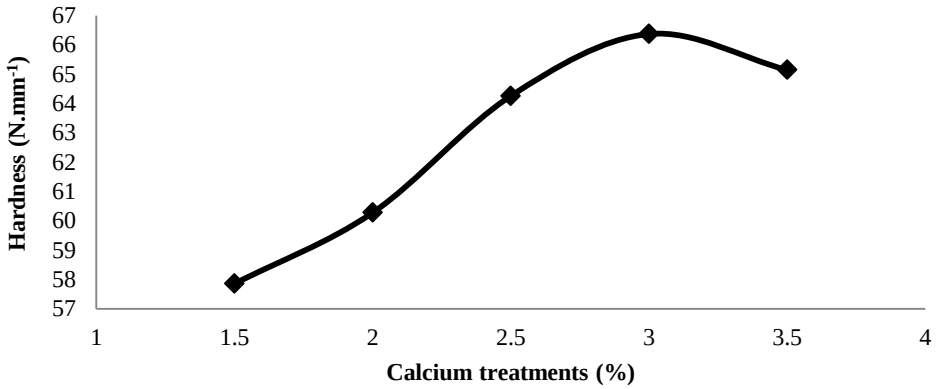

Fig.5. Variation in the slope of rupture curve (hardness) of quail eggs at different levels of calcium

Table 5- The slope of rupture curve along the longitudinal axis of quail eggs at different levels of calcium

Age of bird	Calcium treatments (%)	Number of samples	Hardness ($N.mm^{-1}$)	Min ~ Max	SEM	CV (%)
15 weeks	1.5	26	65.152 a	33.9~83.7	2.485184	19.4505
	2	22	66.854 a	35.4~85.7	2.616399	18.35752
	2.5	26	70.929 b	46.2~99.5	2.260435	16.25212
	3	23	71.707 b	5.06~86.4	1.9861	13.28452
	3.5	27	71.235 b	45.5~96.8	2.381955	17.37611
	Total	124	69.2062	33.9~99.5	1.066855	17.16763
19 weeks	1.5	26	54.506 a	39.0~67.7	1.338885	12.52661
	2	19	54.835 a	45.3~72.3	1.688959	13.42696
	2.5	29	61.031 b	39.6~76.6	1.61425	14.24381
	3	21	62.174 b	47.6~78.7	2.061723	15.19704
	3.5	23	62.832 b	46.4~90.7	2.30325	17.58077
	Total	118	59.150	39.0~90.7	0.861474	15.82079
23 weeks	1.5	29	53.9111 a	28.0~72.6	2.098517	20.96246
	2	30	59.142 ab	44.6~82.7	1.652834	15.30765
	2.5	27	60.8067 b	28.3~93.0	2.730575	23.33632
	3	22	65.2219 b	47.6~76.9	1.502526	10.80569
	3.5	28	61.3617 b	35.6~82.9	2.323619	20.03819
	Total	136	59.79775	28.0~93.0	0.992142	19.3515

Means with different letters are significantly different from each other ($P<0.05$).

The effect of various levels of calcium in the diet of quail on the rupture force, rupture energy, and the slope of the rupture curve (hardness) along the transverse axis of the quail egg were similar to that of the longitudinal axis. According to Table 6 and Figure 6, with increasing calcium in the diet of quails from 1.5 to 3%, shell strength was raised in the direction of small diameter, so that the highest strength and the most specific deformation were obtained at 3% treatment of dietary calcium. The results of this study are consistent with previous findings that examined the effect of dietary calcium on eggshell hardness, finding that eggshell strength was improved by calcium (Jiang *et al.*, 2013).

In an experiment on analysis of the resistance of eggshells in different species of chickens several parameters (weight, dynamic stiffness, static stiffness, breaking force and eggshell thickness) were examined (Ketelaere *et al.*, 2002). They reported that changes in these parameters were not consistent, and mechanical strength (e.g. static stiffness, breaking force, and eggshell thickness) of the

shell showed different values. In this study with increasing calcium, shell thickness was improved and resistance to rupture was increased. These results are consistent with the study of Ketta and Tumova (2017), who observed that reinforced eggshell thickness increased the resistance to rupture (Ketta and Tumova, 2018).

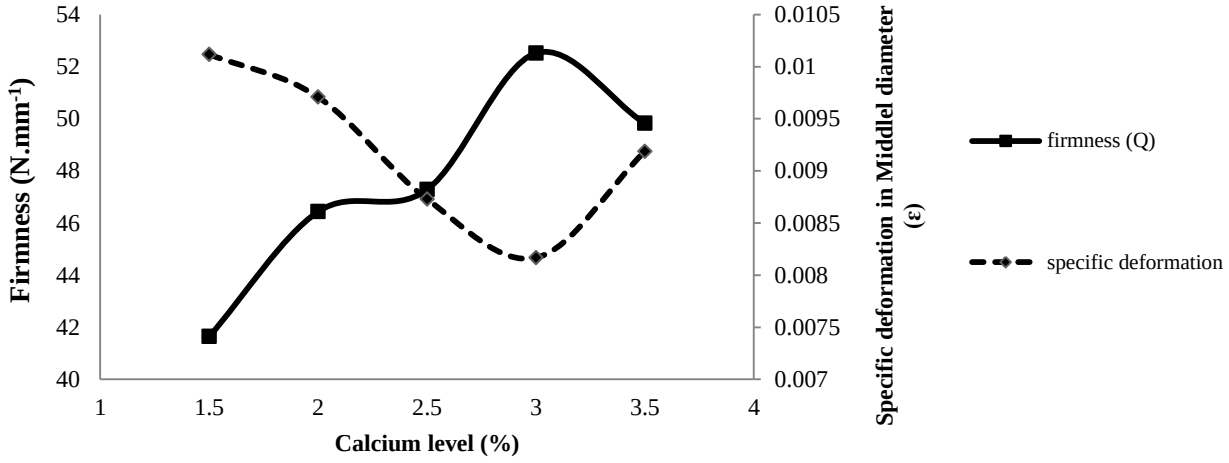

Fig.6. Variation of specific deformation and slope of rupture curve along the transverse axis of quail eggs at different levels of calcium

Table 6- Averages of deformation, specific deformation and hardness of quail eggs along the transverse axis of quail eggs at different levels of dietary calcium

	Level of calcium (%)					Min	Max	SEM	CV
	1.5	2	2.5	3	3.5				
Deformation (mm)	0.269c	0.2532bc	0.2253ab	0.2107a	0.2408abc	0.1161	0.6444	0.00545	0.23871
Specific deformation	0.0101c	0.0097bc	0.0087ab	0.0081a	0.0091abc	0.004324	0.023824	0.00020	0.23393
Hardness ($N.mm^{-1}$)	41.640a	46.432ab	47.278b	52.517c	49.824bc	15.754	72.606	0.84448	0.18500

Mean with different letters are significantly different from each other (P<0.05)

The mean values of the rupture force, rupture energy, the slope of the rupture curve and the deformation to the rupture point along the central diameter of the quail eggs were 10.94 N, 1.53 $N.mm^{-1}$, 47.65 $N.mm^{-1}$, and 0.238 mm, respectively. The mean rupture force and slope of the rupture curve along the transverse axis were lower than the longitudinal axis, while the rupture energy and deformation to the rupture point along the transverse axis of quail eggs were much greater compared to the longitudinal axis. The results are in line with the findings reported by (Polat *et al.*, 2007; Altuntas and Sekeroglu, 2008; Buchar *et al.*, 2015; Nedomova *et al.*, 2016).

Conclusions

The results of this study suggested that by increasing calcium in the diet of quail eggs from 1.5% of the diet to 3 wt%, the strength and thickness of eggshell were reinforced. The highest shell strength of quail eggs was obtained when calcium constituted 3% of the diet weight. By more increasing calcium content, the thickness of the shell remained constant, but the shell strength declined.

The characters of the specific mass, shell thickness, rupture force, and slope of the rupture curve of quail eggs all indicate the degree of shell strength for quail eggs. Increasing each of these characters will translate into enhanced shell strength of quail eggs. In this study, variations in all parameters exhibit that shell strength at different levels of dietary calcium is identical.

In the present study, with an increase in calcium intake, shell thickness was improved and resistance to rupture increased. A comparison of quail eggs in two longitudinal and transverse axes suggested that quail eggs displayed lower strength and greater flexibility along the transverse axis (central diameter) compared to the longitudinal axis.

References

1. Alahdadi, I., H. Oraki, and F. ParhizkarKhajani. 2012. Grain Physical Properties of Some Sunflower Cultivars Influenced by Water Deficit Stress. Journal of Agricultural Machinery Engineering 2 (1): 58-66. (In Farsi).
2. Altuntas, E., and A. Sekeroglu. 2008. Effect of egg shape index on mechanical properties of chicken eggs. Journal of Food Engineering 85: 606-612.
3. Ancel, A., and H. Girard. 1992. Eggshell of the domestic guinea fowl. British poultry science 33: 993-1001.
4. Baghani, M., and M. H. Aghkhani. 2016. Effects of Divergent Selection Body Weight and the Quail Laying Eggs on some Physical and Mechanical Properties of Japanese quail Eggs. Iranian Journal of Animal Science Research 8 (1): 216-226. (In Farsi).
5. Buchar, J., S. Nedomova, J. Trnka, and J. Strnkova. 2015. Behaviour of Japanese quail Eggs under Mechanical Compression. International Journal of Food Properties 18: 1110-1118.
6. Corrêa P. C., G. H. H. Oliveira, P. L. Rodrigues, S. C. Campos, and F. M. Botelho. 2010. Hygroscopic equilibrium and physical properties evaluation affected by parchment presence of coffee grain. Spanish Journal of Agricultural Research 8: 694-702.
7. Gonzalez, M. 1995. Influence of age on physical traits of Japanese quail (*Coturnixcoturnix japonica*) eggs. Ann Zootech 44: 307-312.
8. Jiang, S., C. Luying, S. Cheng, K. Xiao, L. Jingwen, and H. 2013. Jiafa. Effects of dietary energy and calcium levels on performance, egg shell quality and bone metabolism in hens. The Veterinary Journal 198: 252-258.
9. Ketelaere B., T. Govaerts, P. Coucke, E. Dewil, J. Visscher, E. Decuypere, and J. De Baerdemaeker. 2002. Measuring the eggshell strength of 6 different genetic strains of laying hens: Techniques and comparisons. British Poultry Science 43: 238-244.
10. Ketta, M., and E. Tumova. 2016. Eggshell structure, measurements, and quality-affecting factors in laying hens: a review. Czech Journal of Animal Science 7: 299-309.
11. Ketta, M., and E. Tumova. 2018. Relationship between eggshell thickness and other eggshell measurements in eggs from litter and cages. Italian Journal of Animal Science 17 (1): 234-239.
12. Mazzuco, H., and P. Y. Hester. 2005. The effect of an induced molt and a second cycle of lay on skeletal integrity of White Leghorns. Poultry Science 84: 771-781.
13. Mohsenin N. N. 1986. Physical properties of plant and animal materials. Second edition. Gordon and Breach Science Publishers. New York, USA.
14. National Research Council. 1994. Nutrient requirements of poultry. 9th ed. Washington (DC): National Academy of Sciences.
15. Nedomova, S., V. Kumbar, J. Trnka, and J. Buchar. 2016. Effect of the loading rate on compressive properties of goose eggs. Journal of Biological Physics.42: 223-233.
16. North M. O. 1984. Commercial production manual, Third Edition. Van Nostrand Reinhold, New York.

17. Polat, R., S. Tarhan, M. Cetin, and U. Atay. 2007. Mechanical behavior under compression loading and some physical parameters of Japanese quail (*Coturnixcoturnix japonica*) eggs. Czech Journal of Animal Science 52 (2): 50-56.
18. Robert, J. R., and M. Ball. 1998. Egg shell quality problems: causes and solutions. University of Newengland. Armidals, New south Wales, Australia, 2351.
19. Rohani, A., S. I. Saedi, H. Gerailue, and M. H. Aghkhani. 2015. Prediction of lateral surface, volume and sphericity of pomegranate using MLP artificial neural network. Journal of Agricultural Machinery 5 (2): 292-301. (In Farsi).
20. Roque, L., and M. C. 1994. Soares. Effects of eggshell quality and broiler breeder age on hatchability. Poultry Science 73: 1938-1845.
21. Velayati, E., B. Emadi, M. Khojastehpour, and M. H. Saidirad. The Effect of Moisture Content on Physical Properties of Berberis 1 (1): 1-9.
22. Yannakopoulos, A. L., and A. S. Tserveni-Goussi. 1986. Quality characteristics of quail eggs. British Poultry Science 27: 171-176.

نشریه ماشین‌های کشاورزی
جلد ۱۰، شماره ۱، نیمسال اول ۱۳۹۹، ص ۱۰۲-۹۳

Journal of Agricultural Machinery
Vol. 10, No. 1, Spring- Summer 2020, p. 93-102

ویژگی‌های مهندسی تخم بلدرچین ژاپنی در سطوح مختلف کلسیم جیره غذایی

محمد حسین آق خانی[1*]، موسی الرضا باغانی[2]

تاریخ دریافت: ۱۳۹۷/۰۳/۰۵
تاریخ پذیرش: ۱۳۹۷/۰۶/۰۳

چکیده

پوسته تخم پرندگان، به‌عنوان یک بسته‌بندی طبیعی، از مواد موجود در تخم در برابر آسیب‌های میکروبی و مکانیکی محافظت می‌کند. مصرف مقادیر مناسب کلسیم در جیره غذایی پرنده، به‌عنوان یک عامل مهم و مؤثر در افزایش قدرت و کیفیت پوسته تخم می‌تواند عوارض ناشی از مشکلات پوسته را کاهش دهد. در این مقاله، تأثیر کلسیم جیره غذایی در پنج سطح مختلف بر ویژگی‌های مهندسی تخم بلدرچین ژاپنی در گله بلدرچین مادر در اولین دوره تخم‌گذاری آن‌ها بررسی شده است. مقادیر میانگین جرم، حجم، جرم مخصوص، ضخامت پوسته، قطر بزرگ، قطر میانی و نیروی شکست در امتداد محورهای طولی و عرضی اندازه‌گیری شد. انرژی شکست یا چقرمگی، شیب منحنی پارگی (سختی)، تغییر شکل در امتداد محور طولی و عرضی تا نقطه شکست و همچنین تغییر شکل طولی و عرضی ۴۵۰ عدد تخم بلدرچین مورد آزمایش بررسی و اندازه‌گیری شد. پارامترهای جرم مخصوص، ضخامت پوسته، نیروی شکست و شیب منحنی شکست تخم بلدرچین همگی بیانگر استحکام پوسته تخم بلدرچین بوده و در مقالات مختلف از هرکدام از این پارامترها برای نشان دادن استحکام و تغییرات استحکام پوسته استفاده شده است. در مطالعه‌ی حاضر تغییرات تمام پارامترهای بیانگر استحکام پوسته تخم در سطوح مختلف تغذیه‌ی کلسیم با یکدیگر همسو بوده و یکدیگر را تایید کردند. با افزایش مقدار کلسیم جیره غذایی بلدرچین از ۱/۵ به ۳ درصد وزنی، حجم و وزن تخم بلدرچین کاهش یافته و ضخامت پوسته تقویت می‌شود. طبق نتایج به‌دست آمده، مقاومت پوسته تخم بلدرچین در امتداد محور عرضی کمی کمتر از محور طولی است، اما انعطاف‌پذیری و انرژی شکست تخم بلدرچین در محور طولی بسیار بیشتر است.

واژه‌های کلیدی: استحکام، پوسته تخم، کلسیم، ویژگی‌های فیزیکی، ویژگی‌های مکانیکی

۱- استاد، گروه مهندسی بیوسیستم، دانشکده کشاورزی، دانشگاه فردوسی مشهد
۲- دانشجوی دکتری، گروه مهندسی بیوسیستم، دانشکده کشاورزی، دانشگاه فردوسی مشهد
(*- نویسنده مسئول: Email: aghkhani@um.ac.ir)

DOI: 10.22067/jam.v10i1.73027

Journal of Agricultural Machinery
Vol. 10, No. 1, Spring- Summer 2020, p. 103-114

نشریه ماشین‌های کشاورزی
جلد ۱۰، شماره ۱، نیمسال اول ۱۳۹۹، ص ۱۱۴-۱۰۳

Cotton Yield and Water Productivity Affected by Conservation Tillage and Irrigation Methods in Cotton-Wheat Rotation

S. Afzalinia[1*], A. Ziaee[2]

Received: 26-10-2018
Accepted: 10-03-2019

Abstract

In this study, the effect of conservation tillage and irrigation methods on the soil properties, cotton yield, and water productivity was evaluated in a wheat-cotton cropping system in the form of a split-plot experimental design. The main plots were irrigation using the three methods including surface irrigation, drip tape irrigation, and sprinkler irrigation. Tillage methods including zero tillage, reduced tillage, and conventional tillage were considered as subplots in this research. Results showed that tillage methods had no significant effect on cotton yield; whereas, the cotton yield was significantly affected by irrigation methods ($p<0.05$). Tape and sprinkler irrigation methods saved water compared to surface irrigation for 51% and 28%, respectively. The maximum water productivity (0.324 kg m^{-3}) was obtained from the tape irrigation and the minimum water productivity (0.146 kg m^{-3}) was related to surface irrigation. Results also indicated that irrigation and tillage methods had a significant effect on the soil bulk density and infiltration rate so that drip tape irrigation and conventional tillage had the highest infiltration rates, and tape irrigation and reduced tillage had the highest soil bulk density.

Keywords: Cotton, Soil bulk density, Soil infiltration rate, Tillage methods, Water consumption, Water productivity

Introduction

Fars province with 15831 ha of planting area, 50976 tons of production, and 3220 kg ha^{-1} of yield has the second place in producing cotton in Iran (Agricultural Statistics, 2018). Cotton is planted in this province mostly using conventional tillage methods. Using conservation tillage methods in planting cotton has been started recently. Conservation tillage improves soil and water resources (Freebairn *et al.*, 1986), saves energy and time (Afzalinia *et al.*, 2009), and reduces the costs of agricultural products (Erenstein and Laxmi, 2008). The effects of conservation tillage on cotton yield have been evaluated in several studies so far. Conservation tillage under both irrigated and dryland conditions increased cotton profitability compared to the conventional tillage system (Keeling *et al.*, 1989). Strip tillage increased cotton yield and economic return compared to the no-till system (Schomberg *et al.*, 2006). Using crop residue as a soil covering mulch can play a significant role in no-till system success in cotton growing. Results of research conducted in Cameron showed that no-tillage along with crop residue mulch increased cotton yield compared to the conventional tillage and no-till without mulch (Naudin *et al.*, 2010).

Conservation tillage performance may be affected by the irrigation method used on the farm. Conservation tillage had higher water use efficiency in wheat and corn production under the tape irrigation method compared to surface and sprinkler irrigation (Dehghanian and Afzalinia, 2012). Wheat productivity was higher under the flat no-till method compared to the furrow irrigated raised bed and conventional till flat planting in the maize-wheat cropping system (Jat *et al.*, 2005). Conservation tillage reduced water consumption and increased wheat yield for 12% (Freebairn *et al.*, 1986). Soil hydraulic conductivity, soil water absorption, and soil

1- Department of Agricultural Engineering Research, Fars Research and Education Center for Agriculture and Natural Resources, AREEO, Shiraz, Iran
2- Department of Agricultural Engineering Research, Fars Research and Education Center for Agriculture and Natural Resources, Darab Station, AREEO, Darab, Iran
(*- Corresponding Author Email: ja925@mail.usask.ca)
DOI: 10.22067/jam.v10i1.76229

micro-organisms activity were higher in the no-till system compared to the conventional tillage (McGarry *et al.*, 2000). Sprinkler irrigation reduced water consumption compared to surface irrigation for 30% (Haq, 1990). Tape irrigation increased cotton yield compared to the furrow and sprinkler irrigation for 21 and 30%, respectively and had the maximum water use efficiency (4.87 kg ha^{-1} mm^{-1}) compared to these irrigation methods (Cetin and Bilgel, 2002).

No-tillage and permanent bed planting reduced the maize-wheat-mungbean cropping system irrigation water requirement and increased grain yield, biomass yield, and water use efficiency in this cropping system compared to the conventional tillage (Parihar *et al.*, 2017). The zero tillage method decreased evaporation from the topsoil, soil temperature, and corn yield and increased water retention during the critical growth stage of corn, soil bulk density, and soil penetration resistance (Fabrizzi *et al.*, 2005; De Vita *et al.*, 2007). The lower cotton yield and water productivity were obtained from the minimum tillage method compared to the conventional tillage (Jalota *et al.*, 2008). Conservation tillage methods (no-till and minimum tillage) provided higher soil water content, cotton root growth, and cotton yield compared to the conventional tillage (Karamanos *et al.*, 2004). Zero tillage saved soil water content for 23.4% compared to the conventional tillage in dryland vetch-wheat cropping system (Eskandari and Feiziasl, 2017). Overall, researches show that conservation tillage methods increase moisture retention in the soil and decrease water consumption. On the other hand, results show that pressurized irrigation methods, in contrast to surface irrigation methods, significantly reduce water consumption and increase water productivity. The issue that has not been adequately investigated is the effect of interaction between conservation tillage and irrigation methods on water consumption and water productivity. Therefore, the objective of this study was to simultaneously evaluate the effect of conservation tillage and irrigation methods on the cotton yield and water productivity.

Materials and Methods

In order to evaluate the effect of tillage and irrigation methods on the soil bulk density, soil infiltration rate, cotton yield, and cotton water productivity, this research was conducted in Darab region of Fars province (Southern Iran, 28°29′E, 54°57′N, 1080 m above sea level) from 2010 to 2012. Details of the region weather condition are presented in Table 1. The research was conducted based on split-plot experimental design with nine treatments and three replications. The main plots in this research were irrigation methods including 1) surface irrigation; 2) drip tape irrigation; and 3) sprinkler irrigation. Surface irrigation was applied using a gated pipe with a gate space of 75 cm. Drip tape with dripper space of 20 cm and a row space of 75 cm was used in drip irrigation. Traveling gun with Pirot ZK30 sprinkler, operation pressure of 3 bars, the flow rate of 0.7 litter per second, jet length of 19 m, and arrangement of 20 m by 20 m were used in sprinkler irrigation. Tillage methods including zero tillage (ZT), reduced tillage (RT), and conventional tillage (CT) were considered as subplots of this research. Wheat standing residues were retained in the plots and loose residues were taken out of the plots. In the conventional tillage method, primary tillage was performed using a moldboard plow and secondary tillage operation was done using a disk harrow and land leveler then crop seed was planted using seed planter. Seedbed was prepared in the reduced tillage method using a tine and disc cultivator which was able to complete the primary and secondary tillage operations simultaneously then crop seed was planted using seed planter. Cotton and wheat seeds were directly planted using direct planter without any seedbed preparation in the zero-tillage method. The rotation started with cotton and ended with wheat. A local cotton variety (Bakhtegan) was planted with the seed rate of 25 kg ha^{-1}, the row space of 75 cm, and within row space of 20 cm in 20 by 6 m plots in early July and harvested in early December. Wheat

variety of Chamran was planted with the seed rate of 250 kg ha^{-1} and the row space of 17 cm in early December and harvested in late May. Irrigation scheduling was programed every 8, 4, and 2 days for surface, sprinkler, and drip irrigation, respectively based on actual evapotranspiration from the crop, soil water content, and water discharge from the soil. A combination of mechanical and chemical weed control methods was applied to all the treatments identically. Nitrogen, potassium, and phosphorus were applied identically to all the treatments as fertilizers based on the soil elements analysis. Specifications of the soil in which the experiment was performed are presented in Table 2.

Table 1- Climate condition information of the study area

Month	Growing season							
	2010-2011				2011-2012			
	Rainfall (mm)	Evaporation (mm)	Average relative humidity (%)	Average temperature (°C)	Rainfall (mm)	Evaporation (mm)	Average relative humidity (%)	Average temperature (°C)
April	9.1	155.1	45	19.0	13.8	134.7	49	18.6
May	0.0	254.8	31	26.0	6.3	243.9	34	25.4
Jun	0.0	325.5	23	31.5	0.4	368.7	34	30.8
July	0.0	354.2	23	33.7	0..0	364.1	37	33.4
August	3.6	372.7	23	34.1	0.0	375.8	34	33.6
September	0.0	271.3	30	29.8	0.0	274.0	29	30.4
October	0.0	194.2	29	26.0	0.1	186.8	55	24.7
November	0.0	124.9	33	18.6	3.0	115.4	64	17.7
December	0.0	76.7	32	13.2	32.3	57.0	81	11.8
January	39.3	64.9	45	10.7	22.5	60.6	76	10.8
February	210	36.1	71	9.9	62.3	58.8	79	10.2
March	14.1	73.0	55	15.1	31.7	101.8	69	13.0

Table 2- Selected properties of the soil used for the study

Soil depth (mm)	Organic carbon (OC) (%)	Electrical conductivity (EC) (dS m^{-1})	Acidity (pH)	Clay (%)	Silt (%)	Sand (%)	Soil texture
0-100	0.87	0.97	7.7	21.67	36.00	42.33	Loam
100-200	0.79	0.85	7.7	20.00	38.00	42.00	Loam

Soil infiltration rate was determined before crop harvesting each year using the double ring method (Kostiakov, 1932). Soil bulk density was also measured before crop harvesting in the first and second years of study. This parameter was determined in soil depth ranges of 0 to 100 and 100 to 200 mm using core samplers, and drying samples at 105 degrees centigrade for 24 hours in the oven. The following equation was used to calculate the soil bulk density (Black and Harte, 1986):

$$BD = \frac{W_d}{V} \quad (1)$$

Where:
BD = soil bulk density (g cm^{-3}),
W_d = sample dry weight (g), and
V = Sample total volume (cm^3).

The cotton yield per unit area was obtained by harvesting an area of 22.5 m^2 of each plot. Water applied to each main plot was measured using a three inches water flow meter (Abfar Company, Tehran) installed on the pipe supplying water to the main plots. Water productivity was then computed using the following equation (Ali and Talukder, 2008):

$$WP = \frac{Y}{W} \quad (2)$$

Where:
WP = water productivity (kg m^{-3}),
Y= crop yield (kg ha^{-1}), and
W = water consumption (m^3 ha^{-1}).

Data collected from the field experiments were subjected to analysis of variance

(ANOVA) at the confidence level of 95% using SAS software and Duncan's multiple range tests (P=0.05) were used to compare the treatments means.

Results and Discussion

Cotton yield

Variance analysis of cotton yield data showed that year, irrigation method, and interaction between year and irrigation had a significant effect ($p<0.05$) on the cotton yield (Table 3). Tillage methods and interaction between irrigation and tillage methods had no significant influence on the cotton yield. This indicated that the conservation tillage methods did not significantly decrease cotton yield compared to the conventional tillage.

Table 3-Variance analysis of cotton yield data

Variation resources	df	Mean square	F value
Replication	2	3364378.6	6.79**
Year	1	3085968.2	6.23*
Irrigation methods	2	1477009.5	2.98*
Tillage methods	2	552036.8	1.11^{ns}
Year × Irrigation	2	1939510.7	3.92*
Year × Tillage	2	665370.5	1.34^{ns}
Irrigation × Tillage	4	368781.1	0.82^{ns}
Year × Irrigation × Tillage	4	653449.1	1.46^{ns}
Error	28	495325.5	

^{ns}: Non-significant; *: significant at $p<0.05$; **: significant at $p<0.01$.

Means comparison of cotton yield in different irrigation methods is presented in Table 4. According to the results shown in this Table, the cotton yield was significantly higher in the second year (2915 kg ha^{-1}) compared to that of the first year (2437 kg ha^{-1}) due to more moderate climate conditions during the cotton growing season in the second year (Table 1). The maximum cotton yield (2984 kg ha^{-1}) was obtained from the sprinkler irrigation method which was significantly different from those of tape and surface irrigation. There was no significant difference between surface and drip tape irrigation from the cotton yield point of view. Sprinkler irrigation increased cotton yield compared to the surface and drip tape irrigation on average by 23.41 and 13.63%, respectively; while, Cetin and Bilgel (2002) found that drip irrigation increased cotton yield by 21 and 30% compared to the furrow and sprinkler irrigation, respectively. This discrepancy was probably because of the effects of region and climate conditions differences.

There was no significant difference between cotton yields in different tillage methods and conservation tillage methods even increased cotton yield compared to the conventional tillage method (Table 4). These results showed that conventional tillage can be easily replaced by conservation tillage methods (no-till and reduced tillage) in cotton production. These results are in good agreement with the results of research performed by Karamanos *et al.* (2004).

Water applied and water productivity

Results of comparing water applied to different irrigation methods showed that the maximum water application (average of 16483 m^3 ha^{-1}) was occurred in the surface irrigation for cotton production because of its lowest irrigation efficiency and the minimum water application (average of 8113 m^3 ha^{-1}) was related to the drip irrigation (Table 5). The sprinkler irrigation method with an average water application of 11889 m^3 ha^{-1} had the second place from the water application point of view among the irrigation methods tested. As a result, the drip and sprinkler irrigation reduced water application in cotton production compared to surface irrigation for 50% and 28%, respectively. Haq (1990) and Latif (1990) also reported that sprinkler irrigation decreased water application compared to surface irrigation.

Table 4- Means comparison of cotton yield in different treatments

Year		Cotton yield (kg ha^{-1})
First year		2437 b
Second year		2915 a
Irrigation methods		-
Drip tape		2626 b
Surface		2418 b
Sprinkler		2984 a
Tillage methods		-
Conventional tillage		2474 a
Reduced tillage		2768 a
No-tillage		2786 a
Year × Irrigation		-
First year	Drip tape	2290 b
First year	Surface	1910 c
First year	Sprinkler	3111 a
Second year	Drip tape	2962 a
Second year	Surface	2926 a
Second year	Sprinkler	2857 a

a, b, c: Averages with different letters in each column are statistically different at $p<0.05$.

Table 5- Water applied for cotton growing in different irrigation methods

Irrigation methods	Water applied (m^3 ha^{-1})		
	2010	2011	Average
Drip tape	8139	8087	8113
Surface	16320	16645	16483
Sprinkler	11692	12086	11889

Variance analysis of water productivity data revealed that year and irrigation methods had a significant effect on water productivity in cotton production, while tillage methods and interaction between irrigation and tillage methods had no remarkable influence on cotton water productivity (Table 6). Since water applied to the various irrigation methods was different, a significant effect of irrigation methods on water productivity was expected. On the other hand, cotton yields were not significantly different in the various tillage methods and identical water was applied to the tillage methods in this research; therefore, tillage methods had no drastic effect on the cotton water productivity.

Table 6- Variance analysis of cotton water productivity data

Variation resources	df	Mean square	F value
Replication	2	0.029	7.53^{**}
Year	1	0.020	5.00^{*}
Irrigation methods	2	0.143	36.68^{**}
Tillage methods	2	0.007	1.76^{ns}
Year × Irrigation	2	0.016	4.15^{*}
Year × Tillage	2	0.007	1.78^{ns}
Irrigation × Tillage	4	0.004	0.98^{ns}
Year × Irrigation × tillage	4	0.007	1.87^{ns}
Error	28	0.004	

^{ns}: Non-significant; *: significant at $p<0.05$; **: significant at $p<0.01$.

Means comparison of cotton water productivity showed that cotton had higher water productivity in the second year (0.26 kg m^{-3}) compared to the first year (0.22 kg m^{-3}) (Table 7). This was mostly because of the more moderate climate condition of the second year which resulted in higher crop yield this year. Results also indicated that drip tape irrigation had the maximum water productivity (0.324 kg m^{-3}) and surface irrigation had the

minimum water productivity (0.146 kg m^{-3}). Means comparison of interaction between year and irrigation method revealed that there was no significant difference between drip tape and sprinkler irrigation from the water productivity point of view in the first year; while, this difference was significant in the second year. Drip tape irrigation had maximum water productivity in both years.

Water productivity is a function of two factors including water consumption (inverse relationship) and crop yield (direct relationship); therefore, in spite of having higher water application, the sprinkler irrigation had water productivity close to that of drip irrigation in 2010 because of having higher crop yield in this year. The results of this study also revealed that pressurized irrigation methods (drip tape and sprinkler irrigation) had higher water productivity in cotton production compared to surface irrigation; thus, surface irrigation should be replaced by pressurized irrigation systems in cotton growing. Cetin and Bilgel (2002) also reported that drip irrigation improved water use efficiency compared to furrow and sprinkler irrigation methods.

Results of means comparison of water productivity in different tillage methods indicated that there was no significant difference between tillage methods for water productivity; however, conservation tillage methods increased cotton water productivity for an average of 16% compared to the conventional tillage (Table 7).

Table 7- Means comparison of cotton water productivity in different treatments

Year		Water Productivity (kg m^{-3})
First year		0.222 b
Second year		0.260 a
Irrigation methods		-
Drip tape		0.324 a
Surface		0.146 c
Sprinkler		0.251 b
Tillage methods		-
Conventional tillage		0.218 a
Reduced tillage		0.253 a
No-tillage		0.250 a
Year × Irrigation		-
First year	Drip tape	0.281 a
First year	Surface	0.117 b
First year	Sprinkler	0.266 a
Second year	Drip tape	0.366 a
Second year	Surface	0.176 c
Second year	Sprinkler	0.236 b

a, b, c: Averages with different letters in each column are statistically different at $p<0.05$.

Soil bulk density

Variance analysis of soil bulk density data indicated that bulk density was affected by year and irrigation method at the soil depth of 0-100 mm; while, soil bulk density was affected by year and tillage method at the soil depth of 100-200 mm (Table 8). Results also showed that soil bulk density was not influenced by the interaction between irrigation and tillage methods.

Results revealed that soil had a higher bulk density in the first year compared to the second year that was probably because of more decomposed crop residue at the end of the second year (Table 9). Comparing soil bulk density in different irrigation methods showed that drip tape irrigation had the highest soil bulk density and surface irrigation had the lowest soil bulk density at the soil depth of 0-100 mm. Soil bulk density amount was inversely related to the soil organic matter, and soil organic matter was affected by the amount of decomposed crop residue. In drip tape irrigation, only a small fraction of crop residue was wetted by irrigation water; while, all crop residues were exposed to the irrigation water in the sprinkler and surface irrigation.

Therefore, soil organic matter was usually higher in the plots irrigated by tape irrigation compared to that of plots irrigated by sprinkler and surface irrigation. For this reason, plots irrigated with tape irrigation had higher soil bulk density compared to plots irrigated with sprinkler and surface irrigation methods.

Table 8- Variance analysis of soil bulk density data

Variation resources	0-100 mm			100-200 mm		
	df	Mean square	F value	df	Mean square	F value
Replication	2	0.005	3.45*	2	0.004	1.68^{ns}
Year	1	0.035	22.42**	1	0.041	18.38**
Irrigation methods	2	0.007	4.69*	2	0.004	1.77^{ns}
Tillage methods	2	0.003	2.16^{ns}	2	0.019	8.39**
Year × Irrigation	2	0.002	1.55^{ns}	2	0.005	2.14^{ns}
Year × Tillage	2	0.003	1.66^{ns}	2	0.002	0.95^{ns}
Irrigation × Tillage	4	0.001	0.80^{ns}	4	0.001	0.48^{ns}
Year × Irrigation × tillage	4	0.001	0.94^{ns}	4	0.005	2.18^{ns}
Error	28	0.002		28	0.002	

^{ns}: Non-significant; *: significant at $p<0.05$; **: significant at $p<0.01$.

Conservation tillage methods (reduced and zero tillage) had a higher soil bulk density compared to the conventional tillage at the soil depth of 100-200 mm (Table 9). In the conservation tillage methods, soil disturbance was less than conventional tillage; therefore, soil bulk density was higher in conservation tillage methods compared to the conventional tillage. Results of some previous studies also show the higher soil bulk density in the conservation tillage methods compared to the conventional tillage (Afzalinia *et al.*, 2012; Liu *et al.*, 2005; Taser and Metinoglu, 2005). It should be noted that the difference between conservation and conventional tillage methods from the soil bulk density point of view is bigger at the beginning of the growing season compared to the end of growth season (Afzalinia and Zabihi, 2014).

Table 9- Means comparison of soil bulk density (g cm^{-3})

Treatments	0-100 mm	100-200 mm
Year	-	-
First year	1.37 a	1.44 a
Second year	1.32 b	1.38 b
Irrigation methods	-	-
Drip tape	1.36 a	1.43 a
Surface	1.33 b	1.40 a
Sprinkler	1.33 b	1.41 a
Tillage methods	-	-
Conventional tillage	1.36 a	1.37 b
Reduced tillage	1.34 a	1.44 a
No-tillage	1.33 a	1.42 a

a, b: Averages with different letters in each column are statistically different at $p<0.05$.

Table 10- Variance analysis of soil infiltration rate data

Variation resources	df	Mean square	F value
Replication	2	0.144	6.53**
Year	1	0.735	33.36*
Irrigation methods	2	0.584	26.50**
Tillage methods	2	0.319	14.47**
Year × Irrigation	2	0.132	5.98*
Year × Tillage	2	0.084	3.79*
Irrigation × Tillage	4	0.275	12.49**
Year × Irrigation × Tillage	4	0.122	5.55**
Error	28	0.022	

^{ns}: Non-significant; *: significant at $p<0.05$; **: significant at $p<0.01$.

Soil infiltration rate

Variance analysis of soil infiltration rate data showed that year, irrigation methods, tillage methods, and interaction between irrigation and tillage methods had a significant influence on the soil infiltration rate (Table 10). Since soil disturbance and crop residue decomposition were different in various irrigation and tillage methods, a significant effect of irrigation and tillage methods on the soil infiltration rate was expected.

Results of means comparison of soil infiltration rate showed that plots had significantly higher infiltration rate in the second year compared to the first year which was probably because of the increase of soil organic matter due to crop residue retention on the soil in this research (Table 11). Comparing irrigation treatments for soil infiltration rate indicated that drip tape irrigation had the maximum soil infiltration rate which was not significantly different from that of sprinkler and surface irrigation had the minimum infiltration rate. Water reached the soil gradually in tape irrigation and clay leaching in this irrigation method was low; therefore, the soil had a more porous structure and higher infiltration rate in this irrigation system. In contrast, more clay leaching and adhesion of soil aggregates in surface irrigation slowed down the water movement in the soil in this irrigation system.

Table 11- Soil infiltration rate in different irrigation and tillage methods

Year			Soil infiltration rate (mm min^{-1})
First year			0.79 b
Second year			1.03 a
Irrigation methods			-
Drip tape			1.08 a
Surface			0.72 b
Sprinkler			0.92 ab
Tillage methods			-
Conventional tillage			1.06 a
Reduced tillage			0.80 b
No-tillage			0.88 b
Year × Irrigation× Tillage			-
		Conventional tillage	1.07 c
First year	Drip tape	Reduced tillage	0.81 d
		No-tillage	0.86 d
		Conventional tillage	0.53 e
First year	Surface	Reduced tillage	0.59 e
		No-tillage	0.58 e
		Conventional tillage	1.02 c
First year	Sprinkler	Reduced tillage	0.63 e
		No-tillage	1.06 c
		Conventional tillage	1.62 a
Second year	Drip tape	Reduced tillage	1.36 b
		No-tillage	0.78 d
		Conventional tillage	0.81 d
Second year	Surface	Reduced tillage	0.72 d
		No-tillage	1.11 c
		Conventional tillage	1.28 b
Second year	Sprinkler	Reduced tillage	0.67 de
		No-tillage	0.88 d

a, b, c: Averages with different letters in each column are statistically different at $p<0.05$.

Results of means comparison of soil infiltration rate in different tillage methods revealed that conventional tillage had the highest soil infiltration rate compared to the conservation tillage methods (Table 11). The minimum soil infiltration rate was related to the reduced tillage; however, there was no significant difference between reduced and no-

tillage for soil infiltration rate. The higher soil infiltration rate in the conventional tillage was probably because of more soil disturbance in this tillage method. Means comparison of soil infiltration rates affected by the interaction between irrigation and tillage methods indicated that conventional tillage method irrigated by tape irrigation had the maximum soil infiltration rate and the reduced tillage method irrigated by sprinkler and surface irrigation had the minimum soil infiltration rate (Table 11).

Conclusions

The following conclusions can be drawn from the results of this research:

1. The cotton yield was not affected by tillage methods in a short research period; while, irrigation methods had a significant effect on cotton yield. Pressurized irrigation systems produced more cotton yield on average compared to surface irrigation; therefore, conservation tillage methods irrigating with drip tape and sprinkler irrigation system was recommended for cotton growing in semi-arid climate conditions of Iran.
2. The maximum water was applied in surface irrigation and the minimum water application was related to the drip tape irrigation. Drip tape and sprinkler irrigation methods saved water for 51 and 28% and increased water productivity for 120 and 71% in growing cotton compared to surface irrigation, respectively.
3. Conservation tillage methods increased the soil bulk density compared to the conventional tillage in growing cotton. Tape irrigation had also the higher soil bulk density among the irrigation systems tested.
4. Drip tape irrigation treatment had the maximum soil infiltration rate and the minimum infiltration rate belonged to surface irrigation. Among the tillage methods tested, the conventional tillage treatment had a higher infiltration rate.

Acknowledgments

The authors would like to acknowledge the financial support extended by the Agriculture Organization of Fars province and Agricultural Engineering Research Institute. Technical supports from colleagues in the Department of Agricultural Engineering Research during the experimental works are also appreciated.

References

1. Afzalinia, S., E. Dehghanian, and M. H. Talati. 2009. Effect of conservation tillage on soil physical properties, fuel consumption, and wheat yield. Fourth Conference on Energy Efficiency and Agricultural Engineering, Rousse, Bulgaria.
2. Afzalinia, S., A. Karami, and S. M. Alavimanesh. 2012. Comparing Conservation and Conventional Tillage Methods in Corn-Wheat Rotation. International Conference of Agricultural Engineering, Valencia, Spain.
3. Afzalinia, S., and J. Zabihi. 2014. Soil compaction variation during corn growing season under conservation tillage. Soil and Tillage Research 137: 1-6.
4. Ahmadi, K., H. R. Ebadzadeh, H. Abdshah, A. Kazemian, and M. Rafiee. 2018. Agricultural statistics of 2016-2017 growing season. Ministry of Jehad-e-Agriculture, Tehran, pp 116.
5. Ali, M. H., and M. S. U. Talukder. 2008. Increasing water productivity in crop production-A synthesis. Agricultural Water Management 95: 1201-1213.
6. Black, G. R., and K. H. Harte. 1986. Bulk density, core method in methods of soil analysis, part 1. Agronomy Monograph 9: 363-366.
7. Cetin, O., and L. Bilgel. 2002. Effects of different irrigation methods on shedding and yield of cotton. Agricultural Water Management 54: 1-15.
8. Dehghanian, S. E., and S. Afzalinia. 2012. Effect of conservation tillage and irrigation methods on the crop yield and water use efficiency in wheat-corn rotation. International Conference of Agricultural Engineering, Valencia, Spain.

9. De Vita, P., E. Di Paolo, G. Fecondo, N. Di Fonzo, and M. Pisante. 2007. No-tillage and conventional tillage effects on durum wheat yield, grain quality and soil moisture content in southern Italy. Soil & Tillage Research 92: 69-78.
10. Erenstein, O., and V. Laxmi. 2008. Zero tillage impacts in India's rice–wheat systems: A review. Soil & Tillage Research 100: 1-14.
11. Eskandari, I., and V. Feiziasl. 2017. Influence of conservation tillage on some soil physical properties and crop yield in vetch-wheat rotation in dryland cold region. Journal of Agricultural Machinery 7 (2): 451-467. (In Farsi).
12. Fabrizzi, K. P., F. O. Garc´, J. L. Costa, and L. I. Picone. 2005. Soil water dynamics, physical properties and corn and wheat responses to minimum and no-tillage systems in the southern Pampas of Argentina. Soil & Tillage Research 81: 57-69.
13. Freebairn, D. M., L. D. Ward, A. L. Clarke, and G. D. Smith. 1986. Research and development of reduced tillage systems for vertisols in Queensland, Australia. Soil & Tillage Research 8: 211-229.
14. Haq, N. 1990. Evaluation of modern irrigation techniques for sandy loam soil having low slopes. Department of Irrigation and Drainage, University of Agriculture, Faisalabad.
15. Jalota, S. K., G. S. Buttar, A. Sood, G. B. S. Chahal, S. S. Ray, and S. Panigrahy. 2008. Effects of sowing date, tillage and residue management on productivity of cotton (*Gossypium hirsutum* L.)-wheat (*Triticum aestivum* L.) system in northwest India. Soil & Tillage Research 99: 76-83.
16. Jat, M. L., A. Srivastava, S. K. Sharma, R. K. Gupta, P. H. Zaidi, H. K. Rai, and G. Srinivasan. 2005. Evaluation of maize-wheat cropping system under double no-till practice in Indo-Gangetic Plains of India. 9th Asian Regional Maize Workshop, Beijing, China.
17. Karamanos, A. J., D. Bilalis, and N. Sidiras. 2004. Effects of reduced tillage and fertilization practices on soil characteristics, plant water status, growth and yield of upland cotton. Journal of Agronomy and Crop Science 190: 262-276.
18. Keeling, W., E. Searra, and J. R. Abernathy. 1989. Evaluation of conservation cropping systems for cotton on the Texas southern high Plains. Journal of Production Agriculture 2 (3): 269-273.
19. Kostiakov, A. N. 1932. On the dynamics of the coefficient of water percolation in soils and on the necessity for studying it from a dynamic point of view for purposes of amelioration. Trans. 6 Comm. Intern. Soil Sci. Russian, Part A, 17-21.
20. Latif, M. 1990. Sprinkler irrigation to harness potential of water scarcity area in Pakistan. Technical Report No. 41. CEWRE. Pub. No. 37.
21. Liu, S., H. Zhang, Q. Dai, H. Huo, Z. K. Xu, and H. Ruan. 2005. Effects of no-tillage plus inter-planting and remaining straw on the field on cropland eco-environment and wheat growth. Ying Yong Sheng Tai Xue Bao 16: 393-396.
22. McGarry, D., B. J. Bridge, and B. J. Radford. 2000. Contrasting soil physical properties after zero and traditional tillage of an alluvial soil in semi-arid subtropics. Soil &Tillage Research 53: 105-115.
23. Naudin, K., E. Goze, O. Balarabe, K. E. Giller, and E. Scopel. 2010. Impact of no tillage and mulching practices on cotton production in North Cameroon: A multi-locational on-farm assessment. Soil & Tillage Research 108: 68-76.
24. Parihar, C. M., S. L. Jat, A. K. Singh, A. Ghosh, N. S. Rathore, B. Kumar, S. Pradhan, K. Majumdar, T. Satyanarayana, M. L. Jat, Y. S. Saharawat, B. R. Kuri, and D. Saveipune. 2017. Effects of precision conservation agriculture in a maize-wheat-mungbean rotation on crop yield, water-use and radiation conversion under a semiarid agro-ecosystem. Agricultural Water Management 192: 306-319.

25. Schomberg, H. H., R. G. McDaniel, E. Mallard, D. M. Endale, D. S. Fisher, and M. L. Cabrera. 2006. Conservation tillage and cover crop influences on cotton production on a southeastern U.S. Coastal Plain soil. Agronomy Journal 98: 1247-1256.
26. Taser, O., and F. Metinoglu. 2005. Physical and mechanical properties of a clay soil as affected by tillage systems for wheat growth. Acta Agriculture Scandinavica Section B-soil and Plant 55: 186-191.

نشریه ماشین‌های کشاورزی
جلد ۱۰، شماره ۱، نیمسال اول ۱۳۹۹، ص ۱۱۴-۱۰۳

Journal of Agricultural Machinery
Vol. 10, No. 1, Spring- Summer 2020, p. 103-114

عملکرد پنبه و بهره‌وری مصرف آب تحت تأثیر روش‌های خاک‌ورزی حفاظتی و آبیاری در تناوب پنبه-گندم

صادق افضلی نیا[1*]، علیرضا ضیایی[2]

تاریخ دریافت: ۱۳۹۷/۰۸/۰۴
تاریخ پذیرش: ۱۳۹۷/۱۲/۱۹

چکیده

در این تحقیق، اثر روش‌های خاک‌ورزی حفاظتی و آبیاری بر خصوصیات خاک، عملکرد پنبه و کارایی مصرف آب در تناوب گندم-پنبه در قالب طرح آزمایشی اسپلیت پلات بررسی شد. فاکتور اصلی روش آبیاری شامل آبیاری سطحی، قطره‌ای نواری و بارانی بود. روش‌های خاک‌ورزی شامل بی‌خاک‌ورزی، کم‌خاک‌ورزی و خاک‌ورزی مرسوم نیز به‌عنوان فاکتور فرعی در نظر گرفته شدند. نتایج نشان داد که روش خاک‌ورزی اثر معنی‌داری بر عملکرد پنبه نداشت، در حالی‌که عملکرد پنبه تحت تأثیر معنی‌دار روش آبیاری قرار گرفت ($p<0.05$). روش‌های آبیاری قطره‌ای نواری و بارانی در مقایسه با آبیاری سطحی مصرف آب را به‌ترتیب ۵۱ و ۲۸ درصد کاهش دادند. آبیاری قطره‌ای نواری بیشترین مقدار کارایی مصرف آب (۰/۳۲۴ کیلوگرم بر متر مکعب) را داشت و کمترین مقدار کارایی مصرف آب (۰/۱۴۶ کیلوگرم بر متر مکعب) مربوط به آبیاری سطحی بود. همچنین، نتایج نشان داد که روش‌های خاک‌ورزی و آبیاری اثر معنی‌داری بر جرم مخصوص ظاهری و نفوذپذیری خاک داشتند، به‌طوری‌که آبیاری قطره‌ای نواری و خاک‌ورزی مرسوم بیشترین نفوذپذیری خاک را داشتند و بیشترین جرم مخصوص ظاهری خاک مربوط به آبیاری قطره‌ای نواری و کم‌خاک‌ورزی بود.

واژه‌های کلیدی: پنبه، جرم مخصوص ظاهری خاک، روش‌های خاک‌ورزی، کارایی مصرف آب، نفوذپذیری خاک، مصرف آب

۱- بخش تحقیقات فنی و مهندسی کشاورزی، مرکز تحقیقات و آموزش کشاورزی و منابع طبیعی فارس، سازمان تحقیقات، آموزش و ترویج کشاورزی، شیراز، ایران
۲- بخش تحقیقات فنی و مهندسی کشاورزی، مرکز تحقیقات و آموزش کشاورزی و منابع طبیعی فارس، ایستگاه تحقیقات داراب، سازمان تحقیقات، آموزش و ترویج کشاورزی، داراب، ایران
(*- نویسنده مسئول: Email: sja925@mail.usask.ca)

DOI: 10.22067/jam.v10i1.76229

FORMAT OF MANUSCRIPT PREPARATION FOR JOURNAL OF AGRICULTURAL MACHINERY

It is important that the manuscript be written according to the Journal format. Submission to this journal proceeds totally online and you will be guided stepwise through the creation and uploading of your files through the web site of the Journal as: http://jame.um.ac.ir

Essential title page information

The title page MUST be prepared and uploaded separately from the main text with the following information:

• Title. Concise and informative and not more than 15 words.

• Author names and affiliations. Present the authors' affiliation addresses (where the work was actually done) below the names. Indicate all affiliations with a superscript number immediately after the author's name and also in front of the appropriate address. Provide the full postal address of each affiliation and if available, the e-mail address of each author.

• Corresponding author. Clearly indicate who will handle correspondence at all stages of refereeing and publication, also post-publication. Ensure that phone numbers (with country and area code) are provided in addition to the e-mail address and the complete postal address. Contact details must be kept up to date by the corresponding author.

• Present/permanent address. If an author has moved since the work described in the article was done, or was visiting at the time, a 'Present address' (or 'Permanent address') may be indicated as a footnote to that author's name. The address at which the author actually did the work must be retained as the main, affiliation address. Superscript numerals are used for such footnotes.

Paper configuration

Each paper should have the following distinct sections: Title, Abstract and up to five Keywords, Introduction, Material and methods, Results and discussion, Conclusion, and References. The Acknowledgment (briefly), Recommendations and Nomenclature can also be added. Each section should be prepared as follow:

Abstract: A concise and factual abstract is required. The abstract should state briefly the purpose of the research, the principal results and major conclusions. It should not exceed 250 words. The abstract is presented separately from the article in a single paragraph, so it must be able to stand alone. For this reason, References should be avoided. Also, non-standard or uncommon abbreviations should be avoided, but if essential they must be defined at their first mention in the abstract itself.

Keywords: Up to five keywords appear immediately after the abstract with alphabetical order.

Introduction: Clearly state the research problem and the necessity of research, the objectives of the work and provide an adequate background, avoiding a detailed literature survey or a summary of the results.

Material and methods: Provide sufficient detail to allow the work to be reproduced. Methods already published should be indicated by a reference: only relevant modifications should be described. For the analytical and modeling works a section may be added as "Theory".

Results and discussion: Results should be clear and concise. The discussion should explore the significance of the results of the work, not repeat them. A combined Results and Discussion section is often appropriate. Avoid extensive citations and discussion of published literature.

Conclusions: The main conclusions of the study is presented in a short Conclusions section, which should be stand alone.

Paper layout

The main text should be prepared in A4 paper size, with 1.5 line spacing and all margins of 3 cm. All pages should be numbered sequentially and not more than 15 pages. All lines should be numbered continuously by applying the "Line numbering" command of MS Word.

Fonts

- All writings should be written using Times New Roman font. Both American and British English format are accepted, but not their mixture!
- The font size for title is 14 point and for the main text is 12 point.
- The subtitles should be written in Bold and font size of 12 point.

Units

Please use SI units only. It is not necessary to give the SI unit and (say) its Imperial equivalent. Engineering Notation, where units are in multiples of 1,000, should be used. Thus, we wish to see the use of mm and m and not cm. Use exponent form instead of conventional format (e.g. m s^{-1} and NOT m/s).

Math formulae

Present simple formulae in the line of normal text where possible. In principle, variables are to be presented in italics. Number consecutively any equations that have to be displayed separately from the text in the right margin (if referred to explicitly in the text).

Tables

Number tables consecutively in accordance with their appearance in the text. Place footnotes to tables below the table body and indicate them with superscript lowercase letters. Avoid vertical rules. Be sparing in the use of tables and ensure that the data presented in tables do not duplicate results described elsewhere in the article. The Table caption appears above the Table with font size of 10. Use no border for the Tables.

Figures

Ensure that each illustration has a caption. Supply captions separately, not attached to the figure. A caption should comprise a brief title (not on the figure itself) and a description of the illustration. Keep text in the illustrations themselves to a minimum but explain all symbols and abbreviations used (preferably in the caption). The caption should allow the reader to understand the main elements of what is being shown without needing to refer to the main text. The Figure caption appears below the Figure and written with font size of 10 points. Use no border for the Figures. The font size within the Figure should not smaller than 8 point and bigger than 10 point. Try to present the Figures in gray scale instead of color illustration. The followings are a sample of Table and Figure.

Table 1- Consumption of inputs during the first year of saffron cultivation

Type of inputs	Consumption (kg ha^{-1})
Consumed corms	3000
Urea	100
Ammonium phosphate	100
Animal manure	32000
Consumed irrigation water	3000 (m^3)*

* The annual water consumption for saffron cultivation was considered equal to 3000 m^3 (Mahdavi, 1999).

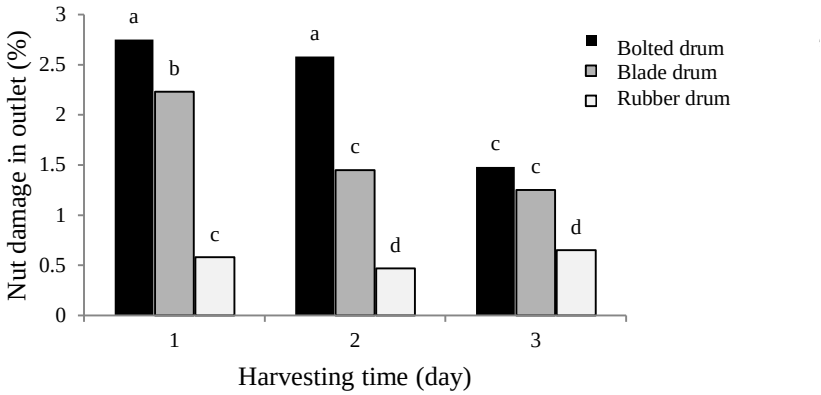

Fig. 3. The effects of harvesting time and machine type on the percentage of cracked shells in the outlet

References

Citation in text

Please ensure that every reference cited in the text is also present in the reference list (and vice versa). Unpublished results and personal communications are not recommended in the reference list, but may be mentioned in the text. If these references are included in the reference list they should follow the standard reference style of the journal and should include a substitution of the publication date with either 'Unpublished results' or 'Personal communication'. Avoid anonymous references. Citation of a reference as 'in press' implies that the item has been accepted for publication.

Reference style

Use "Author, Date" style for list of references and citations all in English language using Times New Roman font size of 10 point as follow:

Citations

Single author: (Loghavi, 2008).

Two authors: (Aghkhani and Abbaspour-Fard, 2009).

Three authors and more: (Abbaspour-Fard *et al.*, 2008).

Multiple citations: (Smith, 1999; Samuel *et al*., 2008; Smith and Samuel, 2009)

Use the complete name of the journals instead of their abbreviations. For those authors using EndNote software for list of References and citations, please use the following style which can be downloaded from Journal of Agricultural Machinery:

Style Name: Jame Endnote Style

List of References

Journal article

Aghkhani, M. H., and M. H. Abbaspour-Fard. 2009. Automatic off-road vehicle steering system with a surface laid cable: Concept and preliminary tests. Biosystems Engineering 103: 265-270.

Special issue

Rice, K. 1992. Theory and conceptual issues. In: Gall, G.A.E., Staton, M. (Eds.), Integrating Conservation Biology and Agricultural Production. Agricultural Ecosystems Environment: 9-26.

Reference to a Book

Gaugh, H. G. 1992. Statistical Analysis of Regional Yield Trials. Elsevier. Amsterdam.

Reference to a chapter in an edited book

Mettam, G. R., and L. B. Adams. 1999. How to prepare an electronic version of your article. PP 281-304 in B. S. Jones and R. Z. Smith eds. Introduction to the Electronic Age. E-Publishing Inc., New York.

Reference to a thesis or dissertation (if you can, avoid this type of reference)

Abbaspour-Fard, M. H. 2001. The dynamic behavior of particulate biomaterials using discrete element method (DEM). Faculty of Agriculture. Newcastle University, Newcastle upon Tyne.

Reference to a conference proceeding

Hemmat, A., V. I. Adamchuk, and P. Jasa. 2007. On-the-go soil strength sensing using an instrumented disc coulter. International Agricultural Engineering Conference (IAEC). Asian Association for Agricultural Engineering, Bangkok, Thailand.

Web references

As a minimum, the full URL should be given and the date when the reference was last accessed. Any further information, if known (DOI, author names, dates, reference to a source publication, etc.), should also be given. Web references can be included in the reference list e.g.:

Brittion, A. 2006. How much and how often should we drink British Medical Journal, 332: 1224-1225. Available from: http://bmj.bjjournals.com/cgi/content/full/332/7552/1224. Accessed 2 June 2006.

Miscellaneous

- All submitted papers will be peer reviewed by some accredited referees under the supervision of the editorial board and if accepted will be put in queue for publication based on the date of acceptance and other journal's rules and regulations.
- The editorial board of the Journal keeps their right to accept or reject any of the submitted papers.
- No change can be made on a paper which has been proof read by the authors.

Persian abstract

The title, abstract, and Persian keywords should be at the bottom of the article.

مندرجات

نشریه ماشین های کشاورزی

با شماره پروانه ۸۹/۱۲۶۳۹ **و درجه علمی – پژوهشی شماره** ۳/۱۱/۳۷۸۱ **از وزارت علوم، تحقیقات و فناوری**

۸۹/۶/۱۳ **۸۹/۳/۱۷**

جلد ۱۰ شماره ۱ نیمسال اول ۱۳۹۹

صاحب امتیاز: دانشگاه فردوسی مشهد

مدیر مسئول: سید محمدرضا مدرس رضوی استاد- گروه مکانیک دانشکده مهندسی (دانشگاه فردوسی مشهد)

سردبیر: محمدحسین عباسپور فرد استاد- گروه مهندسی مکانیک بیوسیستم (دانشگاه فردوسی مشهد)

ناشر: انتشارات دانشگاه فردوسی مشهد **چاپ:** چاپخانه دانشگاه فردوسی مشهد

نشانی: مشهد- کد پستی ۹۱۷۷۵ صندوق پستی ۱۱۶۳

دانشکده کشاورزی- دبیرخانه نشریات علمی - نشریه ماشین‌های کشاورزی - نمابر:۰۵۱۳۸۷۸۷۴۳۰

این نشریه در پایگاه‌های زیر نمایه شده است:

پایگاه استنادی جهان اسلام (ISC)

پایگاه اطلاعات علمی جهاد دانشگاهی (SID)

بانک اطلاعات نشریات کشور (MAGIRAN)

پست الکترونیک: Jame@um.ac.ir

مقالات این شماره در سایت http://jame.um.ac.ir **به‌صورت مقاله کامل نمایه شده است.**

این نشریه به تعداد ۲ شماره در سال منتشر می‌شود.

انجمن مهندسان مکانیک ایران

نشریه علمی
ماشین های کشاورزی

دانشگاه فردوسی مشهد

جلد ۱۰ شماره ۱
سال ۱۳۹۹
(شماره پیاپی: ۱۹)

شاپا: ۶۸۲۹-۲۲۲۸

عنوان مقالات